Democratic and Popular Republic of Algeria
Ministry of Higher Education and Scientific Research
Mohamed Khider University
Faculty of Exact Sciences, and Sciences of Nature and Life
Department of Material Sciences

# Thesis

Presented to obtain the degree of

## Doctorate of Sciences

Speciality: Physics of Materials

# *Study of the type inversion of the semiconductor in irradiated solar cells*

***(Etude de l'inversion du type du semi-conducteur dans les cellules solaires irradiées)***

Presented by:
**Abdelghani HAMACHE**

**To the jury composed by:**

| Full Name | Title | Quality | University |
|---|---|---|---|
| Amjad MEFTAH | Pr | President | Biskra |
| Nouredine SENGOUGA | Pr | Supervisor | Biskra |
| Lakhdar DEHIMI | Pr | Examiner | Batna |
| Lakhdar NACEREDDINE | M.C.A | Examiner | Eloued |

**Academic year: 2017/2018**

**ملخص:**

تتعرض الخلايا الشمسية المستخدمة في التطبيقات الفضائية لجسيمات ذات طاقة عالية مثل البروتونات والإلكترونات. هذه الجسيمات تؤدي إلى تدهور شديد في أداء الخلايا الشمسية. عادة ما يُعزى هذا التدهور إلى العيوب البنيوية في المنطقة النشطة للخلية الشمسية. من بين الظواهر التي لوحظت في خلايا السيليكون المعرضة لإشعاع الإلكترونات ذات الطاقة 1 MeV السلوك الشاذ للتيار الكهربائي للدارة القصيرة (Jsc). ينخفض Jsc في البداية ثم يتزايد من أجل تدفق معين ثم يعود للتناقص مرة أخرى مع زيادة تدفق الإلكترونات. يُعزى هذا السلوك عادة إلى انعكاس نوع نصف الناقل في المنطقة النشطة للخلية الشمسية. من أجل توضيح هذا السلوك، تم تنفيذ محاكاة رقمية باستخدام برنامج SCAPS. تم حساب الخصائص تيار- جهد (J-V) لبنية $n^+$-p-$p^+$ من السيليكون (Si) من أجل الطيف AM0 مع تدفق للإلكترونات ذات الطاقة 1 MeV كعامل متغير. تتم محاكاة تأثير الإشعاعات على الخلية الشمسية من خلال مجموعة من العيوب ذات مستويات طاقة تتموقع عميقا في النطاق الممنوع من عصابة الطاقة للسيليكون. على الرغم من وجود عدة أنواع من المستويات العميقة التي يسببها الإشعاع بما في ذلك العيوب العميقة المانحة و العيوب العميقة الآخذة ومراكز التوليد-الاتحاد فقد تبين أن العيب المانح الأقل عمقا هو المسؤول عن هذه الظاهرة. من جهة أخرى وجد أن هذه الظاهرة ليست مرتبطة بانعكاس نوع الخلية الشمسية وإنما باتساع جانبي لمنطقة شحنة الفضاء. كما وجد أيضًا أن الخلايا الشمسية ذات السمك الأصغر تتمتع بمقاومة أفضل للإشعاعات.

**الكلمات المفتاحية:** الخلايا الشمسية، السيليكون ، اشعاع، تيار الدارة القصيرة ، انعكاس النوع، محاكاة رقمية، برنامج سكابس.

**Abstract:**

Solar cells, used for space applications, are exposed to energetic particles such as protons and electrons. These energetic particles induce severe degradation on the performance of solar cells. This degradation is usually attributed to lattice damage in the active region of the solar cell. One of the phenomena observed in Silicon solar cells exposed to 1 MeV electron irradiation is the anomalous degradation of the short circuit current (Jsc). It initially decreases followed by a recovery before falling again with increasing electron fluence. This behaviour is usually attributed to type inversion of the semiconductor in the solar cell active region. In order to elucidate this behaviour, a numerical simulation using SCAPS software is carried out. The current-voltage (J-V) characteristics of a Si $n^+$-p-$p^+$ structure are calculated under AM0 spectrum with the fluence of 1 MeV electrons as a variable parameter. The effect of irradiation on the solar cell is simulated by a set of defects of which the energy levels lie deep in energy gap of Silicon. Although several types of deep levels are induced by irradiation including deep donors, deep acceptors, and generation-recombination centres. It was found that the shallower donor trap is responsible for this behaviour and this not related to type inversion but to a lateral widening of the space charge region. It is also found that solar cells with smaller thickness have better radiation tolerance.

**Keywords:** Solar cells, Silicon, Irradiation, short circuit current, Type inversion, Numerical simulation, SCAPS.

**Résumé :**

Les cellules solaires utilisées pour les applications spatiales, sont exposées à des particules énergétiques telles que les protons et les électrons. Ces particules énergétiques induisent une dégradation importante dans les performances des cellules solaires. Cette dégradation est généralement attribuée aux dommages du réseau dans la région active de la cellule solaire. L'un des phénomènes observés dans les cellules solaires au Silicium, exposées à une irradiation des électrons de 1 MeV, est la dégradation anormale du courant de court-circuit (Jsc). Ce dernier diminue dans un premier temps, puis il croît pour une certaine fluence. Ensuite, il décroît de nouveau avec l'augmentation de la fluence des électrons. Ce comportement est généralement attribué à l'inversion de type du semi-conducteur dans la région active de la cellule solaire. Afin d'élucider ce comportement, une simulation numérique utilisant le logiciel SCAPS est réalisée. Les caractéristiques courant-tension (J-V) d'une structure Si $n^+$-p-$p^+$ sont calculées sous un spectre AM0 avec une fluence des électrons 1 MeV comme paramètre variable. L'effet de l'irradiation sur la cellule solaire est simulé par un ensemble de défauts dont les niveaux d'énergie se trouvent profondément dans le gap d'énergie du Silicium. Bien que plusieurs types de niveaux profonds soient induits par l'irradiation, y compris les donneurs profonds, les accepteurs profonds et les centres de génération-recombinaison, il a été constaté que le piège donneur le moins profond est responsable de ce comportement. Néanmoins ceci n'est pas lié à l'inversion de type mais à un élargissement latéral de la région de charge d'espace. Il est constaté également que les cellules solaires de plus faible épaisseur ont une meilleure résistance aux irradiations.

**Mots clés** : Cellules solaires, Silicium, Irradiation, Courant de court-circuit, Inversion de type, Simulation numérique, SCAPS.

# Acknowledgements

**First and foremost, I would like to thank Allah the almighty, who has allowed me to accomplish this work with his mercy.**

I would like to express my sincere gratitude and thanks to my supervisor Pr.Nouredine Sengouga for his guidance, support, patience, and immense knowledge.

My gratitude also goes to the members of the jury who accepted to examine and evaluate my work. I would like to thank Pr. Amjad Meftah (University of Biskra) for her acceptance to be president of the jury. I would like also to thank Pr.Lakhdar Dehimi (University of Batna), and Dr.Lakhdar Nacereddine (University of Eloued) who honoured me by their acceptance to examine my thesis.

My deepest gratitude goes also to my parents, my wife, and my sister for their extraordinary support and constant encouragement.

Finally, i would like to sincerely thank all of the people who directly or indirectly contributed to complete this thesis.

# Dedication

To my dear parents

To my dearest wife and my beloved kids: Meriem, Oussama and Loudjaine

To my sister

To my brothers

To all my family

## *Table of contents*

# List of Figures

# List of Tables

# Introduction

**S**emiconducting materials and semiconductor devices play a fundamental role in modern technology. Semiconductor devices are not only essential parts of systems, such as computers, biomedical equipment, solar cells, which are important in our daily life, but also from the basis for development of novel technology through their operational principles.

The first semiconductor device (a germanium transistor) has been built in 1947 by Bardeen, Brattain and Shockley, who have been awarded the Nobel Prize in 1956 **[1]**. In the following decades, a lot of different devices for special applications have been invented such as, semiconductor lasers, solar cells, light-emitting diodes (LED), metal-oxide semiconductor (MOS) transistors…

A very important fact of the success of the semiconductor technology is that the device length is much smaller than that of previous electronic devices (like tube transistors). The first transistor of Bardeen, Brattain and Shockley had a characteristic length (the emitter collector length) of 20 μm, compared to the size of a few centimeters of a tube transistor. The first Intel processor 4004, built in 1971, consisted of 2250 transistors, each of them with a characteristic length of 10 μm. This length has been reduced to 90 nm for the transistors in the Pentium 4 processor (put on the market in June 2004) **[1]**.

One of the important applications of semiconductors is solar cells. Solar cells convert sunlight directly into electricity using the photovoltaic effect. They are a promising technology for satisfying current and future energy demands in a sustainable and environmentally friendly way. The first commercial use of solar cells was in space applications for powering satellites in the late 1950's **[2]**.

Solar cells have been used on satellites since 1958 when the satellite Vanguard I used a less-than-one watt arrangement to power its radios **[2-4]**. Following this mission, the satellites Explorer III, Vanguard II, and Sputnik 3 were launched, also powered by photovoltaic-powered solar cell arrangements. Although these feats were not completely effective in utilizing the impure Silicon-based solar cell, they opened the door to using solar energy to power satellites. By the 1960s, solar energy became the accepted energy source for many space-associated missions **[3]**.

Solar cells are now widely used to power missions in space because they convert abundant light energy in space into electricity. As the importance of solar cells in space technology increases, there is a need to enhance their reliability and efficiency.

Materials that can be used to powering satellites and space vehicles have to withstand harsh conditions that include high temperature, space dust and energetic particles. Solar cells of compound semiconductors such as gallium arsenide (GaAs) have demonstrated higher conversion efficiencies and radiation-resistance than Silicon solar cells but have much higher prices and nowadays the space solar cell market is still dominated by crystalline Silicon solar cells because they have a better cost effectiveness and reliability as a space power source **[5-7]**.

The effects of high-energy particle irradiation on materials and devices, used in space, are among the principal reasons for spacecraft operation failure and lifetime reduction. The study of radiation damage in semiconductor devices and solar cells has been an important subject of research. High-energy particle induced defects, causing a permanent deterioration of the electrical characteristics of the semiconductor material, are one of the primary reasons for the failure of the crystalline Silicon space solar cells **[4]**. Main sources of radiation affecting solar cells are protons and electrons trapped by the terrestrial magnetic field and protons coming from the Sun, the particle flux depending on the orbit of the mission **[4]**. However, in some particular orbits or during a space-wind storm the radiation levels may be much higher **[8]**. These space-wind storms can last up to a few days and may lead to a significant efficiency decrease of solar cells on satellites. For example, on July 14, 2000, the efficiency of solar cells on the solar heliospheric observatory satellite dropped from 14% to 12% **[8]**.

A lot of works have been done on defects introduced by radiation in materials used for space solar cells in the last few decades, such as Silicon (Si) and gallium arsenide (GaAs) **[7-9]**. According to traditional point of view, the increase of density of high energy particles results in an increase of deep defects density, which causes decrease in the output parameters of the solar cell ( the short circuit current, the open circuit voltage, the maximum output power, the fill factor and the conversion efficiency). However, an accidental injection of satellite used Silicon solar cells passing through the Van Allen radiation belt, where the planetary magnetic field traps belts of high-energy protons and electrons shows an anomalous behaviour, which is the increase of the short circuit current and decrease in open-circuit voltage, followed by an abrupt decrease of the short circuit current and cell failure **[10]**. Yamaguchi et al **[9]** proposed a model to explain these

phenomena by expressing the change in carrier concentration of the base region of the cell, in addition to the decrease of the short circuit current by minority carrier lifetime (diffusion length) reduction with radiation.

Another model proposed by Karashanov **[11]** explain the anomalous behaviour of the short circuit current by the conversion of conductivity type and the increase of minority lifetime with respect to that of majority carriers when he choose only defects whose energy level is close to the middle of the band gap.

In these models several simplifications were made. In particular, the defects created by irradiation are assumed to act as one effective deep level. In reality and as it is well known, irradiation creates several defects of different types.

The aim of the work presented in this thesis is to develop a model to explain the anomalous behaviour observed in Silicon solar cells and which of the defects introduced by electron radiation is responsible for this behaviour. For this aim we have studied numerically the effect of the most commonly defects observed in Silicon solar cells irradiated by electrons considering their parameter as given by the literature **[7, 12]**.

This thesis is divided into five chapters in addition to an introduction and a conclusion. The problematic of the present work is presented in the introduction.

In the first chapter the device physics of solar cells is presented. The main materials used in the manufacture of solar cells are also presented.

In chapter II, different types of defects in semiconductors are discussed. The theory of deep level defects is also presented.

Chapter III is devoted to the description of the space radiation environment and its impact on solar cells.

Chapter IV consists of two main parts: in the first part the mathematical model used to the modelling of semiconductor devices such as solar cells is presented. In the second part, a description of the solar cell capacitance simulator (SCAPS) that is used in this work is also presented.

The last chapter describes the results achieved in this work in addition to their discussion and interpretation. The thesis concludes with a general conclusion in which the obtained results are summarized.

# Chapter I

# Physics of solar cells

## I.1. Introduction:

Solar cells convert sunlight into electrical energy. In the near future, this technology may well occupy an increasingly prominent role in global electricity generation in order to limit environmental pollution.

This chapter gives the basic concepts to understand the solar cells physics. In the first section, we give a brief history of the solar cells. Next, we explain the principle of the photovoltaic effect, and the principle function of the p-n junction which is the basic component of a solar cell, followed by their main parameters. Then we present the most important materials in the technology of the solar cells. In the last section we review the most important materials used in the manufacture of space solar cells.

## I.2. History of the solar cell:

The photovoltaic solar cells are materials able to convert directly the light into electricity, this conversion, called the photovoltaic effect. The photovoltaic effect was first reported by Edmund Becquerel in 1839 when he observed that the action of light on a Silver coated Platinum electrode immerged in electrolyte produced an electric current **[13, 14]** (Figure I.1).

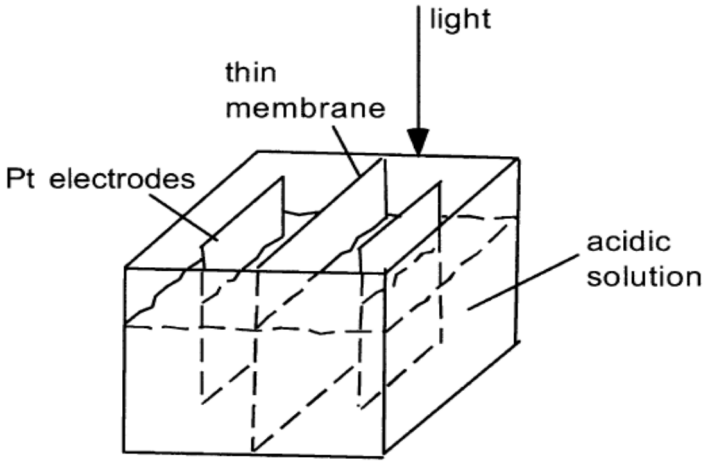


**Figure I.1: Diagram of apparatus described by Becquerel [13].**

Later in 1876, W. G. Adam, W. Smith, and R. E. Day found that a photocurrent could be produced in a sample of Selenium when contacted by two heated Platinum contacts **[14, 15]** (Figure I.2).

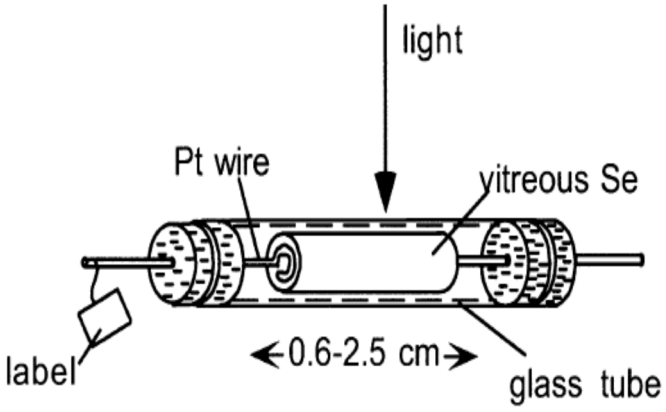


**Figure I.2: Sample geometry used by Adams and Day for the investigation of the photovoltaic effect in Selenium [13].**

A few years later (in 1883) an American named C. E. Fritts placed a sheet of amorphous Selenium on a metal backing and covered the Selenium with a transparent gold leaf film.
He reported that this selenium array produced a current "that is continuous, constant, and of considerable force with exposure to sunlight." At the time, there was no quantum theory and there was considerable skepticism about his claim of converting sunlight into electricity **[15]**.
Around 75 years passed while quantum mechanics was discovered, the importance of single-crystal semiconductors was recognized, and p-n junction behaviour was explained. By 1954, the first Silicon solar cell was reported by Chapin et al, and converted sunlight with an efficiency of 6% **[14, 15]**. These Silicon solar cells were not seriously considered for power generation for several decades. Nevertheless, the early Silicon solar cell did introduce the possibility generation in remote locations where fuel could not easily be delivered. The obvious application was to satellites where the requirement of reliability and low weight made the cost of the cells unimportant and during the 1950s and 60s, Silicon solar cells were widely developed for applications in space.
Also in 1954, a Cadmium Sulfide p-n junction was produced with an efficiency of 6% **[14]**, and in the following years studies of p-n junction photovoltaic devices in Gallium Arsenide (GaAs), Indium Phosphide (InP) and Cadmium Telluride (CdTe) were stimulated by theoretical work indicating that these materials would offer a high efficiency. However, Silicon remained and remains the foremost photovoltaic material, benefiting from the

advances of Silicon technology for the microelectronic industry **[15]**. One new feature, introduced in 1974, was the use of crystallographic texturing on the top surface, to reduce reflection loss (Figure I.3). The efficiency of Silicon cells has been improved to about 24% in the early 2000s, very close to the theoretical limit of 28% **[16]**.

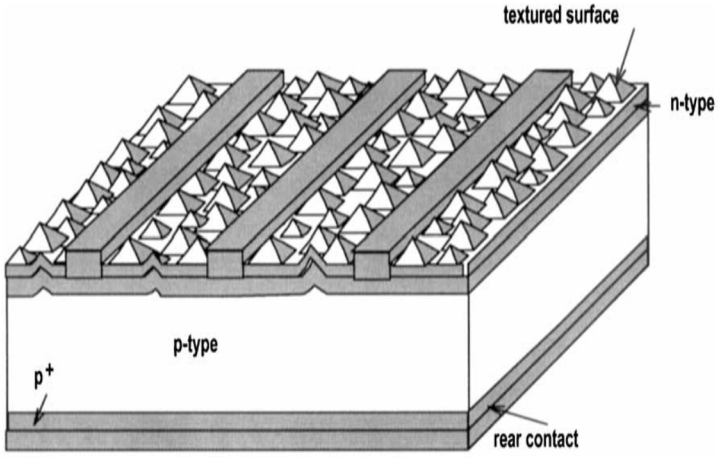


**Figure I.3: Standard Silicon solar cell structure developed in the 1970s [13].**

Another significant development in the III–V compound semiconductor area was the use of heterojunctions formed from different III–V compounds or their alloys to produce the rectifying junction. This, along with the other attributes of III–V technology that facilitate 'band-gap engineering', has resulted in the most sophisticated photovoltaic devices to date. These are double and triple-junction devices that allow the monolithic stacking of multiple cells on top of one another, so each efficiently converts a relatively narrow range of photon energies suited to its band gap (Figure I.4).

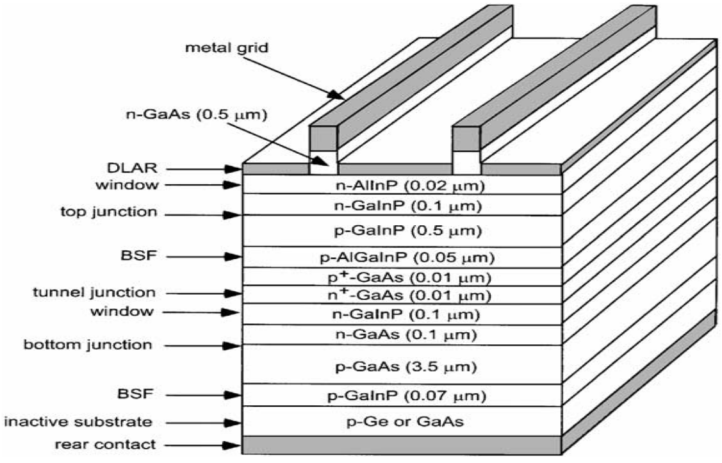


**Figure I.4: Monolithic tandem space cell using two stacked p-n junctions connected by a tunneling junction [13].**

Recent developments that considerably broaden the base of photovoltaic from mainstream homo or hetero-junction semiconductor approaches include dye-sensitized nanocrystalline semiconductors and organic solar cells **[17, 18]**.

## I.3. The physics of photovoltaics:

### I.3.1. The photovoltaic effect:

The origin of the word "photovoltaic" is made up from the Greek word phos (light), and voltaic (electrical) from the name of Italian physicist Alessandro Volta. The physical basis for photovoltaic is the "photovoltaic effect". An appropriate definition of the photovoltaic effect is the transformation of solar energy into electrical energy.

The device that is designed to generate an electrical current when it is illuminated is usually known as solar cell. To date, most solar cells are made of semiconductors (roughly 90% of the market share). Especially, Silicon solar cells (more than 80% of the solar cell market) **[16, 19]**.

The photovoltaic effect is the basic physical process through which a solar cell converts sunlight into electricity. Sunlight is composed of photons (like energy accumulations), or particles of solar energy. These photons contain various amounts of energy corresponding to the different wavelengths of the solar spectrum. When photons hit a PV cell, they may be reflected or absorbed. Only the absorbed photons generate electricity. When this happens, the energy of the photon is transferred to an electron in an atom of the cell (usually Silicon atoms). The electron is able to escape for its normal position associated in the atom to become part of the current in an electrical circuit **[20]**.

### I.3.2. Solar radiation spectrum:

The development, the optimization and the characterization of photovoltaic cells imply certain knowledge of the source of energy used: the sun. This one is our main source of energy; it is essentially a sphere of gas heated by a nuclear fusion at its centre (hydrogen-helium fusion reaction), its diameter is about of 1.39 million Km. The mass of the sun is about $2.9 \times 10^{30}$ Kg, it accounts for about 99.86 % of the total mass of the solar system. The mean distance between the sun and the earth is 149.6 million km and is known as the astronomical unit (AU).

The spectral distribution of the radiation emitted from the sun is determined by the temperature of the surface (photosphere) of the sun which is about 6000 K. The

wavelength distribution of the sunlight (power per unit area and per unit wavelength) follows approximately the radiation distribution of a black body at this temperature as shown in Figure I.5.

The total energy per unit area integrated over the entire spectrum and measured outside the atmosphere perpendicular to the direction of the sun is essentially constant. This radiation power is referred to as the solar constant or air mass zero (AM0) radiation. Measurements taken at high altitudes have yielded the currently accepted average value of 1353W/m$^2$ **[21, 22]**.

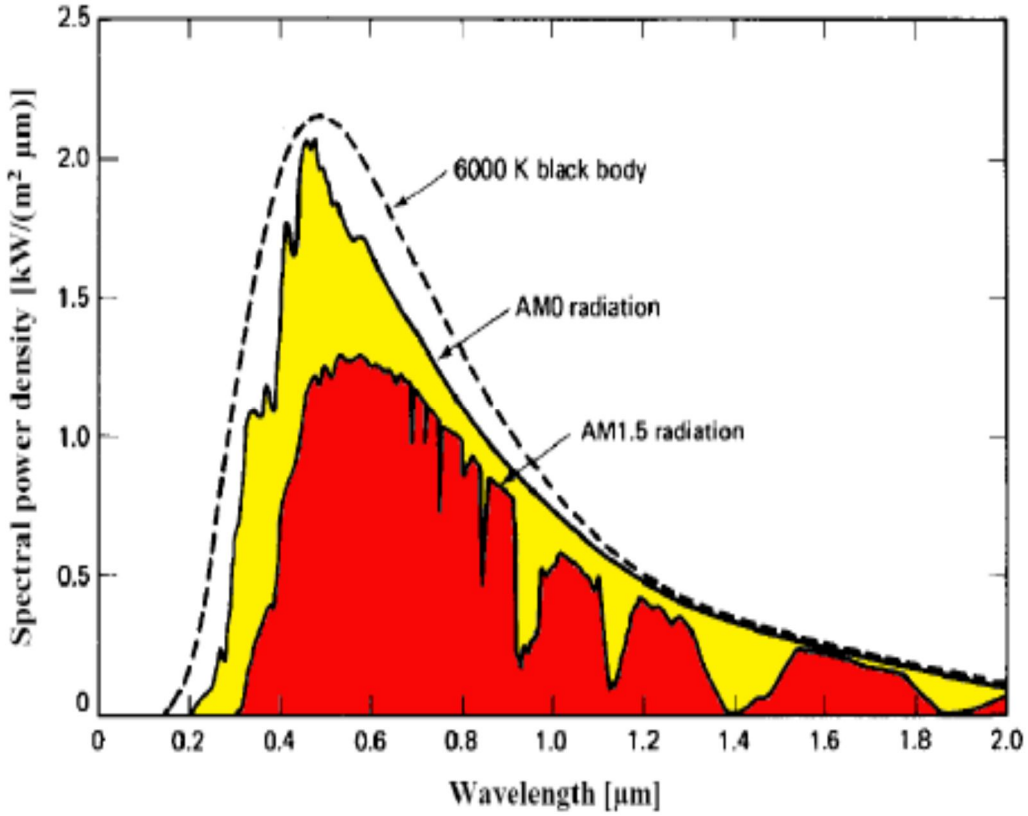


**Figure I.5: Spectral power density of sunlight showing AM0 (extraterrestrial radiation), AM1.5 (terrestrial) and the black body radiation at 6000 K [23].**

When the solar radiation passes through the earth's atmosphere, the spectral distribution is attenuated and changed as a result of absorption and scattering phenomena in the gas, water and dust. Atmospheric absorption is commonly caused by ozone ($O_3$), oxygen ($O_2$), nitrogen ($N_2$),carbon dioxide ($CO_2$), carbon oxide (CO) and water vapour ($H_2O$) while scattering is mostly caused by aerosols, air molecules (Rayleigh scattering), dust and water droplets (Figure I.6) **[24]**.

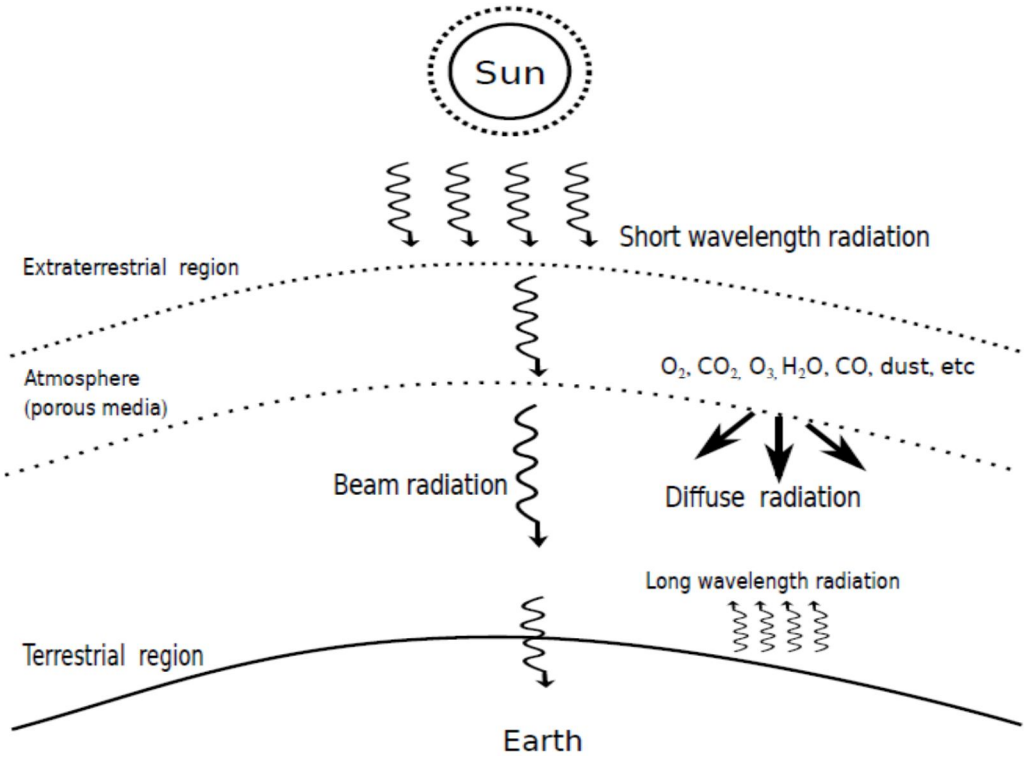


**Figure I.6: Terrestrial, extra-terrestrial regions and atmospheric effects [24].**

The degree to which the atmosphere affects the sunlight received at the earth's surface is quantified by the air mass. The secant of the angle between the sun and the zenith is defined as the air mass (AM) number and it measures the atmospheric path length relative to the minimum path length when the sun is directly overhead.

The Air Mass number is given by:

$$Air\ Mass = \frac{1}{\cos\theta} \qquad \text{I.1}$$

$\theta$ is the angle of incidence ($\theta = 0$ when the sun is directly overhead). The Air Mass number is always greater than or equal to one at the earth's surface.

The AM1spectrum represents the sunlight at the earth's surface when the sun is at zenith, and the incident power is about 925 W/m$^2$.

The most widely used terrestrial standard is the AM1.5 spectral distribution (for $\theta = 48.2°$), while the AM0 spectrum is the relevant one for satellite and space-vehicle applications (see Figure I.5).

### I.3.3. Photon-semiconductor interaction:

Physics of photovoltaics is based on the optical and electrical properties of semiconductors. A semiconductor is generally characterised by a bandgap energy $E_g$, the energy needed to create an electron-hole (e-h) pair.

The sunlight consists of photons that each has a different energy and wavelength. The relationship between photon energy ($E$) in electron Volts and the wavelength (λ) of the incident light in micrometers is given as:

$$E(eV) = \frac{1.24}{\lambda(\mu m)} \qquad \text{I.2}$$

Depending on the relation between energy and the semiconductors bandgap three things can happen as shown in Figure I.7.

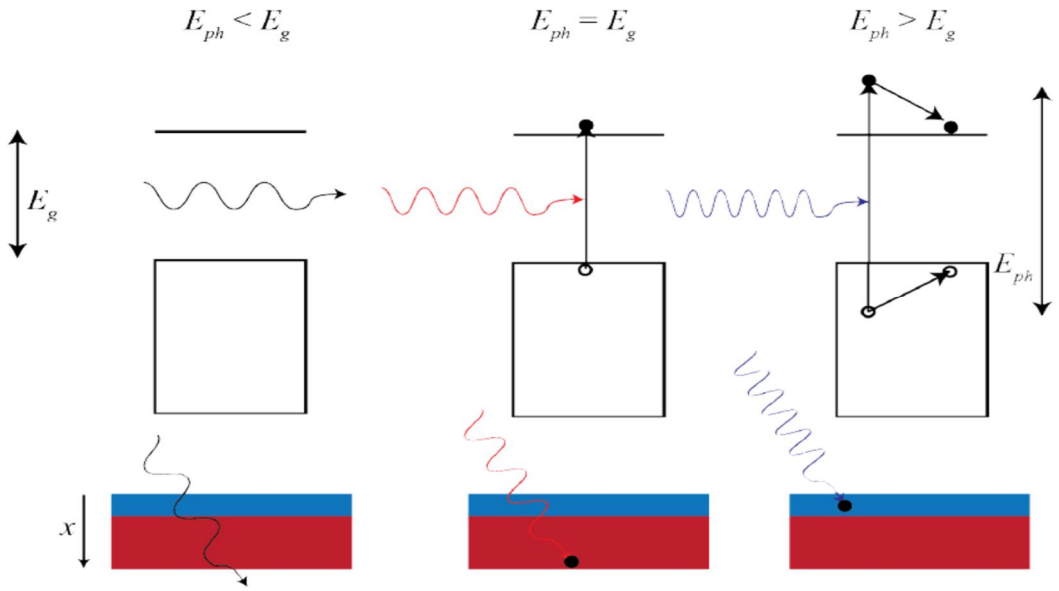


**Figure I.7: Photon Transition in a Semiconductor [25].**

When a photon with energy larger than the bandgap of the semiconductor ($E_{ph}$>$E_g$) is absorbed, an electron-hole pair is created. This means that an electron is stimulated from the valence band ($E_v$) to the conduction band ($E_c$) leaving a hole behind. This pair needs to be separated then by electric field in order to avoid recombination: this field is provided by a p-n junction (see section I.4) which is the core of a photovoltaic device. A photon hitting on the surface of a semiconductor could be either reflected from the surface, absorbed in the material or transmitted throughout the material itself. In the case of PV devices, photons which are not absorbed (thus reflected or transmitted) are typically considered as a loss since they do not generate power. Considering the energy of the photon and the

bandgap of the semiconductor it is possible to establish if a photon is absorbed or transmitted:

-If ($E_{ph}<E_g$): The photons pass through the semiconductor without being absorbed (transmitted).

- If ($E_{ph}= E_g$): In this case the photons are absorbed (they have just enough energy to create an electron-hole pair).

- If ($E_{ph}>E_g$): Photons with energy higher than the band gap are also absorbed. However, for PV applications, part of the energy of these photons is released since electrons quickly thermalize down to the $E_c$ lower energy states.

## I.4. The P-N junction:

Understanding the fundamentals of the p-n junction is important to understanding how a solar cell works because the principles that allow solar cells to work are based on these basic concepts.

The most predominant semiconductor material currently used in solar cells is Silicon. It is abundant, and its material properties have been extensively studied. Silicon (Si) is a group IV element which alludes to the four valence electrons of an isolated Si atom has in its outer shell. When in the vicinity of other Si atoms these valence electrons are shared to form covalent bonds between atoms in order to fill the atoms outer shells. These bonds allow for the formation of orderly crystal structures.

If a Silicon atom is replaced with another type of atom, such as a group III material (Boron atom for example) that only has three valence electrons, there will be a Silicon atom that does not have four electrons it can share. The vacancy results in a hole that easily accepts a free electron. If more Silicon atoms are replaced, there will be more holes. The resulting material is called p-type (Figure I.8-b). If the Silicon atom was instead replaced with a group V material (Arsenide atom for example) that has five electrons in its outermost shell, there is instead an extra electron. Since this electron is not tightly bound, it is free to move throughout the material, making it n-type (Figure I.8-a).

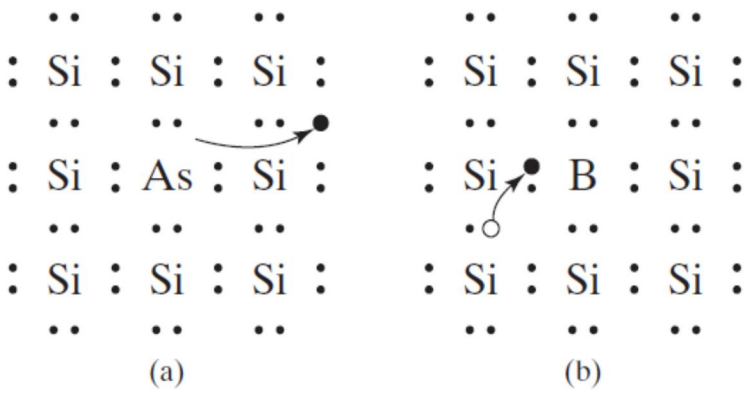


**Figure I.8: *n*-type material (a) and *p*-type material (b); created by replacing a Silicon atom with Arsenide atom and Bore atom respectively.**

In a doped semiconductor the more abundant carriers are named "majority carriers", while the less abundant carriers are named "minority carriers". Majority carriers are electrons (holes) in n-type semiconductors (p-type semiconductors). Minority carriers are electrons (holes) in p-type semiconductors (n-type semiconductors). At equilibrium, the product of the majority and minority carrier concentration is a constant:

$$n_i^2 = n_0 p_0 \qquad \text{I.3}$$

Where $n_i$ is the intrinsic carrier concentration, $n_0$ and $p_0$ are the electron and hole equilibrium carrier concentrations respectively.

A p-n junction is a semiconductor junction where a p-doped region is in contact with a n-doped region as seen in Figure I.9. Where an n-type semiconductor comes into contact with a p-type semiconductor, a p-n junction is formed. In p-n junctions the p-side and n-side can be made from different semiconductors, which are called heterojunctions, or the p-side and n-side can be differently doped regions of the same material, which is called homojunctions **[25]**. Once the two semiconductors are in contact, electrons from the n-region near the junction interface diffuse in the p-region leaving donor atoms electrically unshielded by the majority carriers. In the same way, holes from the p-region near the interface diffuse in the n-region, leaving acceptors unshielded behind. This phenomenon is called "diffusion". The region nearby the p-n interface, common at the two semiconductors, which lost its neutrality and become actively charged, is called the "space charge region" (SCR). The rest of the two semiconductors which is not influenced by the metallurgical junction is called "quasi neutral region" (QNR). The consequence of the formation of the SCR is an electric field $\vec{E}$ which fights the diffusion for both electrons and holes. $\vec{E}$ will superimpose on the random movement of carriers accelerating holes in

the same direction of the field and electron in the opposite. This phenomenon is called "drift". When an equilibrium condition is reached, a potential difference ($V_D$) is formed across the p-n junction. A schematic of the p-n junction is shown in Figure I.9 **[26]**.

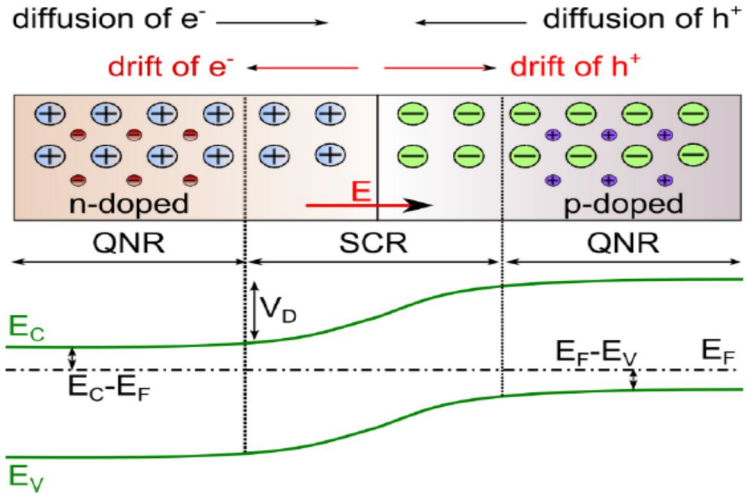


**Figure I.9: p-n junction in thermal equilibrium with zero-bias voltage applied [26].**

### I.4.1. Current voltage characteristics of a diode:

The diode is a p-n junction connected to two contacts. The diode current density in the dark (no illumination) can be written by the following equation:

$$J_{Diode}(V) = J_0[exp\left(\frac{qV}{K_BT}\right) - 1] \qquad \text{I.4}$$

$J_0$ is the dark saturation current density, which depends on the type, the doping density and quality of the p-n junction. $q$ is the elementary charge, $V$ is the voltage, $K_B$ is the Boltzmann constant ($1.38x10^{-23}$ J/K), $T$ is the absolute temperature (Kelvin).

$$J_0 = q\left(\frac{D_n n_i^2}{L_n N_A} + \frac{D_p n_i^2}{L_p N_D}\right) \qquad \text{I.5}$$

$N_{A,D}$ the acceptor and the donor concentration in the p-type and n-type material, respectively. $D_{n,p}$ are the diffusion coefficients, and $L_{n,p}$ are the diffusion lengths of electrons and holes. Equation (I.4) is usually called the Shockley equation or the ideal diode equation. In the current form the equation (I.4) behaves:

$$I_{Diode}(V) = I_0[exp\left(\frac{qV}{K_BT}\right) - 1] \qquad \text{I.6}$$

Thus, the p-n junction has an exponential current-voltage characteristic as shown in Figure I.10. $I_0$ is the saturation current.

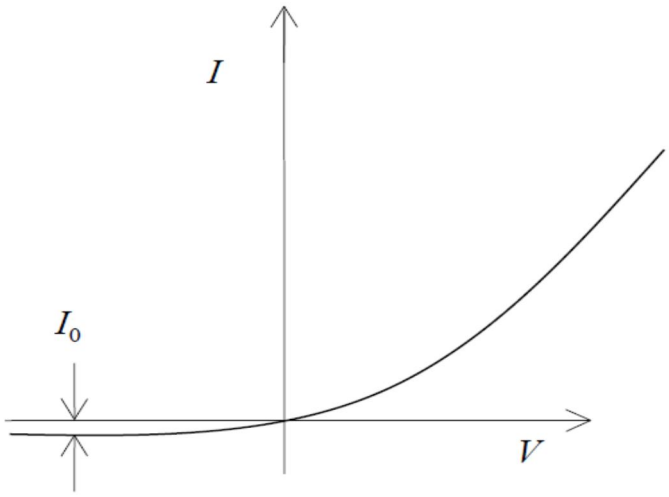


**Figure I.10: I-V characteristics of a diode.**

In practice, the diode equation is usually modified by addition of an empirical ideality factor, n, as follows:

$$J_{Diode}(V) = J_0[exp\left(\frac{qV}{nK_BT}\right) - 1] \qquad \text{I.7}$$

The ideality factor tells us how close the junction's behaviour to an ideal diode ($n$ = 1). Physically, the ideality factor is related to geometry of the junction and distribution of electron-hole recombination with respect to the associated depletion region. Also, for any junction that approximates an infinite planar junction, recombination is generally negligible in the depletion region and, consequently, ($n \approx 1$). Conversely, if geometry is non-ideal and recombination in the depletion region dominates then ($n \approx 2$).

### I.4.2. Current voltage characteristics of the solar cell:

#### I.4.2.1. Ideal solar cell:

When the p-n junction is illuminated electron-hole pairs are created by the photons giving rise to the so-called photogenerated ($J_L$) current which could be modelled as a current generator in parallel to the diode as shown in Figure I.11.

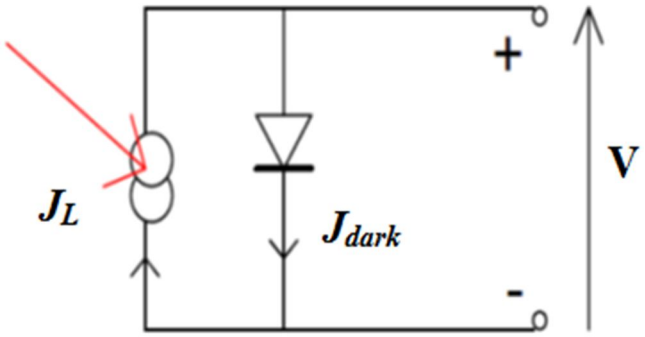


**Figure I.11: Equivalent circuit of ideal solar cell.**

If the carriers are created inside the SCR, or within a diffusion length (the average distance a carrier can travel from the point where it is created until it recombines) so they are able to diffuse into it, they are separated by the built-in electric field across the SCR. If electron-hole pairs are created away from the SCR the minority carriers will recombine before they can be caught. If the carriers reach all the way to the external load, they deliver a current **[25, 26]**. Figure I.12 shows the light and the dark J-V characteristics of the solar cell for an ideal case.

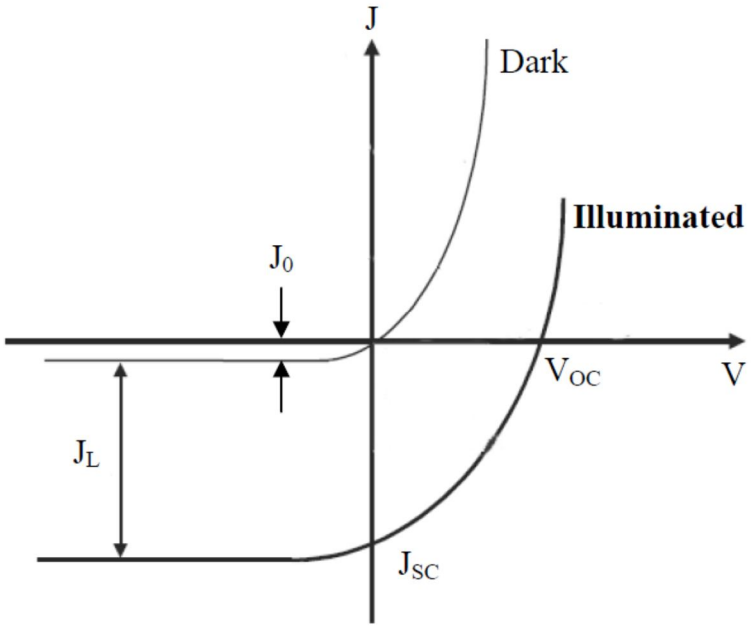


**Figure I.12: I-V characteristic of a solar cell in the dark and under illumination [27].**

Equation I.7 (diode law) needs to be modified by adding the photogenerated current, so the output current becomes:

$$J(V) = J_0 \left[ exp\left(\frac{qV}{nK_BT}\right) - 1 \right] - J_L \qquad \text{I.8}$$

Note that the photocurrent current is negative because the direction of current flow is, by definition, in the direction opposite to the flow of electrons. Conventionally however, the photocurrent in solar cells is written as a positive current and equation I.8 is also often written in terms of a current density, $J$ (A/cm$^2$):

$$J(V) = J_L - J_0 \left[ exp\left(\frac{qV}{nK_BT}\right) - 1 \right] \qquad \text{I.9}$$

### I.4.2.2. Real solar cell:

In reality, solar cells have a parasitic series ($R_s$) and shunt resistance ($R_{sh}$) associated with them, as shown in Figure I.13

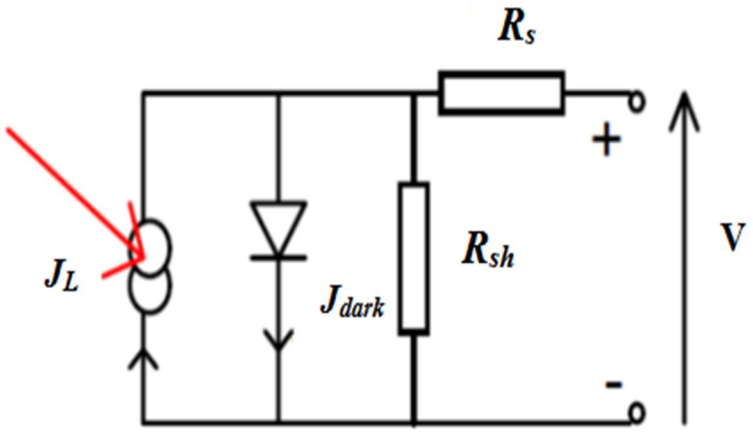


**Figure I.13: Solar cell model including parasitic resistances.**

In the presence of both series and shunt resistances, the J-V curve of a solar cell is given by:

$$J = J_0 \left[ exp\left(\frac{(qV - JR_S)}{nK_BT}\right) - 1 \right] - J_L + \frac{V - JR_S}{R_{sh}} \qquad \text{I.10}$$

The series resistance is a result of the material's resistance to current flow. The most important contributors to the series resistance ($R_s$) are the bulk resistance of the semiconductor material, the metallic contacts and interconnections, carrier transport through the top diffused layer, and contact resistance between the metallic contacts and the semiconductor **[28]**. The effect of series resistance on the current–voltage characteristic of a solar cell is shown in Figure I.14.

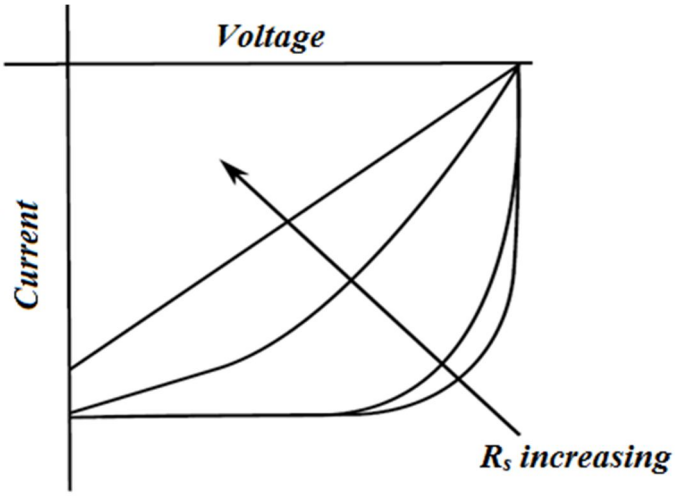


**Figure I.14: The effect of increasing series resistance on the J-V curve ($R_{sh}$=0).**

The shunt resistance could be due from leakage of current through the cell, around the edges of the cell and between contacts of different polarity. The effect of shunt resistance on the current-voltage characteristic of a solar cell is shown in Figure I.15.

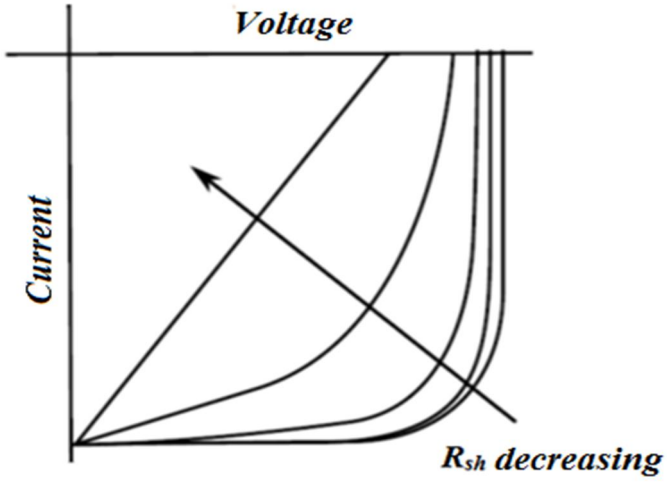


**Figure I.15: The effect of increasing shunt resistance on the J-V curve.**

Series and shunt resistances reduce the fill factor as shown in Figures I.14 and I.15.
For an efficient cell we want $R_s$ to be as small and $R_{sh}$ to be as large as possible. Thus, low $R_s$ and high $R_{sh}$ are needed for the best performance.

## I.5. Solar cell parameters (Solar Cell Figures of Merit):

The main parameters that determine the quality of a solar cell (solar cell figures of merit) are the short circuit current $I_{sc}$, the open circuit voltage $V_{oc}$, the fill factor $FF$, and the efficiency $\eta$. These parameters are important to the full interpretation of the current-voltage characteristics of a solar cell. They can be extracted from the illuminated J-V curve (see Figure I.16).

### I.5.1. Short circuit current:

The short circuit current $I_{sc}$ is defined as the current through the solar cell when the terminals are in short circuit (i.e., the voltage across the solar cell is zero).
Considering the ideal case in which the effects of $R_s$ and $R_{sh}$ are neglected. When we put $V=0$ in equation I.9 we obtain: $J_L=J_{sc}$. This shows that the short-circuit current density is directly proportional to the incident light, and the current generated by light is generally independent of the voltage.

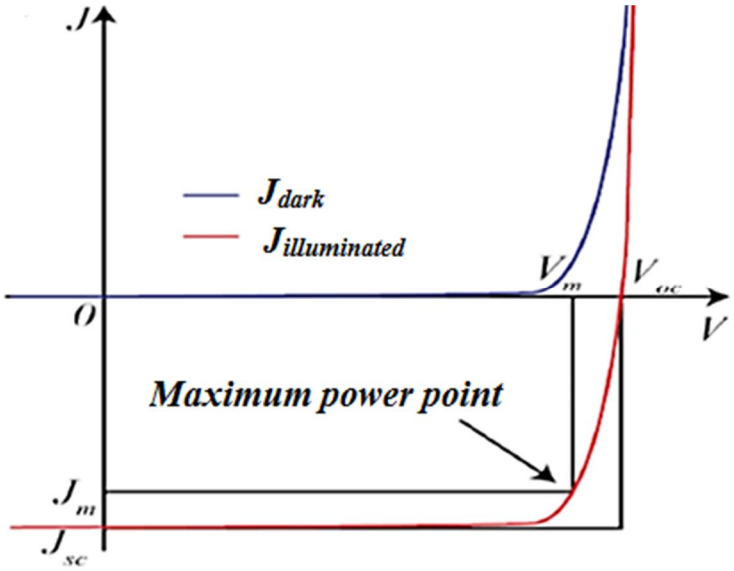


**Figure I.16: Typical J-V curve of a solar cell and its parameters.**

### I.5.2. Open circuit voltage:

Another figure of merit is the open circuit voltage $V_{oc}$, which is the maximum voltage that the cell can deliver when the current is zero.

The open circuit voltage is obtained by setting equation I.9 equal to zero and isolating $V$, therefore we find the ideal open circuit voltage:

$$V_{oc} = \frac{nK_BT}{q}\ln\left(\frac{J_L}{J_0} + 1\right) \qquad \text{I.11}$$

### I.5.3. Fill factor:

The fill factor of a solar cell $FF$ is the ratio between the rectangle drawn by the values of the current density ($J_m$) and voltage ($V_m$) of resulting in its maximum power point ($P_{max}=V_m \times J_m$), and the rectangle given by the product $V_{oc} \times J_{sc}$ (Figure I.16):

The fill factor of a solar cell FF is defined as:

$$FF = \frac{P_{max}}{V_{oc} \cdot J_{sc}} = \frac{V_m \cdot J_m}{V_{oc} \cdot J_{sc}} \qquad \text{I.12}$$

Where, $V_m$ and $J_m$ are voltage and current density at maximum power point respectively.

The fill factor is an indicator of the junction quality and the degree of $R_s$ present in the cell. An ideal solar cell has a $FF$ as closer as possible to 1. In fact the fill factor increases along with $V_m$ and $J_m$ approaching respectively $V_{oc}$ and $j_{sc}$. The typical value of the fill factor is between 0.8 and 0.9 **[16]**.

### I.5.4. Efficiency:

The efficiency of a solar cell ($\eta$) is the most important figure of merit. It is defined as the ratio of the generated maximum power ($P_m$) by the cell and the power of the incident light ($P_{in}$).

It is expressed mathematically as:

$$\eta = \frac{P_m}{P_{in}} = \frac{I_m.V_m}{P_{in}} = \frac{FF.I_{sc}.V_{oc}}{P_{in}} \qquad \text{I.13}$$

The efficiency of a solar cell can be improved by maximising $J_{sc}$, $V_{oc}$ and $FF$. These parameters should be defined under Standard Test Conditions (STM), which are AM 1.5 global spectrum for terrestrial applications, an incident power density of 1000W/m$^2$, and a temperature of 25°C **[29]**.

### I.5.5. Spectral response and Quantum efficiency:

The optical performance of a solar cell can be acquired by a measure of its spectral response (SR) that describes the sensitivity of the solar cell to optical radiation of different wavelengths. The spectral response is the ratio of the current generated by the solar cell to the power incident on the solar cell.

The spectral response is conceptually similar to the quantum efficiency (QE). The quantum efficiency is defined as the number of measured electrons divided by the number of photons, incident on the solar cell.

The quantum efficiency can be determined from the spectral response by replacing the power of the light at a particular wavelength with the photon flux for that wavelength. This gives **[30]**:

$$SR(\lambda) = \frac{q\lambda}{hc} QE(\lambda) = 0.0808.\lambda.QE(\lambda) \qquad \text{I.14}$$

It is possible to define two types of quantum efficiency, one is the internal quantum efficiency (IQE) and one is the external quantum efficiency (EQE). They are defined as follows:

External Quantum Efficiency (EQE) is the ratio of the number of charge carriers collected by the solar cell to the number of photons of a given energy shining on the solar cell from outside (incident photons).

Internal Quantum Efficiency (IQE) is the ratio of the number of charge carriers collected by the solar cell to the number of photons of a given energy that shine on the solar cell from outside and are absorbed by the cell.

The external quantum efficiency therefore depends on both the absorption of light and the collection of charges. The quantum efficiency for a Silicon solar cell is shown in Figure I.17.

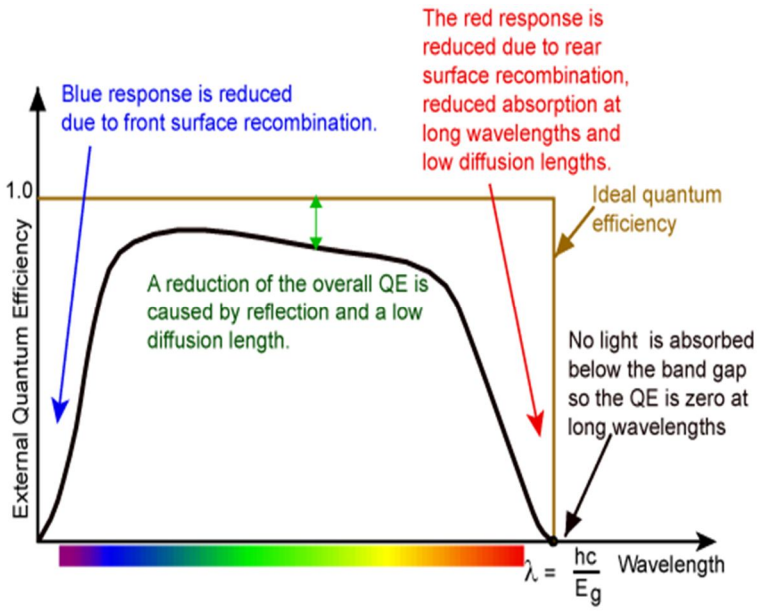


**Figure I.17: The quantum efficiency of a Silicon solar cell [31].**

The ideal quantum efficiency graph has a rectangle shape, where the QE value is fairly constant across the entire spectrum of wavelengths measured. However, the QE for most solar cells is reduced because of the effects of recombination, where charge carriers are not able to move into an external circuit. The same mechanisms that affect the collection probability also affect the QE. For example, modifying the front surface can affect carriers generated near the surface. And because high-energy (blue) light is absorbed very close to the surface, considerable recombination at the front surface will affect the "blue" portion of the QE. Similarly, lower energy (green) light is absorbed in the bulk of a solar cell, and a low diffusion length will affect the collection probability from the solar cell bulk, reducing the QE in the green portion of the spectrum.

## I.6. Solar cell structure:

The semiconductor layers are the most important parts of a solar cell; they form the heart of the solar cell. There are a number of different semiconductor materials that are suitable for the conversion of energy of photons into electrical energy, each having advantages and disadvantages.

The crystalline Silicon (c-Si) solar cell, which dominates the PV market at present, has a simple structure, and provides a good example of a typical solar cell structure. Figure I.18 shows the essential features of c-Si solar cells. An absorber material is typically a moderately doped *p*-type square wafer having thickness around 300 µm and an area of (10 $\times$10 cm$^2$) or (12.5$\times$12.5) cm$^2$. On both sides of the c-Si wafer a highly doped layer is formed, $n^+$-type on the top side and $p^+$-type on the back side, respectively. These highly doped layers help to separate the photo-generated charge carriers from the bulk of the c-Si wafer. The trend in the photovoltaic industry is to reduce the thickness of wafers up to 250 µm and to increase the area to (20 $\times$ 20 cm$^2$) **[32, 33]**.

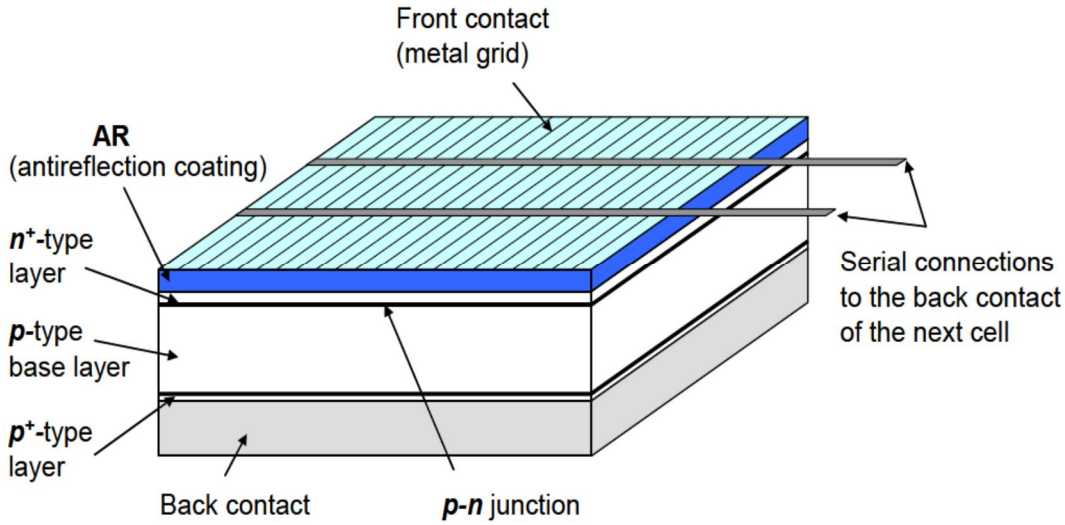


**Figure I.18: A typical structure of a c-Si solar cell [32].**

In addition to semiconductor layers, solar cells consist of a top and bottom metallic grid or another electrical contact that collects the separated charge carriers and connects the cell to a load. Usually, a thin layer that serves as an antireflective coating covers the top side of the cell in order to decrease the reflection of light from the cell. In order to protect the cell against the effects of outer environment during its operation, a glass sheet or other type of transparent encapsulant is attached to both sides of the cell. In case of thin-film solar cells, layers that constitute the cell are deposited on a substrate carrier. When the processing temperature during the deposition of the layers is low, a wide range of low-cost substrates such as glass sheet, metal or polymer foil can be used **[32, 33]**.

## I.7. Materials used for solar cells:

Since the first solar cell was built in 1883 out of Selenium and Gold (with an efficiency of 1%), the variety of technologies for converting solar radiation to electricity has significantly expanded and developed, to the point where efficiencies of 40% are now being achieved. Figure I.19 compares the best achievable efficiencies of different solar cells.

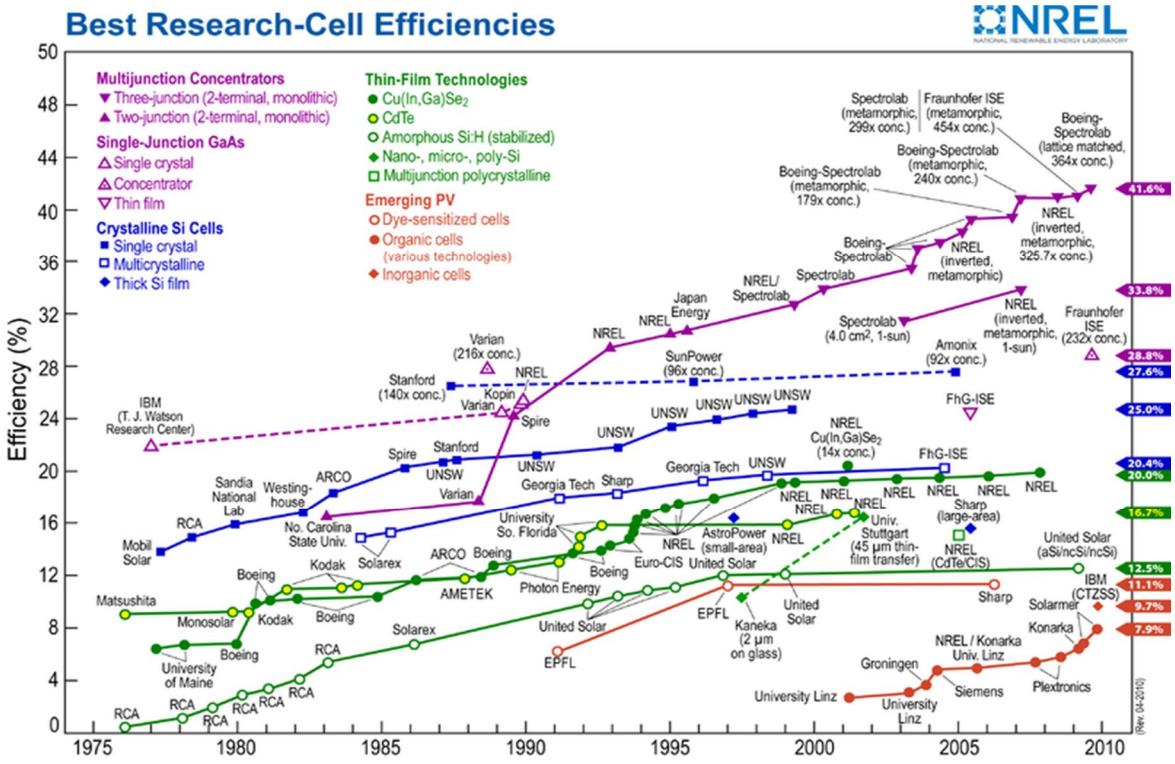


**Figure I.19: Schematic of best achievable efficiencies in different types of solar cells [34].**

The development and application of effective photovoltaic cells is hindered by two primary components: cost and efficiency. Solar cell technology is still largely dominated by cells based on the use of monocrystalline and multicrystalline Silicon, the former material produced using the Czochralski method and the latter material produced using a block casting method. These account for 38% and 46% of modules sold respectively **[24].**

There is a third type, amorphous Silicon, but the efficiency is lower than the previous types so it is less used. Gallium Arsenide (GaAs) is also very popular for solar cells. It is less friable than Silicon, more resistant to radiation damage, so it is preferred in space-based solar cells. Other new solar cells are made of Copper Indium Gallium (di) Selenide (CIGS) or Cadmium Telluride (CdTe). Much research and development effort is being made to develop new materials, but nowadays there are no commercial substitutes to these types of solar cells. In the next sections these different solar cells are more reviewed.

### I.7.1. Crystalline Silicon solar cells:

Silicon is the second most abundant material in the earth's crust; it constitutes about 26% of this crust, It is never occurs free in nature, but in combination with oxygen forming oxides and silicates. In addition to the previous properties, Silicon is a not toxic and stable element. It has dominated the majority semi-conductor applications for a long period.

Monocrystalline and polycrystalline Silicon solar cells are the two major types of Silicon solar cells.

#### I.7.1.1. Mono-crystalline Silicon solar cells:

Silicon is referred to as a group IV element and has a diamond crystal structure. A unit cell of the Diamond structure is shown in Figure I.20.

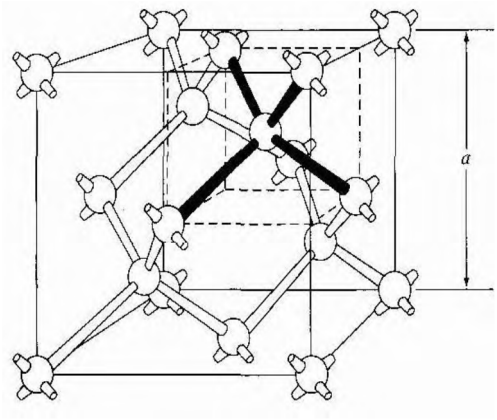


**Figure I.20: The diamond structure [35].**

The diamond structure refers to the particular lattice in which all atoms are of the same species, such as Silicon or Germanium.

Crystalline Silicon has a fundamental indirect band gap $E_G$ = 1.12 eV and a direct gap above 3 eV at ambient temperature as shown in Figure I.21. These characteristics determine the variation of optical properties of Si with wavelength, including the low absorption coefficient for carrier generation for near band gap photons **[28]**.

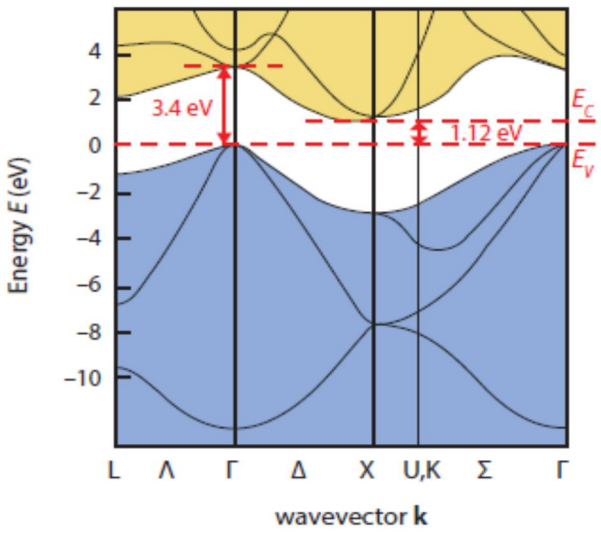


**Figure I.21: The band diagram of crystalline Silicon [36].**

Mono-crystalline or single-crystal Silicon solar cell is a part of Silicon solar cell family. It is one of the first developed and mostly used solar cells. Mono-crystalline Silicon solar cells are the most efficient ones, but are expensive due to the demanding production process.

The main technique for producing single-crystal Silicon is the Czochralski (CZ) method. In this method, high purity Silicon is melted in a quartz crucible. Some doping is added to improve the conductivity of the semiconductor. Generally, Boron or Phosphorous is used as a dopant. A seed crystal is dipped into the molten Silicon and pulled upward and rotates continuously. After sometime, single Silicon ingots is formed from the melting Silicon (Figure I.22).The ingots are then sawed into thin wafers about 200-400 micrometers thick **[30]**. Single crystal Silicon has a uniform molecular structure. However, the fabrication of single crystalline solar cells is a time consuming process, complex, and expensive. The performance of mono-crystalline solar cells is most affected as the temperature increases. However, the life span of these solar cells is large compared to other solar cells. The conversion efficiency of single-crystalline Silicon solar module is about 15-20 % **[37]**.

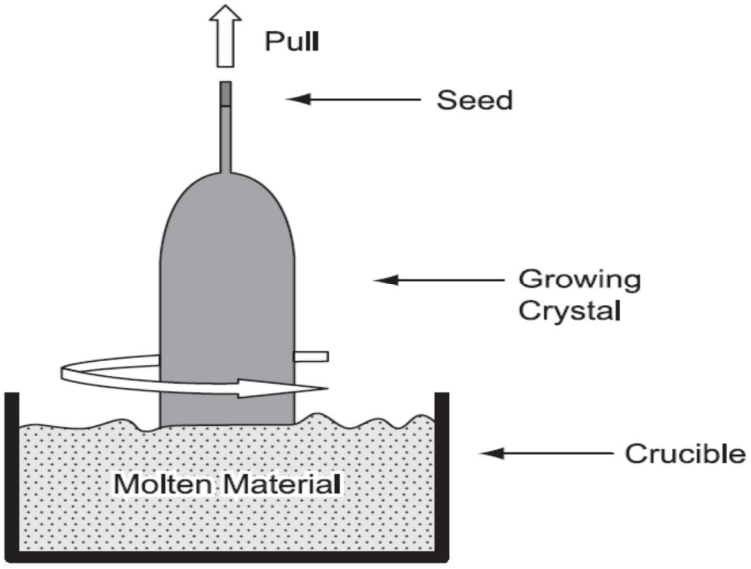


**Figure I.22: A schematic Czochralski (CZ) principle method [30].**

### I.7.1.1. Poly-crystalline Silicon solar cells:

Poly-crystalline or multicrystalline (mc-Si) cells are made of Silicon wafers cut from square cast ingots. Poly-crystalline Silicon solar cells are less expensive to produce than mono-crystalline cells but are less efficient. The efficiency of polycrystalline Silicon cells ranges from 13-14% **[38]**. Figure I.23 shows a wafer of polycrystalline Silicon.

**Figure I.23: Image of a polycrystalline Silicon wafer.**

Polycrystalline Silicon wafers are made by wire-sawing block-cast Silicon ingots into very thin (180 to 350 micrometre) slices or wafers. The wafers are usually lightly p-type doped. To make a solar cell from the wafer, a surface diffusion of n-type dopant is performed on the front side of the wafer. This forms a p-n junction a few hundred nanometres below the surface.

Both mono-crystalline and poly-crystalline Silicon solar cells are single-junction devices with efficiencies limited by thermodynamic considerations. According to Shockley and Quiesser, the maximum theoretical solar conversion efficiency is approximately 31% **[24]**.
Another advantage of poly-crystalline Silicon is the ease with which large structures can be made. Mono-crystalline cells must be carefully interconnected electrically, whereas the poly-crystalline Silicon can be made essentially as large as desired. This has implications for the cost of the two materials.
Mono-crystalline and polycrystalline solar cells constitute what are now called the first generation solar cells. Solar cells of the first generation are relatively expensive to produce, and have low efficiencies.

### I.7.2. Thin films solar cells:

In order to reduce production costs thin film solar cells have been developed. Such devices are fabricated by the deposition of thin films of materials unto cheap substrates.
Generally, thin-film solar cell is a second generation solar cells that is prepared by the deposition of one or more thin layers, or thin film (of about 1 μm to 4 μm thick) of photovoltaic material on a large inexpensive substrate, such as glass, plastic or metal. Thin film solar cells are commercially used in several technologies such as amorphous thin Silicon (a-Si), Cadmium Telluride (CdTe), and Copper Indium Gallium diSelenide (CIGS). These materials have energy bandgaps near the optimum for solar energy conversion and very high optical absorption coefficients such that only few microns of material are needed to absorb most of the incident light, minimising material and production costs **[24]**. In this section we review the most commonly materials used in the second generation solar cells.

#### I.7.2.1. Amorphous Silicon solar cells:

The first produced thin film solar cells developed was based on amorphous Silicon. Amorphous Silicon (a-Si) is the non-crystalline form of the Silicon i.e. it has no crystal structure, and its atoms are ordered only a very short distance. The distances and angles between the silicon atoms are randomly distributed, giving rise to incomplete bonds and a high concentration of defects (Figure I.24). Amorphous Silicon has a higher band gap (1.7 eV) than crystalline Silicon (c-Si) (1.12eV), which means it is a better light absorber than crystalline Silicon, so extremely thin layers of semiconductor may be used (of the order 1 μm).

It was discovered that introducing hydrogen into amorphous Silicon could passivate incomplete bonds known as "dangling bonds", significantly reducing the number of excess energy states within the bandgap. The improved material is referred to as a-Si:H to denote its hydrogen content (Figure I.24.b).

The manufacturing process is simpler, easier and cheaper than in the crystalline cells. However, the cell efficiency of amorphous Silicon is much lower than crystalline Silicon due largely to the increased recombination of the electron-hole pairs that results from the lower carrier mobility.

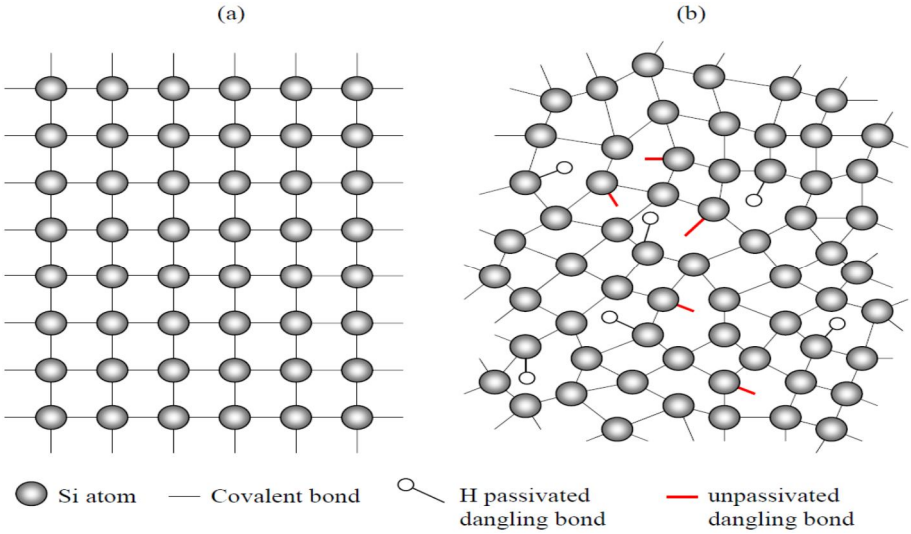


**Figure I.24: Comparison between crystalline and amorphous structure. a- single crystal Silicon, b- hydrogenated amorphous Silicon.**

(a-Si) thin-film cell is mostly made by a method called plasma-enhanced chemical vapour deposition (PECVD) using gases containing silane ($SiH_4$) to deposit a very thin layer of only 1 micrometre (µm) of Silicon on a substrate, such as glass, plastic or metal. There are other methods used to deposit amorphous Silicon on a substrate such as sputtering and chemical vapour deposition (CVD) techniques.

Because of high defect density, the recombination rate in high. The efficiency of the best experimental a-Si:H solar cells is around 10%, and for the mass-produced solar cells, it is around 5% **[16]**.

A notable variant of amorphous Silicon solar cells is the multi-junction thin film Silicon a-Si:H/µc-Si:H which consist of a Si:H cell with additional layers of micro crystalline Silicon (µc-Si:H) applied onto the substrate. In this kind of solar cells the efficiency goes up to 12% **[39]**.

### I.7.2.2. Cadmium Telluride solar cells:

Another semiconductor for thin film solar cells is Cadmium Telluride. CdTe has a direct energy bandgap of about 1.5 eV, and consequently high optical absorption.Its energy bangap is close to the ideal value for photovoltaic conversion efficiency.The theoretical efficiency of CdTe thin-film solar cells is expected to be 28%-30% **[22, 40]**.

To create p-n junction solar cells, a p-type CdTe joined with n-type cadmium sulfide (CdS). A typical fabrication step could be by the deposition of suitable transparent conducting oxide (TCO) on the superstrate, followed by the CdS window layer, the CdTe absorber layer, and then finished off with the back contacts (Figure I.25). The typical thickness of the absorber layer is in the range 3-10 µm compared to the 100-200 µm used in silicon technologies **[24]**.

The best efficiency of CdTe solar cells is 16.5%, and expected to reach 20% **[16]**. However these are still much lower than the theoretical value.

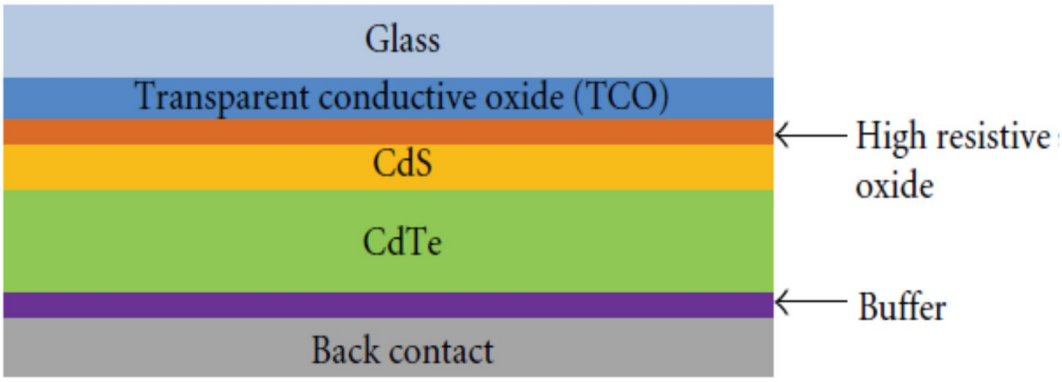


**Figure I.25: Typical structure of CdTe thin film solar cell.**

The most important concern with CdTe solar cells is the toxicity of Cadmium. This concern has been countered by noting that the Cadmium contained in one square meter of a CdTe cell is less than that within a Ni-Cd flashlight battery, and the amount of Cd in CdTe solar cells could be reduced even further as the cells become thinner **[41]**. Also the CdTe is completely sealed by glass. Thus, the environment impact is negligible.

### I.7.2.3. Copper Indium Gallium DiSelenide solar cells:

CIGS is the most promising candidate for efficient and low-cost solar cells, based on the advantages of the optical and electrical properties of this material.

Copper Indium Gallium DiSelenide (CIGS) has also a direct bandgap. The band gap of the semiconductor in CIGS cells can be varied by changing the ratio of Indium to Gallium, allowing the band gap to range continuously from 1 eV to 1.7 eV in the cell **[19]**.

The CIGS solar cell can be produced without requiring the complex vacuum deposition process that some other photovoltaic semiconductors require. Thus, the manufacturing cost can be low. The typical structure of a CIGS solar cell is shown in Figure I.26.

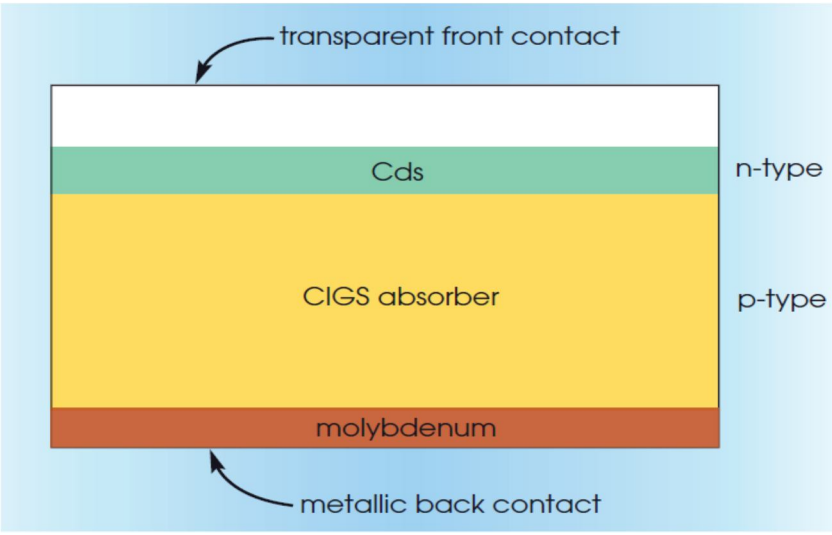


**Figure I.26: Typical structure of CIGS solar cell.**

First, a substrate of soda lime is sputter coated with Molybdenum (Mo), forming the back contact. Then a p-type CIGS absorption layer is vapor deposited over the back contact. Next a chemical bath deposits Cadmium Sulphide (CdS) forming a heterojunction with the adsorption layer. Finally, zinc oxide and indium tin oxide are sputter coated on to form a clear window and the contact grid is e-beam-evaporated on top. In laboratories CIGS solar cells passed the 20% efficiency **[42]**. At that stage commercial module efficiencies were already attaining (10-12%) **[19]**.

### I.7.3. Gallium-Arsenide (GaAs) solar cells:

Among compound semiconductors, Gallium Arsenide (GaAs) is the most studied. It is composed of the element Gallium (Ga) from column III and the element Arsenic (As) from column V of the periodic table of the elements. It is referred as III-V semiconductor.

GaAs has a zinc blend crystal structure. It is very similar to the diamond cubic crystal structure with the difference that it has atoms of alternating elements at its lattice sites (Figure I.27). Due to the fact that it has greater electron mobility than Silicon it can be used in different ways that Silicon cannot.

GaAs cells have been developed and used extensively for space applications, but habitually have been considered too expensive for terrestrial applications despite their high efficiency. Its high efficiency is partly as a result of its direct band gap (1.42 eV).The

absorption coefficient of GaAs is significantly larger than that of Silicon; to absorb the same amount of sunlight, GaAs requires only a layer of few micrometres thick while crystalline Silicon requires a wafer of about 200-300 micrometres thick **[43]**.

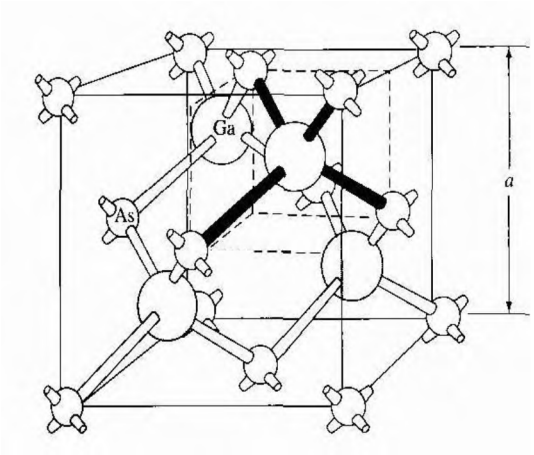


**Figure I.27: The zincblende lattice of GaAS [35].**

GaAs is less friable than Silicon, less susceptible to suffer damage from the space radiation than Silicon, and so the material of choice in space-based solar cells. Also, its high resistance to heat makes it an ideal choice for concentrator systems in which cell temperatures are high.

The main disadvantage of GaAs PV cells is the high cost of the single-crystal substrate that GaAs is grown on. Therefore it is most often used in concentrator systems where only a small area of GaAs cells is needed **[43]**.

### I.7.4. Other semiconductor solar cells:

In addition to the materials used in the manufacture of solar cells previously mentioned, there are other materials referred in the so-called solar cells of the third generation. This new generation solar cells are being made of new materials besides Silicon, including nanocrystal based solar cells, organic solar cells, dye sensitized solar cells, concentrated solar cells…

Most of the works on third generation solar cells is being done in the laboratories, and for the most part is not commercially available. The goal is to make solar cells cheap to produce and more efficient.We will focus as follows on the organic and dye sensitized solar cells.

### I.7.4.1. Organic solar cells:

While the external behaviour of organic photovoltaics is the same as that of inorganic PVs, the mechanism by which the voltage and current are generated is slightly different. The organic PV material is not crystalline, so instead of semiconductor p-n junctions, organic cells use electron donor and acceptor species. Typical choices are polymers for the electron donors and fullerenes for the electron acceptors **[44]**.

Single layer organic photovoltaic cells are the simplest form. These cells are made by sandwiching a layer of organic electronic materials between two metallic conductors, typically a layer of indium tin oxide (ITO) and a layer of metal such as Aluminium, Magnesium or Calcium. An example of a basic structure of an organic solar cell is shown in Figure I.28. Efficiencies of organic solar cells are currently around 10% **[28, 45]**.

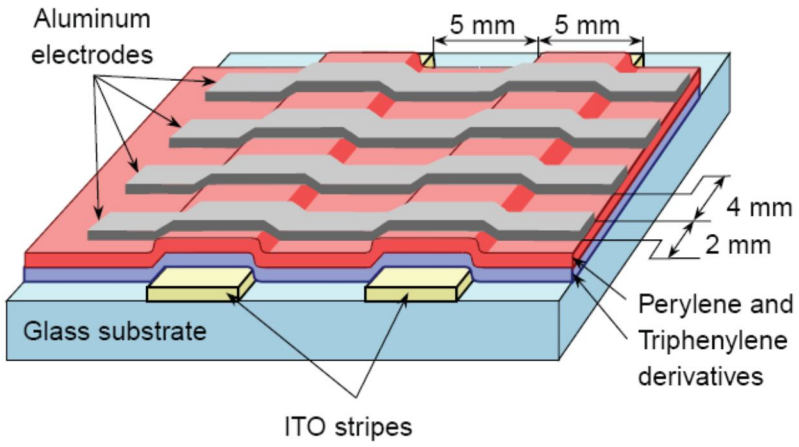


**Figure I.28: Basic structure of an organic cell, adapted from [46].**

Because organic materials can have high absorption coefficients, a layer of only a few hundred nanometers is often enough to absorb a large fraction of light in the material's absorption spectrum **[47]**.The use of thin layers reduces the amount of active material needed and also makes light-weight and flexible devices possible. For these and other reasons, organic solar cells have gained significant attention.

### I.7.4.2. Dye-Sensitized solar cells:

Dye-sensitized solar cells (DSSCs) were first invented in 1991 by Michael Gratzel and co-workers of the Swiss Polytechnic of Lausanne. A Dye-sensitized solar cell contains titanium dioxide ($TiO_2$) nanoparticles, organic dye particles, an electrolyte and platinum contact. Figure I.29 shows an illustration of a basic structure of a DSSC.

In a Dye sensitized solar cell, the incident photons excite electrons in the dye molecules. If given sufficient energy, the excited electrons will escape from the dye to the conduction band of the $TiO_2$ particles and will then diffuse to the electrode, generating a current. The electrons return to the dye through the electrolyte.

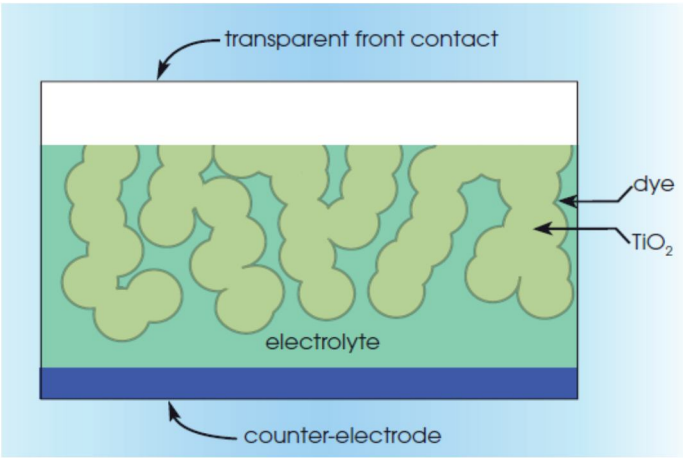


**Figure I.29: The basic structure of a dye-sensitized solar cell [19].**

The record efficiency of dye-sensitised PV devices on lab-scale is 11.9% and was achieved by Sharp **[36]**. Commercial efficiencies are low, typically under 4% to 5%, the reason why efficiencies are low is because there are very few dyes that can absorb a broad spectral range.

Dye sensitized solar cells are attractive because they are made of low-cost materials, and they are easy to manufacture. However, there performance can degrade over time with exposure to ultra violet (UV) light, and at low temperatures the electrolyte can freeze, which stops the device from generating power and might even result in physical damage. Another challenge is the high cost of the Platinum electrodes, hence replacing the Platinum with cheaper materials is a topic of on-going research. Secondly, more stable and resistive electrolyte materials must be developed. Thirdly, research is done on improved dyes that enhance the spectral and band gap utilisation of the solar cells **[36]**.

## I.8. Materials used for space solar cells:

Solar cells that are developed for use in space must take into account the unique aspects of the space environment. The spectral illumination that is available in space is not filtered by the earth's atmosphere and thus is different from what is experienced on earth. Space solar cells are designed and tested under an Air Mass Zero (AM0) spectrum. The main

characteristics of solar cells required for many space missions are: high efficiency, high reliability, good radiation tolerance, long life, and low cost.

In addition to these characteristics, some planetary missions may require operational capabilities at low or high temperatures, at low or high solar intensities, and in high radiation fields. Inner planetary missions require solar cells that can function at very high temperatures and high solar fluxes. Outer planetary missions require solar cells that can function at very low solar intensity flux and very low temperatures **[48]**.

Up to now, the two major materials used for space solar cells are Silicon and Gallium Arsenide. Currently, there are other materials used in the manufacture of space solar cells such as, Gallium Indium Phosphide (GaInP), thin film cells of amorphous Silicon (a-Si), Cadmium Telluride (CdTe), and Copper Indium Gallium diSelenide (CIGS). CIGS cells, which are still under development, have efficiencies of 20% measured under laboratory conditions. Their advantages over other cells are radiation insensitivity, low weight, and low cost, and thus make it a very promising technology for future applications **[49]**.

Silicon solar cells are the most mature of all space solar cell technologies. In the early 1960s, the efficiency of Silicon solar cells were ~11%, relatively inexpensive, and well suited for short mission duration (3-5 years). The conversion efficiency of current "standard-technology" Silicon ranges from around 12 to 15% under standard AM0 test conditions **[28]**.

There have been many enhancements to Silicon solar cells over the years to improve their efficiency and make them more suitable to space utilisation. Textured front surfaces for better light absorption, extremely thin cells with back surface reflectors for internal light trapping, and passivated cell surfaces to reduce losses due to recombination effects are just a few examples. Currently, high-efficiency Si cells approaching 17% AM0 efficiency **[28]**. The advantage of the high-efficiency Si cell to that of a III-V lies in their relatively lower cost and lower material density. However, Silicon solar cells are less tolerant of the radiation environment of space **[28]**.

III–V solar cells such as (GaAs) cells have some advantages over Silicon cells for space applications. Their higher efficiencies and radiation resistance have made them attractive as replacements for Silicon cells on many satellites and space vehicles. One of the most important advances in recent years has been the development of triple-junction cells based on Gallium Arsenide (GaAs) and related compounds, which now achieve 30% efficiency under AM0 conditions **[19]**. Typically, a triple-junction device consists of a 'sandwich' of layers of Gallium Indium Phosphide (GaInP), Gallium Arsenide, and Germanium (Ge). In

addition to the properties of single-junction GaAs solar cells, GaInP/GaAs/Ge cells have the added advantage of operating at high voltage and low current, as well as having excellent radiation resistance. They also have a smaller temperature coefficient than Silicon cells, which implies better performance under the operating conditions encountered in space applications **[28]**.However, these cells are relatively expensive to produce due to the difficulty in growing high quality crystals of these materials.

Because of the potential for low-cost production, significant research has gone into developing low-cost thin-film solar cells for the terrestrial market. Thin-film solar cells have been primarily based on CIGS, amorphous Silicon, or CdTe alloys. Application of these technologies for use in space has been, and continues to be, the stronger driver for developing higher performance both in terms of specific power and efficiency.

Currently, CIGS and CdTe solar cells are attracting considerable interest for space applications, because proton and electron irradiation tests of CIGS and CdTe solar cells have proven that their stability against particle irradiation is superior to conventional Si or III-V solar cells **[50]**, possibly extending mission lifetimes. Moreover, lightweight and flexibility of these cells can yield a high specific power (W/kg) and open numerous possibilities for a variety of applications.

# Chapter II
# Defects in semiconductor devices

## II.1. Introduction:

A perfect crystal is an idealization; it is formed by the repetition of infinite number of unit cells along the crystal orientation, there is no such thing in the nature. Atom arrangements in real materials do not follow perfect crystalline patterns and any deviation from this perfect structure is said to contain imperfections or defects. Defects are not always unfavourable, and do in general contribute to various mechanical and electronic properties of the material. In fact a part of modern electronic engineering is based on the manipulation of these defects to produce desired properties for efficient use of the material in the operation of devices.

In this chapter we give an overview on the types of defects that are found in semiconductors such as point defects. The theory of deep level defects is also presented.

## II.2. Semiconductors:

Semiconductor materials are called semiconductors because their conductivity is not as high as conductors (generally metals), and not as low as insulators (such as ceramics and glasses). The conductivity of a typical semiconductor can be controlled by temperature to such an extent that most can appear to be insulators at sufficiently low temperatures and metals at sufficiently high temperatures. Also, the electrical properties of these materials are extremely sensitive to the presence of even little concentrations of impurities.

Semiconductors are categorised into two classes; elementary semiconductors such as Silicon (Si), and compounds semiconductors containing two or more elements. For example, compounds semiconductors made by two elements from the periodic table are called binary compounds such as gallium arsenide (GaAs) and those which are made by three elements are known as ternary compounds semiconductors such as indium gallium arsenide (InGaAs).

A semiconductor free of significant impurities is termed “intrinsic” while those doped with impurities are termed “extrinsic”. Both of these behaviours are important to the operation of microelectronic devices.

### II.2.1. Intrinsic semiconductors:

An intrinsic semiconductor also called an undoped semiconductor or i-type semiconductor is a pure semiconductor without any significant dopant species present. The conductivity of such semiconductors is many orders of magnitude lower than metallic conductors. The number of charge carriers is determined by the properties of the material itself instead of the amount of impurities. In intrinsic semiconductors the number of excited electrons n and the number of holes p are equal ($n = p$). The number of electrons or holes is named the intrinsic carrier concentration $n_i$. For example, thermally excited electrons in Si and GaAs are $1.5 \times 10^{10}$ $cm^{-3}$ and $1.1 \times 10^{6}$ $cm^{-3}$, respectively, at room temperature **[51]**.

Intrinsic semi- conductors (especially Si and Ge) are used as optical and x-ray detectors (at low temperature) where a low concentration of charge carriers is required **[52]**.

### II.2.2. Extrinsic semiconductors:

One of the important advantages of semiconductor materials is that their electrical properties can be modified significantly by adding small amounts of impurities into the host material (known as dopants), or other kinds of defects. However, while one type of defect can make a semiconductor useful for fabricating a device, another type can have undesirable effects which render the device useless. The doped semiconductor, called an extrinsic material, is the primary reason we can fabricate the various semiconductor devices. The quantity of dopants necessary to change the properties of a semiconductor is often considerably less than one impurity atom per million host atoms **[53]**.

If the atom has one fewer electron than the host, it is likely to accept an electron from the relatively electron-rich semiconductor. Consequently, it is referred to as an acceptor dopant. If the atom has one extra electron it is generally a donor.

## II.3. Types of defects in semiconductors (classification of defects):

One of the most important keys to manufacturing a semiconductor is the control of defects in its structure. Defects may be classified in four categories according to their dimension as follows:

- Zero dimensional defects (Point defects).
- One dimensional defects (line defects).
- Two dimensional defects (plane defects).
- Three dimensional defects (volume defects).

In general, the intrinsic lattice defects can be broadly classified in terms of dimensionality, viz., point, line, plane, and spatial or volume defects. Moreover, any foreign species present within the crystal lattice (extrinsic defects) may evidently also be regarded as a kind of defects.

In the next sections we will discuss each kind of defects separately.

### II.3.1. Point defects:

Point defects are the simplest kinds of defects that can exist in any crystal. When an atom is missing or is an irregular place, then the material is said to have point defects.

It is useful to distinguish intrinsic defects, which can appear in a pure material, from extrinsic defects, which are caused by impurity atoms.

#### II.3.1.1. Vacancies:

Vacancies are the empty spaces where an atom should be, but is missing (Figure II.1). They are common in metals and semiconductors, especially at high temperatures when atoms are found to change their positions leaving behind empty lattice sites.

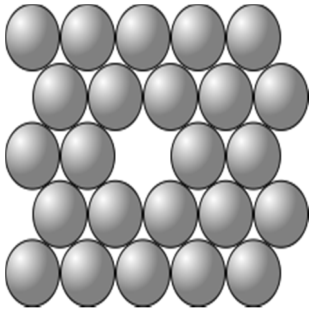

**Figure II.1: Illustration of a Vacancy in a two-dimensional lattice.**

The number of vacancies, $N_{Va}$ increases exponentially with the absolute temperature, T, and can be estimated by the equation **[54]**:

$$N_{Va} = N_S . \exp(-\frac{E_{Va}}{K_B . T}) \qquad \text{II.1}$$

Where $N_s$ is the number of regular lattice sites, $K_B$ is the Boltzmann constant, and $E_{Va}$ is the energy needed to form a vacancy in a perfect crystal.

In an elemental semiconductor (such as Silicon) there is only one type of vacancy, although it may have multiple allowed charge states. Compounds consist of ordered arrangements of chemically different atoms. Vacancies can occur on any of these positions. Thus, in GaAs, one can have a Ga vacancy ($V_{Ga}$) or an As vacancy ($V_{As}$). More complex

compounds can have more types of vacancies, one for each distinct lattice site. Vacancies always occur in crystalline solids, and are therefore intrinsic to materials **[55]**.

### II.3.1.2. Substitutional defects:

Substitutional defects are either impurities or antisites. "Impurities", as one would expect, refers to atoms which are not constituents of the semiconductor host (Figure II.2). They are not intrinsic to the nature of a solid, but result from its incomplete purification or intentional contamination. Thus, they are referred to as extrinsic defects.

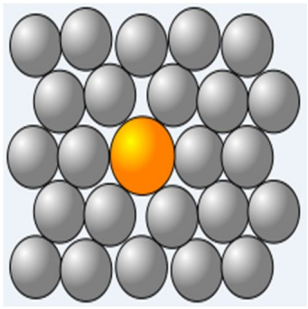

**Figure II.2: Illustration of a substititional impurity.**

Antisites, as with vacancies, are intrinsic to compounds. When a host atom occupies the site of another host atom in a material, the impurity formed is called antisite (Figure II.3). Antisite defects are found only in crystals with more than one sublattice and having different atoms on each **[55]**. For example in GaSb material when Sb atom occupies the Ga site the resulting defect, SbGa, is called antisite.

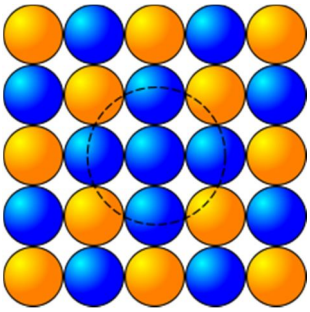

**Figure II.3: Illustration of an antisite.**

### II.3.1.3. Interstitials:

Interstitials are atoms that occupy a place outside the normal lattice position. There are two types of interstitials; self-interstitial and interstitial impurity.

A self-interstitial is an atom from the host material occupies a site other than its regular site in the crystal structure. On the other hand, if a foreign atom occupies an irregular site in the

lattice structure it is called interstitial impurity. Thus, both intrinsic and extrinsic interstitials are found in semiconductors. These two types of interstitials are shown in Figure II.4.

Interstitials are generally high-energy configurations. Once again, the introduction of an interstitial induces a relaxation and distortion of the lattice, which surrounds it. The type of configuration the interstitial assumes depends on its ability to make bonds with its neighbours and therefore can change with its charge state **[56]**.

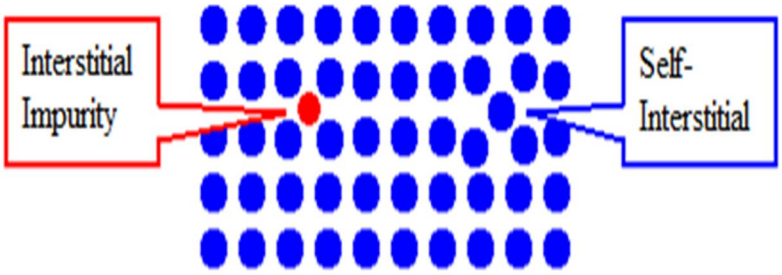


**Figure II.4: A two-dimensional illustration of the two types of interstitial.**

### II.3.1.4. Complexes of point defects:

The combination of simple point defects is possible and the resultant defects will be complexes. In this section selected complexes are discussed.

#### a- Frenkel defects:

Frenkel defect (Figure II.5) was first observed by a Russian scientist Yakov Frenkel in 1926 **[57]**. In general the defect forms when an atom or cation leaves its normal position in the lattice, creating a vacancy, and becomes an interstitial by lodging in a nearby location not usually occupied by an atom. In ionic crystals there is no change in charge because the cation maintains the same positive charge as an interstitial **[58]**.

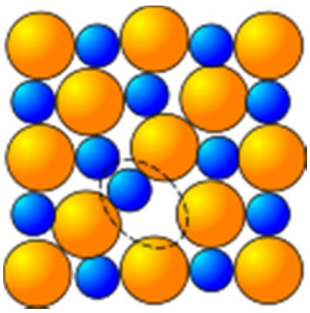

**Figure II.5: Illustration of a Frenkel defect.**

**b- Schottky defects:**

This defect was first discovered by German scientist Walter H. Schottky **[57]**. This defect is unique to ionic materials. It forms when oppositely charged ions leave their lattice sites, creating vacancies (Figure II.6). These vacancies are formed in stoichiometric units, to maintain an overall neutral charge in the material. The vacancies are then free to move about as their own entities **[59]**.

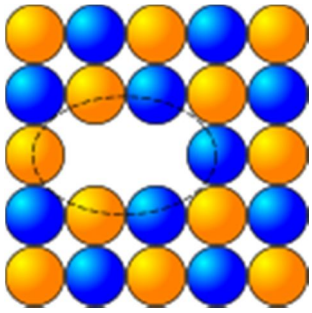

**Figure II.6: Illustration of a Schottky defect.**

There are other types of complexes defects such as split interstitial, Di-vacancy, vacancy-impurity pair, impurity pair **[51, 56]**.

It is worth to mention that the point defects may occur during growth, heating, doping, plastic deformation, and as a result of radiation exposure.

### II.3.2. Line defects:

Line defects are one-dimensional and are commonly known as dislocations. These defects are found in the material when an array of atoms is displaced in the crystal structure. Dislocations are generated and move when a stress is applied. They affect the physical properties of the material to a large extent, in fact the motion of dislocations cause the occurrence of plastic deformations in the material.

Broadly, there are two basic forms of dislocations, the edge dislocation and the screw dislocation.

#### II.3.2.1. Edge dislocation:

An edge dislocation is formed when an extra half-plane of atoms is introduced half way in the middle through the crystal, and disturbs the symmetry of nearby planes of atoms (Figure II.7). In the figure, the atoms above the dislocation line are squeezed together, and those below are pulled apart; this is reflected in the slight curvature for the vertical planes of atoms as they bend around this extra half-plane. The magnitude of this distortion

decreases with distance away from the dislocation line; at positions far removed, the crystal lattice is virtually perfect **[58]**.

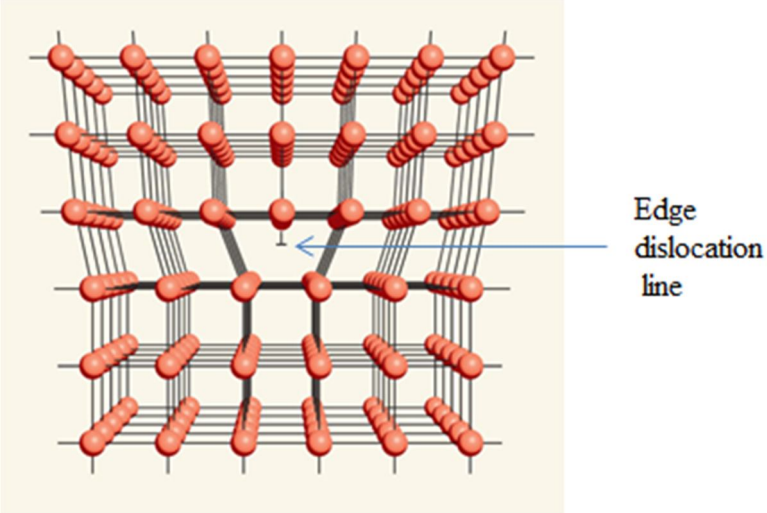


**Figure II.7: Lattice structure illustrating an edge dislocation within a semiconductor.**

### II.3.2.2. Screw dislocation:

There is a second basic type of dislocation, called screw dislocation. It is not very straightforward to understand. The motion of a screw dislocation is also a result of shear stress, but the defect line movement is perpendicular to direction of the stress and the atom displacement, rather than parallel as shown in Figure II.8.

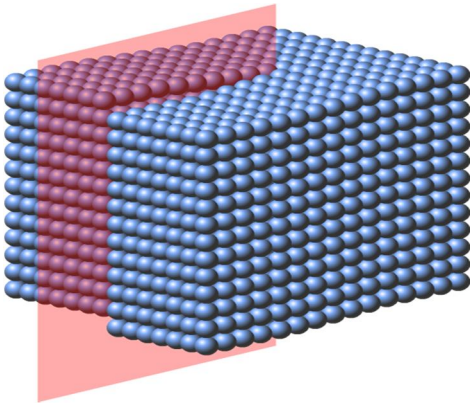

**Figure II.8: Lattice structure indicating a screw dislocation.**

Dislocations affect the electrical properties of materials as they often contain many charges. In crystals, dislocations can also cause lattice distortions or strain and have also been proposed to account for the shear stresses above which single crystals of metals undergo permanent plastic deformation.

Charge carriers can build up in a line and gradually start repelling accumulation of additional charges. This in turn reduces the effective capture cross section as the amount of

accumulated charge increases, causing the emission of carriers to follow a non-exponential process **[60]**.

### II.3.3. Planar defects (two dimensional defects):

Defects like the Stacking faults, Twin boundaries, and Grain boundaries are examples of planar defects. In this section we discuss two types of planar defects which are Stacking faults and Grain boundaries.

#### II.3.3.1 Stacking faults:

A stacking fault is a one or two layer interruption in the stacking sequence of atom planes (Figure II.9 a and b). Stacking faults occur in a number of crystal structures. One of the simplest forms of stacking fault occurs in fcc and hcp crystals, converting one to the other. For example, fcc crystals have a stacking sequence denoted "ABCABC", in which the letters represent the positions of planes of atoms with respect to each other. Likewise, the hcp structure has an "ABABAB" stacking sequence. So, if the hcp structure is going along as ABABAB and suddenly switches to ABABAB**C**ABAB, there is a stacking fault present. In the fcc lattice the normal stacking sequence of most dense (111) plane is ABCABCABC. A stacking fault in an fcc structure would appear as one of the C planes (say) missing. In other words, the stacking sequence would become ABCABCAB↕ABCABC.

#### II.3.3.2 Grain boundaries:

Up to this point, the discussion has focused on defects of single crystal. However solids generally consist of a number of crystallites or grains (Figure II.9 c). The interface between two grains or crystallites in a polycrystalline material is known as grain boundary.

Grain boundaries are such defects in the crystal structure which are found to decrease the electrical and thermal conductivity of the material. They limit the lengths and motions of dislocations **[61]**. Therefore, having smaller grains (more grain boundary surface area) strengthens a material. The size of the grains can be controlled by the cooling rate when the material cast or heat treated. Generally, rapid cooling produces smaller grains whereas slow cooling result in larger grains **[59]**.

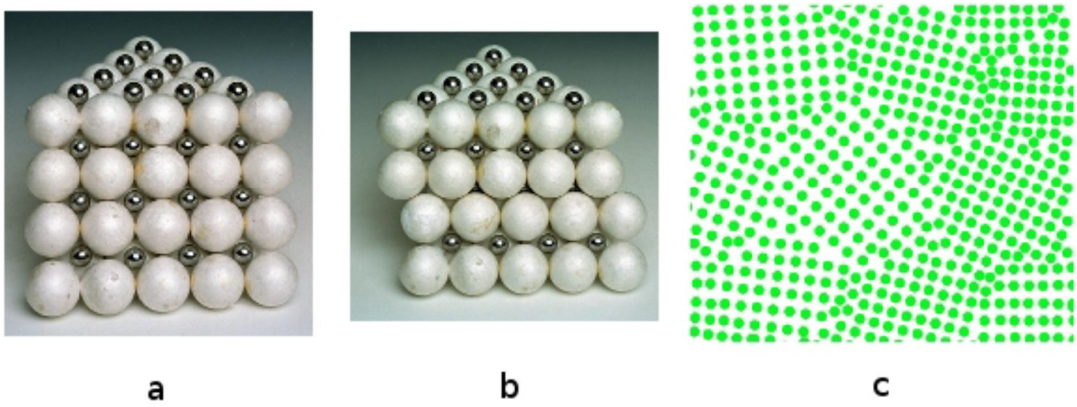


**Figure II.9: (a) ideal packing in the AB FCC structure, (b) a model of the AB FCC structure with a stacking fault (c) Differently oriented crystallites in a polycrystalline material forming boundaries [61].**

### II.3.4. Spatial (volume) defects:

The last class of defects considered are volume defects. These defects occur on a much bigger scale than the rest of the crystal defects. Generally, they are introduced during processing and fabrication steps. A few of the more common volume defects will be briefly mentioned.

**a) Precipitates:** Precipitates are small particles that are introduced into the matrix by solid state reactions. Their most common purpose is to increase the strength of structural alloys by acting as obstacles to the motion of dislocations. Their role in the microstructure is to modify the behaviour of the matrix rather than to act as separate phases in their own right **[62]**.

**b) Dispersants:** They are larger particles that behave as a second phase as well as influencing the behaviour of the primary phase. They may be large precipitates, or grains distributed through the microstructure **[62]**.

**c) Inclusions:** Inclusions are foreign particles or large precipitate particles. They are usually undesirable constituents in the microstructure. For example, inclusions have a deleterious effect on the useful strength of structural alloys since they are preferential sites for failure. They are also often harmful in microelectronic devices since they disturb the geometry of the device by interfering in manufacturing, or alter its electrical properties by introducing undesirable properties of their own **[62]**.

**d) Voids**: Voids (or pores) are caused by gases that are trapped during solidification or by the accumulation of vacancies. They are almost always undesirable defects. Their principal effect is to decrease mechanical strength and promote fracture at small loads **[62]**.

## II.4. Defects and their electronic states:

The presence of defects in the crystal can significantly alter the electrical properties of the semiconductor. Defects can be classified by their atomic structure as discussed in the previous section (section II.3). In addition to this classification, it is common to group defects by the energy level that they introduce into the "forbidden" band gap. The replacement of atoms in a semiconductor crystal with substitutional impurities, interstitials impurities, intrinsic defects, complexes defects, and dislocations can lead to electronic states inside the band gap. These energy states are also called energy levels. Among the hundreds of defects known energy levels, there are only a few that are used to fabricate electronic devices **[63]**.

According to this classification, states that have energies close to either the valence ($E_V$) or conduction band edges ($E_C$) are usually called shallow levels, whereas states with energies that are far from both the bands are called deep levels.

### II.4.1. Shallow defects:

The term shallow defects is used to describe point defects that bind exactly one charge carrier and exhibit an electronic ground state close to either the conduction or the valence band and are therefore either donors or acceptors **[64]**.

For example, in the group IV semiconductors such as Silicon or Germanium the elements of the third group (B, Al, Ga) requires an extra electron to form a complete Lewis octet when they substitute a host atom. We call these impurities shallow acceptors. Elements of the fifth group (P, As, Sb) have one valence electron more than required to form a Lewis octet. This extra electron is given up to the conduction band, and we call these impurities shallow donors. Shallow donors (acceptors) are also called hydrogenic because they can be treated within the theory of the hydrogen atom **[63]**. This approximates the defect as a hydrogen atom in the dielectric medium of the semiconductor. The hydrogenic model can be applied to any monovalent substitutional point defect in either an elemental or a compound semiconductor and to both n and p type dopants **[55]**.

For a donor impurity, the energy difference between the conduction band minimum and the donor level is the ionization energy, or the binding energy ($E_d = E_C - E_D$), this is the amount of energy required to excite an electron from the donor atom into the conduction band. For a shallow donor, the binding energy is small compared to the band gab.

A similar reasoning applies to acceptors; the ionization energy is the energy difference between the acceptor level and the valence band maximum ($E_a = E_A - E_V$). The acceptor binding energy is the energy required to promote a hole from the acceptor atom into the valence band. Equivalently, it is the minimum amount of energy needed to excite an electron from the valence band to the acceptor level.

According to the hydrogen-atom model, the ionization energy for the hydrogen atom in vacuum is **[22]**:

$$E_H = \frac{m_{0q^4}}{32\pi^2\varepsilon_0^2\hbar^2} = 13.6\ eV \qquad \text{II.2}$$

The ionization energy $E_d$ for a donor in a lattice can be obtained by replacing the electron rest mass ($m_0$) by the conductivity effective mass of electron ($m_{ce}$), and by replacing the vacuum permittivity ($\varepsilon_0$) by the permittivity of the semiconductor ($\varepsilon_s$):

$$E_d = E_C - E_D = \left(\frac{\varepsilon_0}{\varepsilon_s}\right)^2 \left(\frac{m_{ce}}{m_0}\right) E_H \qquad \text{II.3}$$

For Silicon, the ionization energy for donors as calculated from Eq. II.3 is 25 meV **[22]**. Since the small ionization energies of shallow defects are comparable to the thermal energy $k_BT$, ionization is usually complete at room temperature. Generally, Impurity elements which are used as dopants in semiconductors create shallow levels which are ionized at room temperature and provide additional free carriers to form p-type or n-type semiconductor.

### II.4.2. Deep defects:

Defects with properties deviating strongly from those predicted by the hydrogen model are called deep-levels. More generally a deep-level can be defined by the extension of the wave function of a bound charge carrier **[64]**.

Deep levels are positioned deeper in the band gap than the dopant levels and are found to bind the carriers much more strongly into highly compact, localized states.

The deep levels have higher ionization energies (greater than 100meV); therefore contribute very little to the free charge carriers.

Depending on its position in the band gap and on relative capture cross-section of minority and majority carriers, a deep level may act as a minority carrier trap, majority carrier trap or recombination centre. A majority carrier trap is an electron trap in n-type semiconductor or a hole trap in p-type semiconductor. Conversely a minority carrier is a hole trap in n-type semiconductor or an electron in p-type semiconductor. If a majority- or minority-carrier lives a mean lifetime in the captured state and is thermally ejected to the band from which it came, the centre may be considered as majority carrier trap or minority carrier trap respectively. Recombination centres are deep levels with approximately equal capture cross sections for both electrons and holes and these centres are generally located near the middle of the band gap. After capturing a majority carrier, if the majority carrier stays trapped at the centre long enough for the trap to capture a minority carrier, then recombination takes place and the centre is acting as a recombination centre **[56].**

Deep levels play an important role in semiconductors since they modify the properties of the semiconductors devices. In a defect free diode or bipolar junction transistor the speed of the device can be limited by the time to remove charge from the base. Because recombination centres reduce this time, they can, in theory, make a transistor switch faster. **[55]**.

Deep levels may also non-desirable in some applications, e.g. they cause lower gain in transistors, reduced power production in solar cells by increasing saturation current and decreasing the lifetime of the minority carriers and hence the efficiency, lower output in light emitting devices LEDs, and more reverse leakage current in junctions of all types.

### II.4.2.1. Emission and capture of carriers from deep levels:

In a semiconductor, shallow impurities give rise to dopants, while deep impurities give rise to traps.

The kinetics of charge transfer between the deep levels and the bands are fully described by the Shockley-Read-Hall (SRH) theory (model) **[65, 66]**.

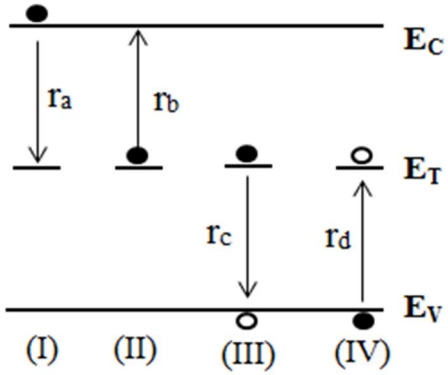


**Figure II.10: A diagram showing the four possible recombination and generation processes: (I) electron capture, (II) electron emission, (III) hole capture, (IV) hole emission. Electrons and holes are represented by filled and open circles, respectively.**

Consider a trap located at $E_T$ from the conduction band with a density $N_T$, the level can interact with the conduction band and the valence band through emission and capture of electrons and holes. There are four competing reactions take place:

As illustrated in Figure II.10, the four common processes for the transition of electrons and holes are:

- Capture of an electron from the conduction band to the trap.
- Electron emission from the trap to the conduction band.
- Capture of a hole from the valence band to the trap (i.e., emission of an electron from the trap to the valence band).
- Hole emission from the trap to the valence band (i.e., capture of an electron from the valence band to the trap).

A process I followed by a process III is known as recombination. A generation process is a process II followed by a process IV.

The capture of electrons by the deep levels, process I, has the rate:

$$r_a = c_n n p_T \qquad \text{II.4}$$

Where $n$, is the number of electrons in the conduction band, $p_T$ is the concentration of the available empty traps, $c_n$ is the capture rate of electrons which is given by:

$$c_n = \sigma_n \langle v_n \rangle_{th} \qquad \text{II.5}$$

Where $\sigma_n$ is the capture cross section for electrons, and $\langle v_n \rangle_{th}$ is the average thermal velocity of electrons which is given by:

$$\langle v_n \rangle_{th} = \sqrt{\frac{3k_B T}{m_e}} \qquad \text{II.6}$$

$m_n$ is the effective mass of electrons.

For the process II, i.e. emission of electrons from the trap to the conduction band, the emission rate is given by:

$$r_b = e_n n_T \qquad \text{II.7}$$

Where $e_n$ is the electron emission rate, $n_T$ is the density of deep levels (traps) that are occupied by electrons.

The capture rate for holes, process III, is analogous to process I with the difference that holes are captured by occupied traps.

$$r_c = c_p p n_T \qquad \text{II.8}$$

Where $p$ is the number of holes in valence band, $p_T$ is the concentration of the available empty traps, $c_p$ is the capture rate for holes which is given by:

$$c_p = \sigma_p \langle v_p \rangle_{th} \qquad \text{II.9}$$

Where $\sigma_p$ is the capture cross section for holes, and $\langle v_p \rangle_{th}$ is the average thermal velocity of holes which is given by:

$$\langle v_p \rangle_{th} = \sqrt{\frac{3k_B T}{m_p}} \qquad \text{II.10}$$

$m_p$ is the effective mass of holes.

Finally, the emission of holes, process IV, has the rate:

$$r_d = e_p p_T \qquad \text{II.11}$$

Where $e_p$ is the hole emission rate.

The overall change of $n$ by unit of time $t$ is given by:

$$\frac{dn}{dt} = r_b - r_a = e_n n_T - c_n n p_T \qquad \text{II.12}$$

Here, no other emission or capture processes than the ones described before are assumed, i.e., the radiative and/or Auger processes are not taken into account.

A similar expression is found for the time rate of change of $p$:

$$\frac{dp}{dt} = r_d - r_c = e_p p_T - c_p p n_T \qquad \text{II.13}$$

Whenever an electron or hole is emitted or captured, the occupancy of the deep level state changes. This rate of change is calculated from equation II.10 and II.11, and is given by:

$$\frac{dn_T}{dt} = \frac{dp}{dt} - \frac{dn}{dt} = e_p p_T - c_p p n_T - e_n n_T + c_n n p_T \qquad \text{II.14}$$

Rearranging terms and using the total density of traps $N_T = n_T + p_T$ , we get:

$$\frac{dn_T}{dt} = \left(c_n n + e_p\right) N_T - \left(c_n n + e_p + c_p p + e_n\right) n_T \qquad \text{II.15}$$

According to the detailed balance principle, in a semiconductor, at thermal equilibrium, the rate of creation and the rate of absorption are the same, thus:

$$e_n n_T = c_n n p_T \quad \text{II.16}$$

$$e_p p_T = c_p n_T p \quad \text{II.17}$$

Using equations II.5 and II.9 we get:

$$e_n n_T = \sigma_n \langle v_n \rangle_{th} p_T n \quad \text{II.18}$$

$$e_p p_T = \sigma_p \langle v_p \rangle_{th} n_T p \quad \text{II.19}$$

If $f(E_T)$ is the Fermi Dirac distribution function which represents the number of states occupied by electrons, then $(1- f(E_T))$ will be the number of states occupied by holes. That is;

$$n_T = N_T f(E_T) \quad \text{II.20}$$

$$p_T = N_T (1 - f(E_T)) \quad \text{II.21}$$

$$f(E_T) = \frac{1}{1+\exp\left(\frac{E_T - E_F}{k_B T}\right)} \quad \text{II.22}$$

The density of electrons in the conduction band is given by:

$$n = N_C \exp\left(\frac{E_F - E_C}{k_B T}\right) = n_i \exp\left(\frac{E_F - E_i}{k_B T}\right) \quad \text{II.23}$$

$n_i$ is the density of states of intrinsic material.

Equation II.18 can be expressed by:

$$e_n N_T f(E_T) = \sigma_n \langle v_n \rangle_{th} (1 - f(E_T)) N_T n \quad \text{II.24}$$

Using equations II.22, II.23, II.24 one can get the thermal emission rate of electrons:

$$e_n = \sigma_n \langle v_n \rangle_{th} N_C \exp\left(-\frac{(E_c - E_T)}{k_B T}\right) = \sigma_n \langle v_n \rangle_{th} n_i \exp\left(\frac{E_T - E_i}{k_B T}\right) \quad \text{II.25}$$

Similar analysis gives the thermal emission rate of holes:

$$e_p = \sigma_p \langle v_p \rangle_{th} N_V \exp\left(-\frac{(E_T - E_V)}{k_B T}\right) = \sigma_p \langle v_n \rangle_{th} n_i \exp\left(\frac{E_i - E_T}{k_B T}\right) \quad \text{II.26}$$

Where $N_C$ and $N_V$ are the density of states in the conduction band and the valence band, respectively.

$$N_C = \left(\frac{2\pi m_e kT}{h^2}\right)^{\frac{3}{2}} \quad \text{II.27}$$

$$N_V = \left(\frac{2\pi m_h kT}{h^2}\right)^{\frac{3}{2}} \quad \text{II.28}$$

The emission rate can be written in a useful form in terms of temperature:

$$e_n = AT^2 \sigma_n \exp\left(-\frac{(E_c - E_T)}{k_B T}\right) \quad \text{II.29}$$

$$e_p = AT^2 \sigma_p \exp \exp\left(-\frac{(E_T - E_V)}{k_B T}\right) \quad \text{II.30}$$

Where $A$ is a constant.

The Arrhenius plot of $(\frac{e_{n,p}}{T^2})$ versus $(\frac{1000}{T^2})$ yields a straight line and the slope of this line gives the activation energy of the deep level [5**1**].

In non-equilibrium $f(E_T)$ is unknown and has to be calculated.

For the steady state condition, $\frac{dn_T}{dt} = 0$. By using II.20 And II.22 we get the new probability of occupancy:

$$f(E_T) = \frac{n_T}{N_T} = \frac{c_n n + e_p}{c_n n + e_p + c_p p + e_n} \qquad \text{II.31}$$

Replacing $c_n$ , $c_p$, $e_n$and $e_p$ by their expression we get:

$$f(E_T) = \frac{\sigma_n n + \sigma_p p_1}{\sigma_n (n + n_1) + \sigma_p (p + p_1)} \qquad \text{II.32}$$

Where $n_1 = n_i \exp\left(\frac{E_T - E_i}{k_B T}\right)$ and $p_1 = n_i \exp\left(\frac{E_i - E_T}{k_B T}\right)$

Assume that non-equilibrium is generated by optical excitation resulting in a generation rate of *G*. we also assume that the emission rates $e_n$, and $e_p$ are not a function of illumination and that the same as calculated at equilibrium, thus:

$$G = r_b - r_a \qquad \text{II.33.a}$$

$$G = r_d - r_c \qquad \text{II.33.b}$$

Replacing $r_a$, $r_b$, $r_c$, and $r_d$ to find a net rate of generation-recombination:

$$G = \frac{pn + {n_i}^2}{\tau_p (n + n_1) + \tau_n (p + p_1)} \qquad \text{II.34}$$

Where $\tau_n = \frac{1}{\sigma_n \langle v_n \rangle_{th} N_T}$ and $\tau_p = \frac{1}{\sigma_p \langle v_p \rangle_{th} N_T}$ are the minority electron lifetime and the minority hole lifetime respectively.

# Chapter III

# Space environment and its effects on solar cells

## III.1. Introduction:

The space radiation environment consists of different kinds of particles such as electrons, protons, and other heavier ions, with different energies (ranging from KeV to GeV and beyond). Reliability of electrical devices in a radiation environment is very important, and extensive studies concerning the development of semiconductor devices that can operate in such conditions have been undertaken **[67-69]**. Possible degradation of the electrical performance of optoelectronic devices in general, induced by irradiation, means that very strict conditions for their application must be predetermined for the worst case scenario. Performance failure in such conditions could have negative impact on both the financial and environmental aspects of the device application **[69]**.

Exposure to charged particles typically degrades the electrical performance of semiconductor devices. These particles can cause both ionization and displacement damage effects in space systems. Concerning solar cells, the most damaging particles are the high-energy electrons and protons that can cause lattice displacement damage. For earth-orbiting and near-earth systems, the most important source of these particles is from the geomagnetically trapped particles in the Van Allen belts **[70]**.

In this chapter we give an overview of the space environment and its effect on semiconductors especially Silicon solar cells and the most important defects induced by radiation in Silicon solar cells.

## III.2. Sources of radiation in space:

The main components of the space radiation environment are classified according to their origin into four categories: solar wind, solar flares, cosmic rays and radiation belts. The electronic components placed in this environment are subjected to the effect of photons, electrons, protons and ions of different origins and energies.

Figure III.1 summarizes the four kinds of radiation distinguished by their energies and their origins.

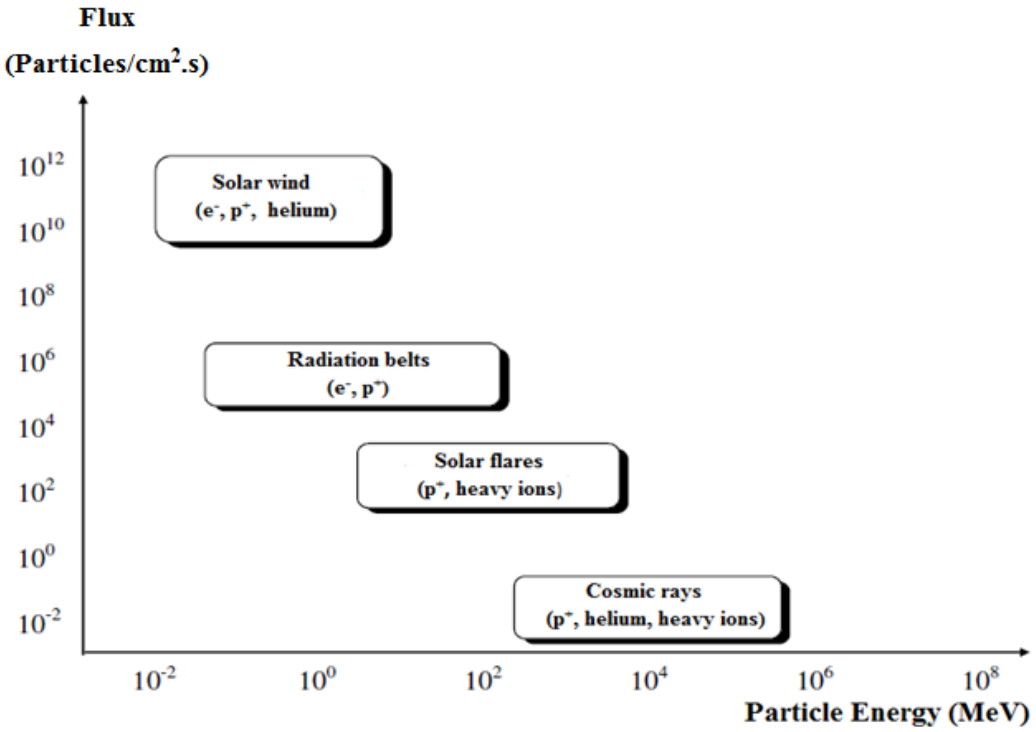


**Figure III.1: Types of space radiation and their fluxes.**

### III.2.1. Solar wind:

Solar wind consists mainly of electrons, protons and an admixture of 5% helium ions, released from the corona (the upper atmosphere of the sun) into the interplanetary space. These charged particles have velocities around 350-500 km/s, and densities typically around 3-5 $cm^{-3}$.

When the supersonic flow of solar wind hits the earth's dipolar magnetic field, it is slowed down generating a shock in the solar wind upstream of the planet known as the bow shock. The region of thermalized subsonic plasma behind the bow shock is called the magnetosheath (Figure III.2), and is characterized by turbulent flows and densities somewhat higher than those in the solar wind.

Plasma inside the magnetosphere is grouped into different regions with quite different densities and temperatures.

The motion of the solar wind compresses the earth's internal magnetic field on the sunward side, sweeping field lines antisunward into a region called the magnetotail (Figure III.2). The boundary between the earth's internal magnetic field and the solar wind is known as the magnetopause; point interior to the magnetopause are referred to as being with the earth's magnetosphere (~5 $cm^{-3}$) **[71].**

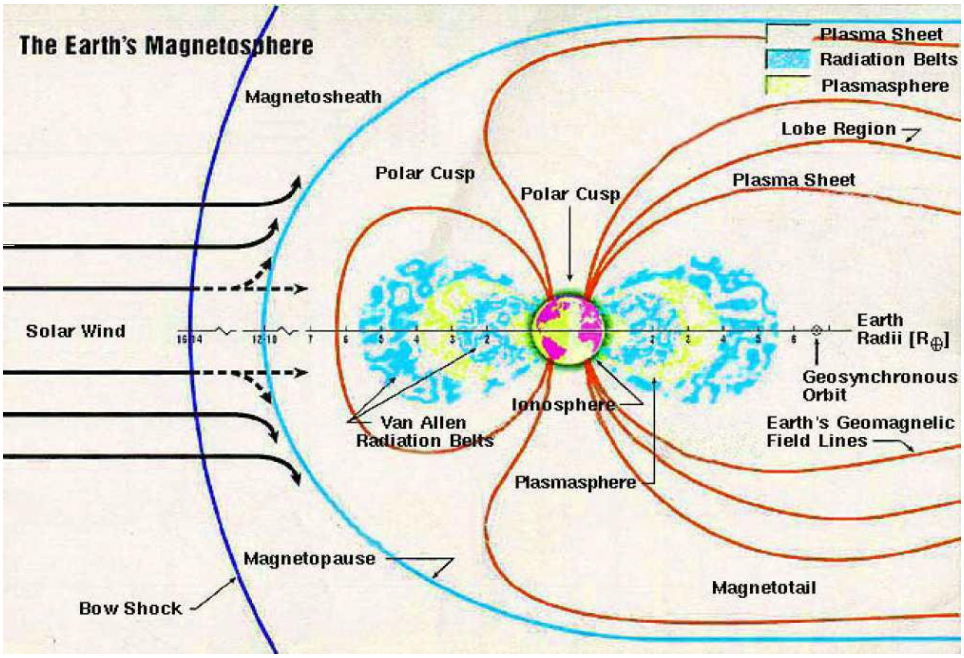


**Figure III.2: The solar wind and radiation belts surrounding the earth.**

### III.2.2. Solar flares:

The other solar-induced radiation environment is solar "flares" (The general term flare is used for convenience to represent all types of solar radiation events). When a magnetic disruption in the solar photosphere occurs, a variety of radiation types and energies erupt from the sun into space. This flare can produce energetic protons (up to 500 MeV) and heavy ions in a lesser extend (up to 10 MeV/nucleon) **[72].**

An important influence on solar particle radiation (and all transient environments) is the earth's magnetic field. The magnetic forces that cause charged particles to be trapped, also act on charged particles in flares. For a given magnetic field strength, an incident particle energy is required to penetrate that magnetic field.

All lower energy particles are deflected along the magnetic field lines. This magnetic screening can be significant for satellites in low-earth orbit **[73]**.

### III.2.3. Cosmic rays:

Cosmic rays originate from two sources, the sun (solar) and sources outside our solar system (galactic). Galactic cosmic rays are always present. In the absence of solar activity, cosmic radiation is composed entirely of galactic radiation. Outside of our solar system, the spectrum of galactic cosmic rays is believed to be uniform. It consists mostly of protons (85%) and alpha particles (helium nuclei) (14%). Less than 1% of the galactic cosmic ray spectrum is composed of high-energy heavy ions.

Heavy ions deposit more energy per unit depth in a material than protons **[74, 75]**. Their flux is usually low. However, during increased solar events the ion flux may increase, and hence it can cause considerable damage to space electronics.

From the point of view of space systems it is particles in the energy range 1-20 GeV per nucleon which have most influence, because it is hard to shield against them and it is not possible to predict a coming impact.

As with the solar flare environment, this radiation source is significant in the near-earth environment. The galactic cosmic rays is affected in the same manner as solar particles due to the effects of the earth's magnetic field (i.e., low altitude equatorial orbits will receive significant screening, while higher inclination or altitude receive less) **[73]**.

As cosmic rays penetrate into the magnetosphere, low-energy particles are attenuated, modifying the cosmic ray spectrum. Only the more energetic particles are able to penetrate the magnetosphere. Since the galactic cosmic rays are energetic. Therefore, they are capable of penetrating deep into semiconductor devices **[76]**.

### III.2.4. Trapped particles in Van Allen Belts:

The Van Allen radiation belts consist mainly of electrons and protons. They originate from the decay of neutrons produced by the interaction of cosmic rays with the low altitude atmospheric particles. These neutrons decay to yield protons, and electrons. Electrons and protons are magnetically trapped by the earth's magnetic field in regions called Van Allen belts. The trapped radiation of the Van Allen belts may also result from the acceleration of particles by magnetic storm activities or from solar flares **[76]**.

The trapped particles move helically around the geomagnetic field lines. There are basically two helical motions of the trapped particles between points near the north and the south poles: sliding motion along the geomagnetic field lines and bouncing motion along a line. Additionally, there is also a longitudinal drift around the earth. Electrons drift to the east, while protons drift to the west **[77]** (Figure III.3).

The trapped radiation belts extend from approximately 500 km to about 12 earth radii (roughly 76,000 km) **[73-74]** (One earth radius is equal to 6380 km, referenced to the centre of the earth, i.e., one earth radius is at the earth's surface).

Radiation belts are divided into two belts (Figure III.4), an inner belt extending to 2.5 earth radii, and an outer belt extending to 12 earth radii **[74]**.

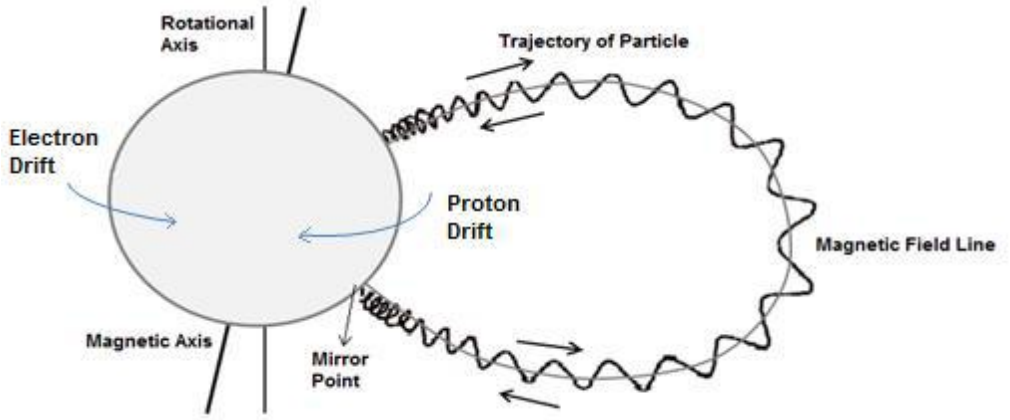


**Figure III.3: Charged particle motion in the earth's magnetic field.**

The electron belts are divided into two zones, an inner zone extending to about 2.8 earth radii and an outer zone extending from 2.8 to 12 earth radii. The outer zone electrons have higher fluxes (~ 10 times) and energies than the inner zone electrons. For electrons with energies greater than 1MeV, the peak in flux is located between 3 and 4 earth radii. The maximum energy of trapped electrons is approximately 7 MeV in the outer zone; whereas, the maximum energy is less than 5 MeV for electrons in the inner zone **[74, 77]**. The inner zone regime is relevant to low earth orbits LEO while the outer zone is relevant to the Geostationary earth orbit GEO environment (see section III.3).

In contrast to electrons, the protons cannot be divided into inner and outer zones since the most energetic protons are concentrated closer to the earth. Also, the energy of the protons varies with position approximately inversely with proton energy. At about 3 earth radii, the proton energy is about 40 MeV, and at 4 earth radii about 8 MeV **[78]**.

There is another region where the radiation belts reach their lowest altitude is called as South Atlantic Anomaly (SAA).

In this region, the flux for protons with energies greater than 30MeV can be as much as $10^4$ times higher than in comparable altitudes over other regions of the earth. At higher altitudes the magnetic sphere is more uniform and the South Atlantic anomaly disappears **[74].**Therefore this region is an important source of radiation exposure for space systems travelling a low orbit inclination and low altitudes.

Here, it is worth to mention that the trapped electrons and protons in Van Allen belts are the most damaging particles on space solar cells.

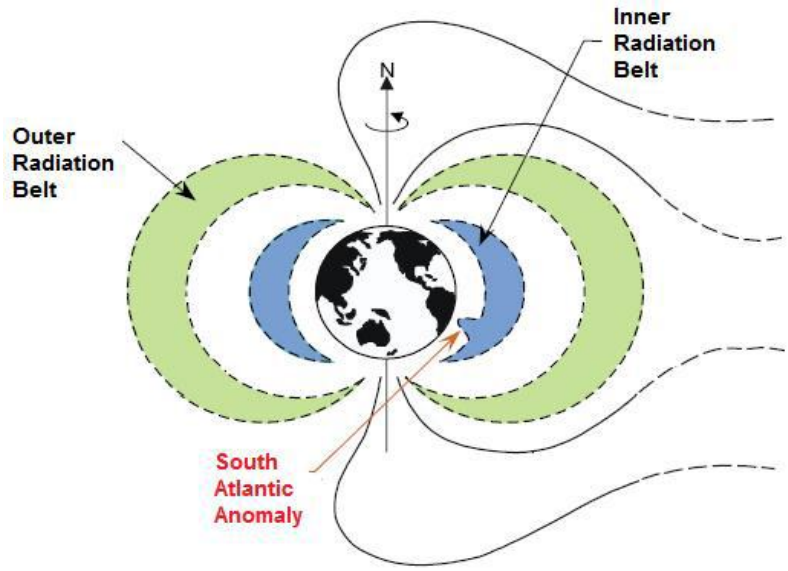


**Figure III.4: Illustration of trapped radiation belts around the earth.**

## III.3. Classification of orbits in a space mission:

The effects of the space environment on semiconductors vary depending on the system's distance from the earth. There are three main orbits for the purposes of radiation effects on orbiting electronic equipment. The detailed description of these orbits is given below.

### III.3.1. Low earth orbit (LEO):

Low earth orbit (LEO) is a circular earth orbit with altitudes in the range of 500–2000 km above the earth's surface. Spacecrafts in LEO are used for shorter missions with less fuel required. Therefore, lower costs in terms of power consumption are required for such missions. The LEO low inclination orbits (those passing near the Equator regions) are characterized by low levels of radiation damage from the trapped electrons and protons. High inclination orbits (those passing near or over the Polar regions) suffer greater radiation damage because shielding by the earth's magnetic field is not as effective as it is near the equator. Additionally, the South Atlantic Anomaly is more susceptible to higher radiation damage because the trapped radiation belts dip to lower altitudes. However, the radiation environment in these altitudes is less than the GEO orbits **[70]**. Therefore LEO is considered as the safest place for spacecrafts.

### III.3.2. Medium earth orbit (MEO):

A medium earth orbit (MEO) is the region of space around the earth above LEO and below GEO. MEO includes the space between 2000 and 36000 km from the earth surface. The

most common useful satellites in this region is for navigation and communication. The orbital periods of MEO satellites range from about 2 to nearly 24 h **[70, 77]**. The MEO orbits are attractive for both military and commercial applications.

Since a space system is mostly within the Van Allen belts in MEO, it is harshly exposed to radiation. The MEO orbit contain high fluences ($>10^{13}/cm^2/year$) of protons with energies less than 1 MeV, and moderate fluences ($>10^{11}/cm^2/year$) of protons with energies greater than 1 MeV. The electron spectrum is similar to GEO, but a higher fluence over 1 MeV **[70]**. For electronics, this is the worst place for, as radiation has the greatest influence due to the loss of shielding from the earth's magnetic field and the Van Allen radiation belts.

### III.3.3. Geostationary earth orbit (GEO):

A geostationary orbits (GEO) is an orbit located at a distance of 36000 km about the earth equator, and circulate in the direction of earth rotation. The satellites in this orbit rotate at the same speed as the earth, meaning that it will continuously be above the same place on the surface of the earth making them valuable for monitoring weather, communication and surveillance.

The GEO spacecrafts are used mainly for commercial telecommunication and designed for longer lifetime (15 ~ 20 years) **[70, 75]**. The main environmental concern on solar array is radiation damage of solar cells primarily from the trapped electrons. Trapped protons are lower in number compared with electrons in this orbit, although still significant. In addition, since the geomagnetic shielding in GEO is significantly weaker, the flux from high-energy proton emission during solar flares may be very damaging to the solar cell. Solar array performance degradation during a single solar flare activity may be equal or greater than that accumulated after a full year or lifetime of spacecraft exposure to the normal trapped radiation fluxes **[70, 75]**. These arrays may also face the temperature extremes while roaming in and out of the eclipse that occurs only for a short period of year **[75]**.

Spacecrafts in GEO are planned for a long operational life times. These longer lifetimes mean solar array is exposed to the higher level of radiation fluxes. The most important solar cell characteristics for these missions are high end-of-life (EOL) efficiency; a characteristic that can be achieved significantly by improved efficiency, resistance to radiation damage, and lightweight **[70, 75]**.

## III.4. Radiation Interaction with matter:

The space radiation environment consists of many forms of radiation which interact with the material and may affect electronic components. Electrons, protons, photons, alpha particles and heavier ions are the primary concern of these interactions.

Radiation interactions can be classified into two categories: charged particle and photon interactions. When the material is bombarded by radiation, the nature of the interaction between the particle and the material depends on several properties. The relevant particle properties are mass, charge, and kinetic energy. Material properties of importance are mass, charge, and density. In the next sections the various types of interactions will be described

### III.4.1. Photon interactions:

Electromagnetic waves have particle-like properties as discrete levels of energy, called photons. Photons have zero rest mass and are electrically neutral. Gamma rays and X-rays are the two examples of high energy photons. The interactions of photons occur through three main processes: the photoelectric effect, Compton scattering and pair production. In all three cases, the interaction produces energetic free electrons.

For the photon energies from 50 keV to 20 MeV, the photoelectric effect, Compton scattering and electron-positron (e-e+) pair production mechanisms of interaction dominate over all others. Among those three effects, the photoelectric effect dominates at the lower photon energies (<50 eV), e-e+ pair production is important only for photon energy higher than 20 MeV. Compton scattering dominates at intermediate energies **[79]**.

#### III.4.1.1. Photo-electric effect:

In the photoelectric (photon-electron) interaction, a photon transfers all its energy to an electron located in one of the atomic shells (usually the K-shell). The electron is ejected from the atom by this energy and begins to pass through the surrounding matter. The photoelectric effect is illustrated in Figure III.5.

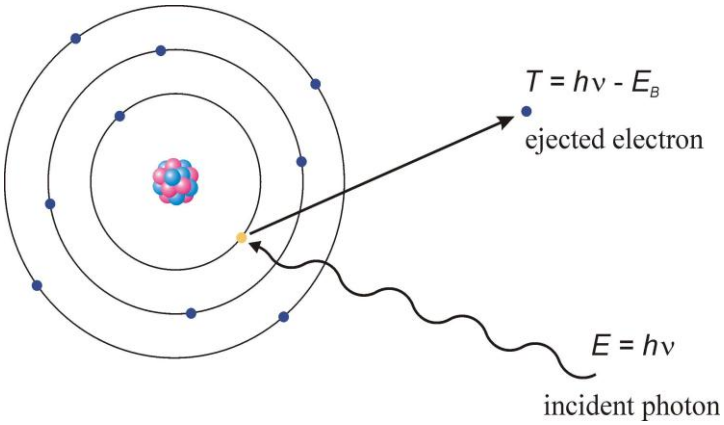


**Figure III.5: Illustration of the photo electric effect.**

The photon's energy is divided into two parts by the interaction. A portion of the energy is used to overcome the electron's binding energy and to remove it from the atom. The remaining energy is transferred to the electron as kinetic energy. The kinetic energy of the ejected electron is given by the Einstein formula:

$$T = h\nu - E_B \qquad \text{III.1}$$

Where $h$ is Planck constant, $\nu$ is the frequency of the incident photon and $E_B$ is the binding energy of the electron.

Since the interaction creates a vacancy in one of the electron shells, typically the K, an electron moves down to fill in. If a K-shell electron was involved, then an L-shell electron will drop into the remaining empty state. Either a characteristic X-ray or a low-energy Auger electron is emitted from the L shell, depending on the value of the atomic number Z of the material **[79]**.

### III.4.1.2. Compton scattering:

In the Compton effect or Compton scattering only a portion of the energy is absorbed and a photon is produced with reduced energy. This photon leaves the site of the interaction in a direction different from that of the original photon. The other part of the initial photon energy is imparted to a free electron. The process of Compton scattering is illustrated in Figure III.6.

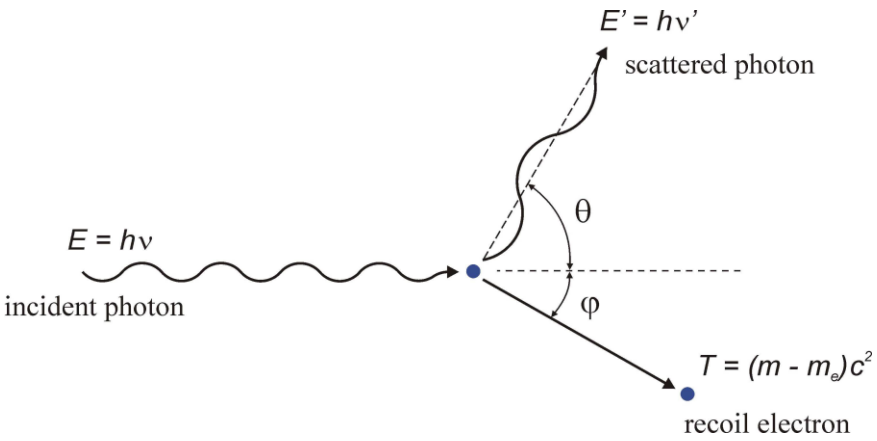


**Figure III.6: Illustration of the Compton scattering.**

In the Compton Scattering, the photon has an energy $E = h\nu = \frac{hc}{\lambda}$ and momentum related by the relativistic equation for particles of zero rest mass, namely $p = \frac{h\nu}{c}$, where $\nu$ is the frequency, $\lambda$ is the wavelength of the photon, c is the speed of light, and $h$ is Plank's constant.

After the Compton Scattering, photon scatters with an angle $\theta$ by giving a portion of energy to the electron. The scattered photon has energy $E' = h\nu'$.

Obviously, $E$ must be less than $E'$. As a result, the wavelength of the scattered photon $\lambda'$ must be longer than the wavelength of the incident photon. The decrease in the energy of the photon appears as a kinetic energy T.

According to the quantum hypothesis and by applying the laws of conservation of momentum and energy, the change in the wavelength is given by:

$$\Delta\lambda = \lambda' - \lambda = \frac{h}{mc}(1 - \cos\theta) \qquad \text{III.2}$$

Where $m$ is the mass of the electron and $\theta$ is the angle between the trajectories of the incident and scattered photon.

### III.4.1.3. Pair production:

In a pair-production interaction, the photon interacts with the nucleus in such a manner that its energy is converted into matter. The interaction produces a pair of particles, an electron and a positron (Positron is the anti-particle of the electron and has the same properties of an electron but positively charged)**.** Figure III.7 shows the process of the pair production phenomenon.

The pair production process occurs only when the energy of the photon is greater than 1.02 MeV **[79, 80]** which is the sum of rest mass energy of electron and positron. If the energy

of the photon is greater than 1.02 MeV, the electron and positron can take away the remaining energy in the form of kinetic energy.

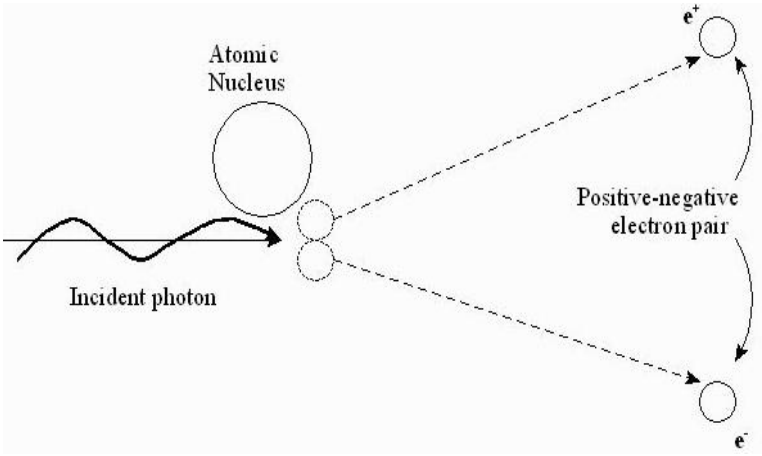


**Figure III.7: Illustration of the pair production process.**

### III.4.2. Charged particle interaction:

The charged particles are considered in two separate groups, the heavy and the light charged particles, Electrons and positrons from the light charged particle group and all others from the heavy charged particle group. Charged particles interact with the electrons and nuclei of atoms. The two major effects that characterize the passage of a charged particle through a material are an energy loss by the particle and a deflection of the same from its incident direction. The interaction mechanism varies with the energy, the mass and the charge of the incoming particle and the characteristics of the target too.

Charged particles can interact with a target material in several ways, the most dominant interactions are:

* Inelastic collisions with the atomic electrons: in this interaction the particle interacts with the surrounding charge of the atom (i.e., the electrons). In the case of heavy charged particles the effect is to transfer energy to the atom. The newly acquired energy raises the energy state of the atom to a higher level and causes an excitation or ionization of electrons within the atom **[73]**. For light charged particles, there are two main processes contributing to the continuous energy loss; ionization and bremsstrahlung (FigureIII.8). The bremsstrahlung process is inversely proportional to the squared mass of the incident particle, thus it substantially accounts for radiation losses only for electrons. At electron energies above a few tens of MeV, bremsstrahlung dominates completely other processes **[81]**.

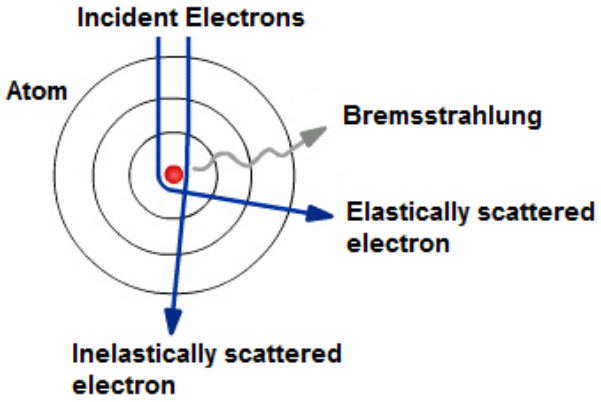


**Figure III.8: Schematic illustration of charge particle interactions.**

* Elastic collisions with atomic nuclei: Energetic charged particles may have coulombic interactions with the positive charge of the atomic nucleus through Rutherford scattering which is schematically shown in Figure III.9. In some cases the amount of energy transferred to the atom can dislodge the atom from its lattice position **[4]**.

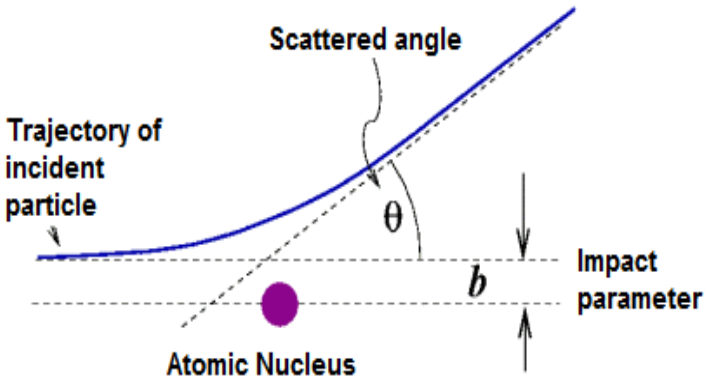


**Figure III.9: Schematic illustration of Rutherford scattering.**

* Inelastic collisions with atomic nuclei: Inelastic scattering involves capture of the incident particle by the nucleus of the target atom, and subsequent emission of that particle at a lower energy. Kinetic energy is lost in this process, and the target nucleus is left in an excited state. The excited nucleus returns to its original state by emission of a gamma ray. The kinetic energy of the emitted particle is reduced, compared to the incident particle, by the energy of the gamma ray. Inelastic scattering can also cause displacement of the target atom to occur **[79]**.

## III.5. Effects of radiation on solar cells:

When energetic particles penetrate a semiconductor material they transfer energy by collisions with the host atoms of the crystal lattice. For radiation effects on electronics in space, two basic mechanisms dominate:

Displacement of atoms from their lattice sites (displacement damage), and generation of electron-hole pairs (ionization). In general, particles passing through electronic materials deposit a portion of their energy into ionization and the remainder into displacement **[79]**.

Figure III.10 classifies the main effects that are produced by radiation in electronic devices.

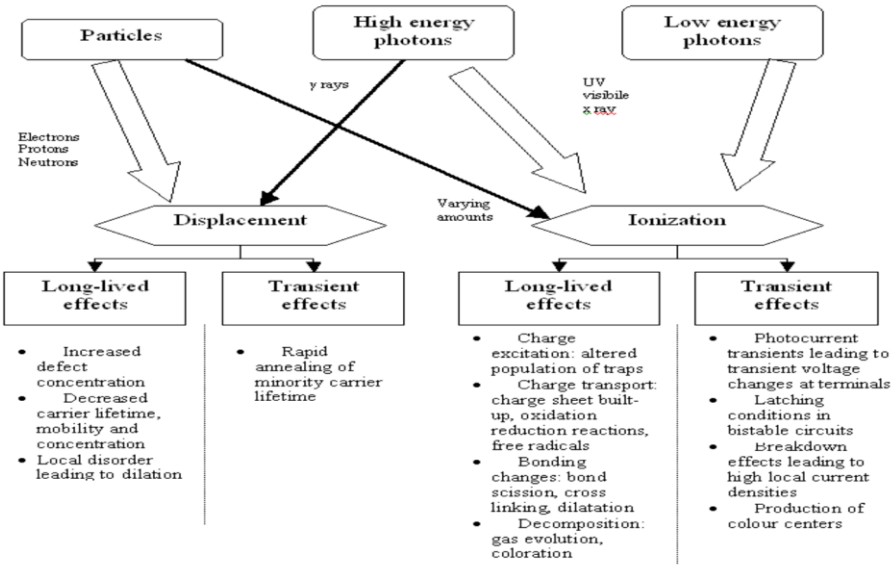


**Figure III.10: Classification of radiation effects [4].**

### III.5.1. Ionization:

In general, Ionization occurs when the bound electrons removed from their parent atoms.

Ionising radiation in Silicon excites the electrons of the valence band to the conduction band, creating electron-hole pairs in much the same way that carrier pairs are generated by visible light. Although an optical photon of energy equal to or greater than 1.1 eV will create an electron-hole pair, roughly three times this amount of energy must be absorbed from a high energy particle to produce the same carriers **[82]**.

Radiation may affect solar cell array materials by several ionisation related effects. The reduction of transmittance in solar cell cover glasses is an important effect of ionising radiation. The darkening is caused by the formation of colour centres in glass or oxide materials. The colour centres form when ionising radiation excites an orbital electron to the

conduction band. These electrons become trapped by impurity atoms in the oxide to form charged defect complexes which can be relatively stable at room temperature.

### III.5.2. Displacement damage:

Displacement damage occurs when sufficient energy is transferred from an incident energetic particle to a lattice atom to dislodge it from its normal location. Using Si as an example, the Si atom initially displaced by an incoming particle is known as the primary knock-on atom (PKA) or the primary recoil. (The PKA, or recoil, carries a net charge that depends on its kinetic energy) **[83]**.The absence of an atom from its normal lattice site is referred to as a vacancy, and this is one example of a radiation-induced defect.

Various types of defects can occur in irradiated Silicon. Simple defects are also referred to as point, or isolated, defects. Regions containing large numbers of relatively closely spaced defects can also occur, and such a grouping is termed a defect cluster, or displacement cascade (Figure III.11). When a displaced atom moves into a nonlattice position, the resulting defect is referred to as an interstitial. The vacancy interstitial combination is called a close pair, or a Frenkel pair. Two adjacent vacancies form a defect known as the divacancy; a di-interstitial can also occur. Larger local groupings of vacancies are also observed in irradiated Silicon. Vacancies and interstitials can also form additional types of simple defects when they are adjacent to impurity atoms. Such defects are termed defect-impurity complexes. For example, the vacancy-phosphorus pair is a defect that is observed in Silicon. If a displaced atom is given a relatively large amount of kinetic energy by an incident particle, the primary knock-on can displace many additional atoms, and thereby cause the formation of a region of disorder, or defect cluster. This process can occur for incident neutrons with energy in the MeV range. On the other hand, MeV electrons and photons produce primarily isolated defects in Silicon **[79]**.

In space, the particles producing displacement damage include protons, electrons, and neutrons. For electrons, an incident particle energy of ~150 keV is the minimum required to produce displacements in Silicon. For protons, the threshold is ~100eV **[79]**.

The primary effect of displacement damage is the creation of deep and shallow level traps in the material. The shallow level traps can compensate majority carriers and cause carrier removal. Deep level traps can act as generation, recombination, or trapping centres. These centres can decrease the minority carrier lifetime, increase the thermal generation rate of electron-hole pairs, and reduce the mobility of carriers **[74]**.

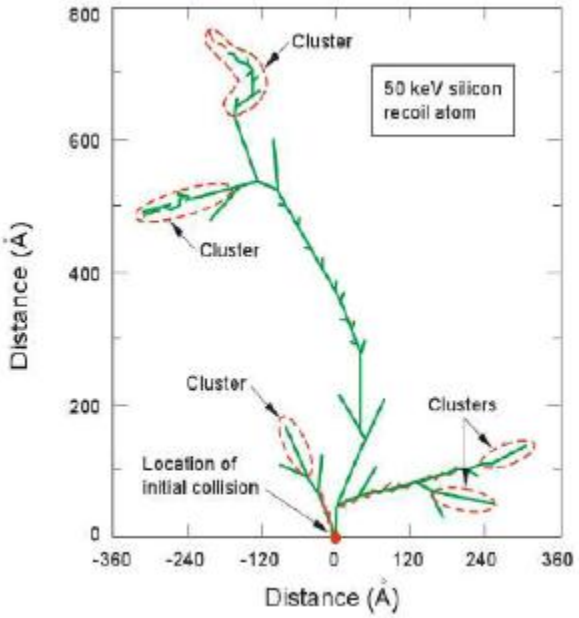


**Figure III.11: Displacement cascade damage from the movement of a Silicon atom after the primary collision [4].**

## III.6. Defects induced by radiation:

As mentioned in the previous section, the primary effect of particle irradiation of a semiconductor material is displacement damage. Displacement damage effects are important for photovoltaic (PV) devices operated in the space radiation environment. Extensive testing and analyses of such effects in solar cells have been performed for many decades. The basic mechanisms of PV device response and representative cell behaviour have been reported widely for Si, GaAs, and multijunction cells **[7, 82, 84]**. The majority of materials used in PV technologies for space applications (i.e., Si, GaAs, InGaP, Ge) are affected almost solely by displacement damage **[83]**.

We will focus in the next section on the defects induced by electrons in Silicon solar cells since it is the material studied in this work.

### III.6.1. Defects induced in Silicon solar cells:

The largest number of studies is found on irradiation of Silicon solar cells with electrons (typically 1 MeV) and protons, because they are the most damaging particles in a space mission. Electrons and protons introduce a variety of defects in the semiconductor lattice. These defects can form energy levels within the forbidden gap of the semiconductor forming charge trapping centres. There have been many studies to determine the properties of these defects. The most widely used technique for the study of radiation-induced defects

is the Deep Level Transient Spectroscopy (DLTS) **[85]**. DLTS is used to measure the energy positions, capture cross sections and concentration of defects.

In n-type Silicon, it has been shown that vacancies react with oxygen impurities to form close coupled vacancy-oxygen pairs (V-O) known as A centre, and with impurity donor atoms, such as phosphorus , to form close coupled vacancy-donor pairs (V-P) known as E centre. Both defects are electrically active and can become negatively charged by accepting an electron from the conduction band. The acceptor energy levels of the V-O and V-P pairs are 0.17 eV and 0.4 eV below the bottom of the conduction band **[82]**. These defects are recombination centres and their formation during electron irradiation of n-type Silicon reduces the minority carrier lifetime.

The V-P pair anneals rapidly near 150°C and the V-O pair anneals rapidly near 350°C. The introduction rates (change in defect concentration per unit fluence) for these defects are in the range of 0.1 to 0.3 $cm^{-1}$ for 1 MeV electrons **[82]**.

P-type Silicon is preferred over n-type because it turned out that it has better tolerance of radiation damage for space applications **[86]**

An example of a radiation-induced defect spectrum as measured in a p-type Si (B doped Silicon) solar cell after 1 MeV electron irradiation using deep level transient spectroscopy (DLTS) is shown in Figure III.12.

A large concentration of a minority-carrier trap with activation energy of about ($E_C$- 0.18 eV) has been observed, as well as the majority-carrier traps at around ($E_V$+0.18 eV), and ($E_V$+0.36 eV).

The defect ($E_C$-0.18 eV) is related to interstitial -Boron-interstitial oxygen complex ($B_i$-$O_i$), While the defects ($E_V$+0.18 eV) and ($E_V$+0.36 eV) are identified as a divacancy V-$V^+$, and an interstitial-carbon–interstitial-oxygen complex ($C_i$–$O_i$) respectively **[7, 12]**.

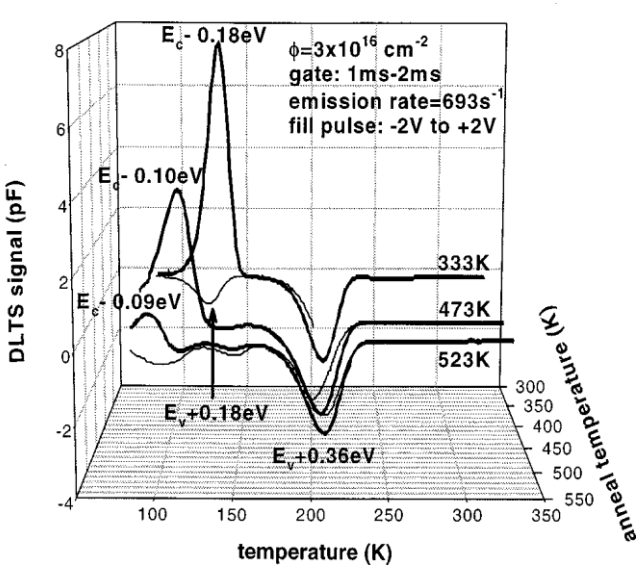


**Figure III.12: DLTS spectra of a Si diode irradiated with $3\times10^{16}$ $cm^{-2}$ 1 MeV electrons as a function of anneal temperature [7, 12].**

The most important defects induced by 1 MeV electrons irradiation in a p-type Silicon solar cell and their possible identification are summarised in Table III.1.

| Activation energy $E_a$(eV) | Possible identification |
|---|---|
| $E_V + 0.18$ | V-V |
| $E_V + 0.36$ | $C_i$–$O_i$<br>$C_s$–$C_i$ |
| $E_C - 0.18$ | $B_i$-$O_i$ |

Table III.1: Trap levels, and possible identifications of defects induced by 1 MeV electrons **[7, 12]**.

The effects of the radiation-induced defects on the solar cell electrical characteristics depend on the location of the defect energy level within the bandgap. Those defect levels lying nearer to mid-gap tend to act as free charge carrier traps and recombination centres. The presence of such defect levels reduces the minority carrier lifetime ($\tau$) and diffusion length ($L$). The decrease in $L$ with the introduction of defects is given by **[20]**:

$$\frac{1}{L_\varphi^2} = \frac{1}{L_0^2} + \sum I_{ri}\sigma_i v\varphi/D = \frac{1}{L_0^2} + K_L\varphi \qquad \text{III.3}$$

where suffixes 0 and $\varphi$ show before and after irradiation, respectively, $I_{ri}$ is the introduction rate of $i_{\text{th}}$ recombination centre by irradiation, $\sigma_i$ the capture cross section of minority-carrier by the $i_{\text{th}}$ recombination centre, $v$ the thermal velocity of minority-carrier,

$D$ the minority-carrier diffusion coefficient, $K_L$ the damage coefficient for minority-carrier diffusion length, and $\varphi$ is the fluence.

Those defects lying closer to one of the bands tend to act as majority charge carrier traps. The capture of a majority carrier can cause compensation of the material thus reducing the carrier concentration. This is referred to as carrier removal and such trapping centres are referred to as compensation centres.

We will see the effect of these defects on the performance of a Silicon solar cell in chapter V.

# Chapter IV
# Simulation of solar cells and SCAPS Simulator

## IV.1. Introduction:

Computational simulation is a technique of studying and analysing the behaviour of a real device or an imaginary system by representing it with a computer application. Simulation is based on a mathematical model that describes the system being studied.

Numerical simulation of semiconductor devices provides an effective tool for device design in many cases of practical relevance. It is an important procedure for the optimization of novel semiconductor devices.

Concerning solar cells; numerical simulation has proven over the years to be a viable tool for studying and understanding the properties of solar cell devices such as the optical, electrical and mechanical properties of complex solar cell devices. Advantages of simulation are the calculation of the electrical behaviour before the fabrication process, the calculation and visualization of inner-electronic values, which are not measurable. It also helps to reduce processing cost and time spent on solar cell device fabrication by providing useful information on how to vary the production parameters to improve the device performance.

In this chapter we will first present the physical model used to simulate the operation of semiconductor-based devices.

We will first detail the calculation of the carrier concentration in a semiconductor. Then, the basic equations of semiconductor physics will be presented. The optical generation model and the recombination phenomena will also be presented. Then, the SCAPS simulator, used during our study, will be reviewed.

## IV.2. Physical basis for semiconductor device modelling:

### IV.2.1. Semiconductors at thermal equilibrium:

Any operation of a semiconductor device depends on the carriers that carry charge inside the semiconductor and cause electrical currents. In order to understand device operation it is important to know the precise number of these charge carriers.

Firstly we assume that the semiconductor is under thermal equilibrium. This implies that no external forces such as voltages, electric fields. Magnetic fields or temperature gradients

are acting on the semiconductor. In this case all properties of the semiconductor will be independent of time **[35]**.

### IV.2.1.1. Carrier concentration:

Firstly, we consider the intrinsic case without impurities added to the semiconductor.

In a semiconductor, two types of charge carrier, the electron and the hole, can contribute to a current. In order to determine the carrier concentration one has to know the function of density of allowed energy states of electrons and the occupation function of the allowed energy states. The density of energy states function, $N(E)$, describes the number of allowed states per unit volume and energy. The occupation function is the well-known Fermi-Dirac distribution function, $f(E)$, which describes the ratio of states filled with an electron to total allowed states at given energy $E$.

The density of energy states at an energy $E$ in the conduction band $N_C(E)$ close to $E_C$ and in the valence band $N_V(E)$ close to $E_V$ are given by **[87]**:

$$N_C(E) = \frac{1}{2\pi^2}\left(\frac{2m_e}{\hbar^2}\right)^{\frac{3}{2}}(E - E_C)^{\frac{1}{2}} \qquad \text{IV.1.a}$$

$$N_V(E) = \frac{1}{2\pi^2}\left(\frac{2m_h}{\hbar^2}\right)^{\frac{3}{2}}(E_V - E)^{\frac{1}{2}} \qquad \text{IV.1.b}$$

Where $m_e$and $m_h$ are the effective mass of electrons and holes, respectively. $E_C$ is the bottom of the conduction band, and $E_V$ is the top of the valence band.

The Fermi-Dirac distribution function is given by:

$$f(E) = \frac{1}{1+\exp\left(\frac{E-E_F}{k_BT}\right)} \qquad \text{IV.2}$$

With $k_B$ is the Boltzmann constant, $T$ the absolute temperature and $E_F$ the Fermi level.

For energy much greater than $k_BT$ (i.e., $E - E_F \gg k_BT$ ) the Fermi function can be approximated by the Boltzmann function:

$$f(E) = \frac{1}{1+\exp\left(\frac{E-E_F}{k_BT}\right)} \cong exp\left[-\frac{(E-E_F)}{k_BT}\right] \qquad \text{IV.3}$$

The density of free electrons $(n)$ (occupied conduction-band levels) is given by the total number of states $N_C(E)$ multiplied by the occupation function $f(E)$, integrated over the conduction band **[22]**:

$$n = \int_{E_C}^{\infty} N_C(E).f(E).dE \qquad \text{IV.4}$$

By replacing equations IV.1a and IV.3 into IV.4 the resulting expression for *n* is obtained after solving the equation. The full derivation can be found for example in references **[22, 35]**:

$$n = N_C exp\left(\frac{E_F - E_C}{k_B T}\right) \qquad \text{IV.5}$$

The parameter $N_C$ is called the effective density of states in the conduction band which is:

$$N_C = \left(\frac{2\pi m_e k_B T}{h^2}\right)^{\frac{3}{2}} \qquad \text{IV.6}$$

An expression for the hole concentration can be derived in the same way. The probability of an energy state being occupied by a hole is the probability of it not being occupied by an electron, i.e., $1 - f(E)$. Therefore,

$$p = \int_{-\infty}^{E_V} N_V(E).[1 - f(E)].dE \qquad \text{IV.7}$$

Applying the Boltzmann approximation we can get:

$$1 - f(E) \cong exp\left[-\frac{(E_F - E)}{k_B T}\right] \qquad \text{IV.8}$$

Substituting Equations (IV.1b) and (IV.8) into Eq. (IV.7) yields

$$p = N_V exp\left(\frac{E_V - E_F}{k_B T}\right) \qquad \text{IV.9}$$

$$N_V = \left(\frac{2\pi m_h k_B T}{h^2}\right)^{\frac{3}{2}} \qquad \text{IV.10}$$

$N_V$ is the effective density of states of the valence band. The values of $N_C$and $N_V$ differ only because $m_e$ and $m_h$ are different. $N_C$ and $N_V$vary somewhat from one semiconductor to another because of the variation in the effective masses, too **[88]**.

$N_C$ and $N_V$ for Ge, Si, and GaAs are listed in Table IV.1.

| Material | Effective density of states of the conduction band ($N_C$) ($cm^{-3}$) | Effective density of states of the valence band ($N_V$) ($cm^{-3}$) |
|---|---|---|
| Ge | $1.04 \times 10^{19}$ $cm^{-3}$ | $6.0 \times 10^{18}$ $cm^{-3}$ |
| Si | $2.8 \times 10^{19}$ $cm^{-3}$ | $1.04 \times 10^{19}$ $cm^{-3}$ |
| GaAs | $4.7 \times 10^{17}$ $cm^{-3}$ | $7.0 \times 10^{18}$ $cm^{-3}$ |

**Table IV.1: Values of $N_C$ and $N_V$ for Ge, Si, and GaAs at $300^0$ K [88].**

### IV.2.1.2. Intrinsic carrier concentration:

In an undoped (intrinsic) semiconductor in thermal equilibrium, the number of electrons in the conduction band and the number of holes in the valence band are equal; $n = p = n_i$, where $n_i$ is the intrinsic carrier concentration.

When multiplying the corresponding sides of Equations IV.5 and IV.9 one obtains:

$$np = N_C N_V exp - \frac{(E_C - E_V)}{k_B T} = N_C N_V exp - \frac{E_g}{k_B T} \quad \text{IV.11}$$

Where $E_g$ is the forbidden gap:

$$E_g = E_C - E_V \quad \text{IV.12}$$

Equation IV.11 states that the $np$ product is a constant for a given semiconductor and *T*, independent of the dopant concentrations. It is an important relationship and is usually expressed in the following form:

$$np = n_i^2 \quad \text{IV.13}$$

$$n_i = \sqrt{N_C N_V} exp\left(-\frac{E_g}{2k_B T}\right) \quad \text{IV.14}$$

The equation IV.13 is called law of mass action and it valid for any semiconductor at equilibrium. The intrinsic carrier concentration in a semiconductor is dependent only on the band gap $E_g$. It is a material property (at a given temperature).

When we denote the position of the Fermi level in the intrinsic material $E_i$ one can write from equations IV.5 and IV.9:

$$n_i = N_C exp\left(\frac{E_i - E_C}{k_B T}\right) = N_V exp\left(\frac{E_V - E_i}{k_B T}\right) \quad \text{IV.15}$$

From Equation IV.15 we can deduce easily the position of $E_i$, which is given by:

$$E_i = \frac{E_C + E_V}{2} + \frac{k_B T}{2} ln\left(\frac{N_V}{N_C}\right) \quad \text{IV.16}$$

The Fermi level $E_i$ lies close to the midgap; a slight shift is caused by the difference in the effective densities of the valence and conduction band.

Also using Equation IV.15 and $E_i$ as the reference energy, we have the alternate equations for N-type materials;

$$n = n_i exp\left(\frac{E_F - E_i}{k_B T}\right) \text{ or } E_F - E_i = k_B T ln \frac{n}{n_i} \quad \text{IV.17}$$

and for P-type materials;

$$p = n_i exp\left(\frac{E_i - E_F}{k_B T}\right) \text{ or } E_i - E_F = k_B T ln \frac{p}{n_i} \quad \text{IV.18}$$

**IV.2.1.3. Donors and acceptors:**

The number of electrons and holes in their respective bands, and hence the conductivity of the semiconductor, can be controlled through the introduction of specific impurities, or dopants, called donors and acceptors. The doped semiconductor, called an extrinsic material.

There are four types of charged species in a semiconductor: electrons, holes, positive donor ions $N_d$, and negative acceptor ions $N_a$. Generally, all samples are free of net charge.

The charge neutrality requires that the densities of the negative particles and positive particles are equal:

$$n + N_a = p + N_d \qquad \text{IV.19}$$

Equations IV.19 and IV.13 can be solved for n and p:

$$n = \frac{N_d - N_a}{2} + \left[\left(\frac{N_d - N_a}{2}\right)^2 + n_i^2\right]^{\frac{1}{2}} \qquad \text{IV.20.a}$$

$$p = \frac{N_a - N_d}{2} + \left[\left(\frac{N_a - N_d}{2}\right)^2 + n_i^2\right]^{\frac{1}{2}} \qquad \text{IV.20.b}$$

The equations IV.20.a and IV.20.b are rarely used. Instead, one of the following two cases is almost always valid:

**1.** $N_d - N_a \gg n_i$ (i.e., N-type material),

$$n = N_d - N_a \qquad \text{IV.21}$$

$$p = \frac{n_i^2}{n} \qquad \text{IV.22}$$

If furthermore, $N_d \gg N_a$, then

$$n = N_d \text{ and } p = \frac{n_i^2}{N_d} \qquad \text{IV.23}$$

The Fermi energy can then be written as:

$$E_F = E_i + k_B T ln\frac{N_d}{n_i} \qquad \text{IV.24}$$

**2.** $N_a - N_d \gg n_i$ (i.e., P-type material)

$$p = N_a - N_d \qquad \text{IV.25}$$

$$n = \frac{n_i^2}{p} \qquad \text{IV.26}$$

If furthermore, $N_a \gg N_d$, then

$$p = N_a \text{ and } n = \frac{n_i^2}{N_a} \qquad \text{IV.27}$$

The Fermi energy can then be written as:

$$E_F = E_i - k_B T ln\frac{N_A}{n_i} \qquad \text{IV.28}$$

**IV.2.2. Non-equilibrium carrier concentration:**

Most of semiconductor devices operate by the creation of charge carriers in excess of the thermal equilibrium values, these excess carriers can be created by optical excitation or by applying an electric field.

The creation of excess carriers (electrons and holes) means that the semiconductor is no longer in thermal equilibrium and the Fermi energy is strictly no longer defined. We can define two new parameters that apply to the non-equilibrium semiconductor: the quasi-Fermi energy for electrons and the quasi-Fermi energy for holes.

The concentrations of electrons and holes for the non-equilibrium are then given by:

$$n = N_C exp\left(\frac{E_{Fn\_}E_C}{k_B T}\right) \qquad \text{IV.29}$$

$$p = N_V exp\left(\frac{E_V - E_{Fp}}{k_B T}\right) \qquad \text{IV.30}$$

$E_{Fn}$ and $E_{Fp}$ are the electron and hole quasi-Fermi levels.

When electrons and holes are at equilibrium, $E_{Fn}$ and $E_{Fp}$ coincide and this is known as $E_F$.

### IV.2.3. Basis equations for semiconductor modelling:

The operation of most semiconductor devices, including solar cells, can be described by the so-called semiconductor device equations.

The basic equations for semiconductor-device operation describe the static and dynamic behaviour of carriers in semiconductors under external influences, such as applied field or optical excitation, both of which cause deviations from thermal equilibrium conditions.

#### IV.2.3.1. Poisson's equation:

The Poisson equation relates the electric potential to the space-charge density:

$$div(\varepsilon \nabla \psi) = -\rho \qquad \text{IV.31}$$

Where $\psi$ is the electrostatic potential, $\varepsilon$ is the local permittivity, and $\rho$ is the local space charge density.

The local space charge density is the sum of contributions from all mobile and fixed charges, including electrons, holes, and ionized impurities.

$$\rho = q(N_d + N_a + n + p) \qquad \text{IV.32}$$

Where $q$ is the elementary charge, $n$ is the electron concentration, $p$ represents the hole concentration, $N_a$ is the ionized acceptor concentration and $N_d$ is the ionized donor concentration.

The electric field is obtained from the gradient of the potential:

$$\vec{E} = \nabla \psi \qquad \text{IV.33}$$

**IV.2.3.2. Continuity equations:**

The continuity equation describes the behaviour of excess carriers with time and in space in the presence of electric fields and density gradients:

$$\frac{\partial n}{\partial t} = \frac{1}{q} div\overrightarrow{J_n} + G_n - R_n \qquad \text{IV.34}$$

$$\frac{\partial p}{\partial t} = -\frac{1}{q} div\overrightarrow{J_p} + G_p - R_p \qquad \text{IV.35}$$

where $n$ and $p$ are the electron and hole concentration, $J_n$and $J_p$ are the electron and hole current densities, $G_n$ and $G_p$ are the generation rates for electrons and holes, $R_n$and $R_p$are the recombination rates for electrons and holes.

In steady state $\frac{\partial n}{\partial t} = 0$ and $\frac{\partial p}{\partial t} = 0$.

**IV.2.3.3. Current-density equations:**

Derivations based upon the Boltzmann transport theory have shown that the current densities in the continuity equations may be approximated by a drift-diffusion model **[87]**. In this case, the current densities are expressed in terms of the quasi-Fermi levels $E_{Fn}$ and $E_{Fp}$ as **[22]**:

$$\vec{J}_n = \mu_n n \nabla E_{Fn} \qquad \text{IV.36}$$

$$\vec{J}_p = \mu_p p \nabla E_{Fp} \qquad \text{IV.37}$$

Where $\mu_n$ and $\mu_p$ are the electron and hole mobilities. The quasi-Fermi levels are linked to the carrier concentrations and the potential through the two Boltzmann approximations **[87, 89]**:

$$n = n_i exp\left(\frac{q\psi - E_{Fn}}{k_B T}\right) \qquad \text{IV.38}$$

$$p = n_i exp\left(\frac{-q\psi + E_{Fp}}{k_B T}\right) \qquad \text{IV.39}$$

These two equations may then be rewritten to define the quasi-Fermi levels **[89]**:

$$E_{Fn} = q\psi - k_B T ln\left(\frac{n}{n_i}\right) \qquad \text{IV.40}$$

$$E_{Fp} = q\psi + k_B T ln\left(\frac{p}{n_i}\right) \qquad \text{IV.41}$$

By substituting these equations into the current density expressions, the following current relationships are obtained:

$$\vec{J}_n = qD_n \nabla n - qn\mu_n \nabla\psi - \mu_n n(k_B T \nabla(lnn_i)) \qquad \text{IV.42}$$

$$\vec{J}_p = -qD_p \nabla p - qp\mu_n \nabla\psi - \mu_p p(k_B T \nabla(lnn_i)) \qquad \text{IV.43}$$

Where $D_n$ and $D_p$ are the diffusion constants for electrons and holes, respectively:

$$D_n = \frac{k_B T}{q}\mu_n \quad \text{IV.44}$$

$$D_p = \frac{k_B T}{q}\mu_p \quad \text{IV.45}$$

The final term in (IV.42) and (IV.43) accounts for the gradient in the effective intrinsic carrier concentration, which takes account of band-gap narrowing effects. Effective electric fields are defined whereby:

$$\overrightarrow{E_n} = -\nabla\left(\psi + \frac{k_B T}{q} lnn_i\right) \quad \text{IV.46}$$

$$\overrightarrow{E_p} = -\nabla\left(\psi - \frac{k_B T}{q} lnn_i\right) \quad \text{IV.47}$$

Which then allows the more conventional formulation of drift-diffusion equations to be written.

$$\vec{J_n} = qn\mu_n\overrightarrow{E_n} + qD_n\nabla n \quad \text{IV.48}$$

$$\vec{J_p} = qn\mu_p\overrightarrow{E_p} - qD_p\nabla p \quad \text{IV.49}$$

### IV.2.4. Optical generation of electron-hole pairs:

Generation of electron–hole pairs by the absorption of sunlight is important to the operation of solar cells. Electrons and holes, contribute to the transformation of energy carried by light into electrical energy.

The number of generated electron-hole pairs depends on the number of incident photons $S_0\ (v)$ (per unit area, unit time and unit energy). Inside the semiconductor the photon flux $S(x, v)$ decreases exponentially according to **[90]**:

$$S(x, v) = S_0\ (v)\exp(-\alpha x) \quad \text{IV.50}$$

Where $v$ is the frequency. The absorption coefficient $\alpha(v)$ is determined by the absorption process in the semiconductor.

The generation rate $G(x, v)$ of electron-hole pairs at a distance $x$ from the semiconductor surface is given by **[90]**:

$$G(x, v) = \alpha(v)S_0(v)(1 - R)\exp(-\alpha x) \quad \text{IV.51}$$

Where $R$ is the reflectance.

Here it is assumed that each absorbed photon generates one electron-hole pair.

### IV.2.5. Recombination's phenomenon in semiconductors:

Recombination is a process whereby electrons and holes are annihilated or destroyed.

There are several recombination mechanisms important to the operation of solar cells: radiative or band-to-band recombination, Auger recombination, and recombination through defect or traps in the bandgap (often referred to as Shockley-Read-Hall recombination or SRH). These three processes are illustrated in Figure IV.1.

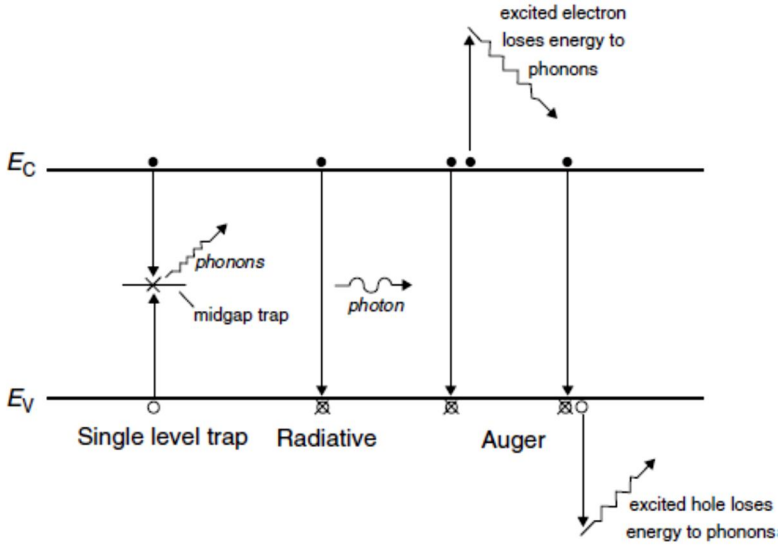


**Figure IV.1: The different recombination processes in semiconductors [28].**

#### IV.2.5.1. Radiative recombination:

Radiative recombination is the inverse of the optical generation. This process occurs when a free electron falls directly from the conduction band and recombines with a free hole in the valence band and emits a photon with energy equal to the difference in energy of the starting and final states. Radiative recombination is very important in direct bandgap semiconductors but not as important in indirect semiconductors such as Silicon since a phonon must also be absorbed or emitted for an electron to make the transition **[28]**.

The net recombination rate due to radiative processes is given by:

$$R_\lambda = B(np - n_i^2) \qquad \text{IV.52}$$

Where $B$ is a material constant.

For n-type semiconductors under low injection ($p_0 \leq p \ll n_0$) the net recombination rate can be written as:

$$R_\lambda \approx \frac{p-p_0}{\tau_{\lambda,p}} \qquad \text{IV.53}$$

The effective lifetime due to radiative recombination, $\tau_{\lambda,p}$, is given by:

$$\tau_{\lambda,p} = \frac{1}{n_0 B} \qquad \text{IV.54}$$

**IV.2.5.2. Auger recombination:**

Auger recombination is fairly similar to radiative recombination, except that the energy of transition is given to an electron or hole which becomes excited in the conduction or the valence band respectively (Figure IV.1). The net recombination due to Auger recombination is given by:

$$R_{Auger} = C_n n^2 p + C_p n p^2 \qquad \text{IV.55}$$

Where $C_n$and $C_p$ are the Auger coefficients for electrons and holes, respectively.

The most commonly used values for the Auger coefficients were determined by Dziewior and Schmid ($C_n$=2.8×10$^{-31}$ cm$^6$s$^{-1}$ and $C_p$=0.99×10$^{-31}$ cm$^6$s$^{-1}$) for Si with a doping concentration greater than 5×10$^{18}$ cm$^{-3}$ **[91]**.

Auger recombination is relevant in semiconductors with high carrier concentration or also under high level injection (e.g. concentrator solar cells).

**IV.2.5.3. Shockley-Read-Hall recombination (SRH):**

The Shockley-Read-Hall Recombination recombination typically dominates the net recombination rate in low quality materials with a high defect density.

The SRH volume recombination rate, $U_{SRH}$, for single-energy level traps is given by:

$$U_{SRH} = N_T \frac{np - n_i^2}{\tau_{p0}(n+n_1) + \tau_{n0}(p+p_1)} \qquad \text{IV.56}$$

where $\tau_{n0}$ and $\tau_{p0}$ are the mean carrier lifetime for electrons and holes, respectively, which are related to the thermal velocity of the charge carrier, $v_{th}$, the defect concentration, $N_T$, and the capture cross-sections of electron and hole of the specific defect, $\sigma_n$and $\sigma_p$ as

$$\tau_n = (N_T v_{th} \sigma_n)^{-1} \quad \tau_p = (N_T v_{th} \sigma_p)^{-1}$$

$n_1$ and $p_1$ are defined as:

$$n_1 = n_i exp\left(\frac{E_T - E_i}{k_B T}\right), p_1 = N_V exp\left(\frac{E_i - E_T}{k_B T}\right) \qquad \text{IV.57}$$

By definition, $n_1$ and $p_1$ are the free-electron and the free-hole concentrations in the case in which the Fermi level ($E_F$) lies at the trap energy level ($E_T$).

In reality, all three recombination processes discussed above take place at the same time. The net recombination can be obtained by adding the three recombination rates as follows:

$$R_{net} = R_\lambda + R_{Auger} + R_{SRH} \qquad \text{IV.58}$$

## IV.3. SCAPS simulator:

At present, a number of simulation software is available for the PV research community such as: PC1D (**P**ersonal **C**omputer One Dimensional) **[92]**, AMPS-1D (**A**nalysis of **M**icroelectronic and **P**hotonic **S**tructures) **[93]**, ASA (**A**morphous **S**emiconductor **A**nalysis) **[94]**, AFORS-HET (**A**utomat **for S**imulation of **Het**erojunction) **[95]**, SILVACO TCAD (**Si**licon **Va**lley **Co**rporation **T**echnology **C**omputer **A**ided **D**esign) **[96]**, and SCAPS-1D. These software programs have been written with a specific reason of modelling solar cells. They have different possibilities and limitations, but the basic principles are the same.

Among the simulation tools available, SCAPS was mainly developed for modelling solar cells based on thin layers (CIGS and the CdTe family). Recent developments make the program successfully applied to model Solar cells based on other materials, such as crystalline solar cells (Si and GaAs), amorphous cells (a-Si and micromorphous Si) **[97]**, and organic solar cells **[98]**. In this work, we used the SCAPS simulator for our calculations.

### IV.3.1. General overview and simulation method:

SCAPS (a Solar Cell Capacitance Simulator) is a one dimensional solar cell simulation program developed at the Department of Electronics and Information Systems (ELIS) of the University of Gent, Belgium **[99]**. It is used for numerical analysis of solar cell performance and characteristics. Multiple measurements of solar cells' output parameters can be done through SCAPS. It can simulate the open circuit voltage (Voc), short circuit current density (Jsc), output J-V characteristic, fill factor (FF), quantum efficiency (QE), cell's output efficiency (η), generation and recombination profiles, etc.

Like any numerical simulation, SCAPS solves the basic semiconductor equations which are: the Poisson equation, relating the charge to the electrostatic potential $\psi$, and the continuity equations for electrons and holes. In one dimension, the total cell length L is divided into N intervals, and the value of $\psi i$ and the electron and hole concentrations $ni$ and $pi$ at each of the intervals constitute the unknowns of the problem. They can be found by numerically solving 3N non-linear equations, i.e. the basic equations at each of the intervals i. Alternatively, one can choose $\psi i$, $E_{Fni}$ and $E_{Fpi}$ as independent variables instead of ($\psi i$, $ni$, $pi$). Here $E_{Fn}$ and $E_{Fp}$ are the quasi-Fermi energy levels for electrons and holes

respectively. The basic equations are non-linear because the continuity equations contain a recombination term, which is non-linear in $n$ and $p$.

The electrical characteristics are calculated following the specified physical structure and bias conditions. This is achieved by approximating the operation of the device into a one dimensional grid, consisting of a number of grid points called nodes. By applying the set of differential equations (Poisson's and continuity equations) onto this grid (or equation's discretization), the transport of carriers through the structure can be simulated. The finite element grid is used to represent the simulation domain.

SCAPS is a Windows application program and few of its main features are listed below **[97]**:

- Up to seven semiconductor layers can be added to the device.
- Almost all physical parameters can be graded in a new window if required.
- Ability to estimate steady-state band diagram, recombination profile and carrier transport.
- Options for variable voltage bias, temperature and illumination.
- Can calculate concentrations, and currents at a given working point, J-V, C-V, C-f and Q-V characteristics, AC characteristics, spectral response.
- Ability to calculate single and batch values.
- Ability to output and export final and intermediate values, graphs and other important data

### IV.3.2. Action panel:

SCAPS is organized in a number of panels, in which the user can set the parameters. The main panel is the "action panel" (Figure IV.2), where the user can set an operating point (temperature, voltage, frequency, illumination), and an action list of calculations to carry out (J-V, C-V, C-f, Q(λ )). In each calculation, the running parameter (V, f or λ) is varied in the specified range, whilst all other parameters have the values specified in the operation point. Also, the user can directly view previously calculated results, namely J-V, C-V, C-f, Q(λ), and also band diagrams, electric field, carrier densities, partial recombination currents.

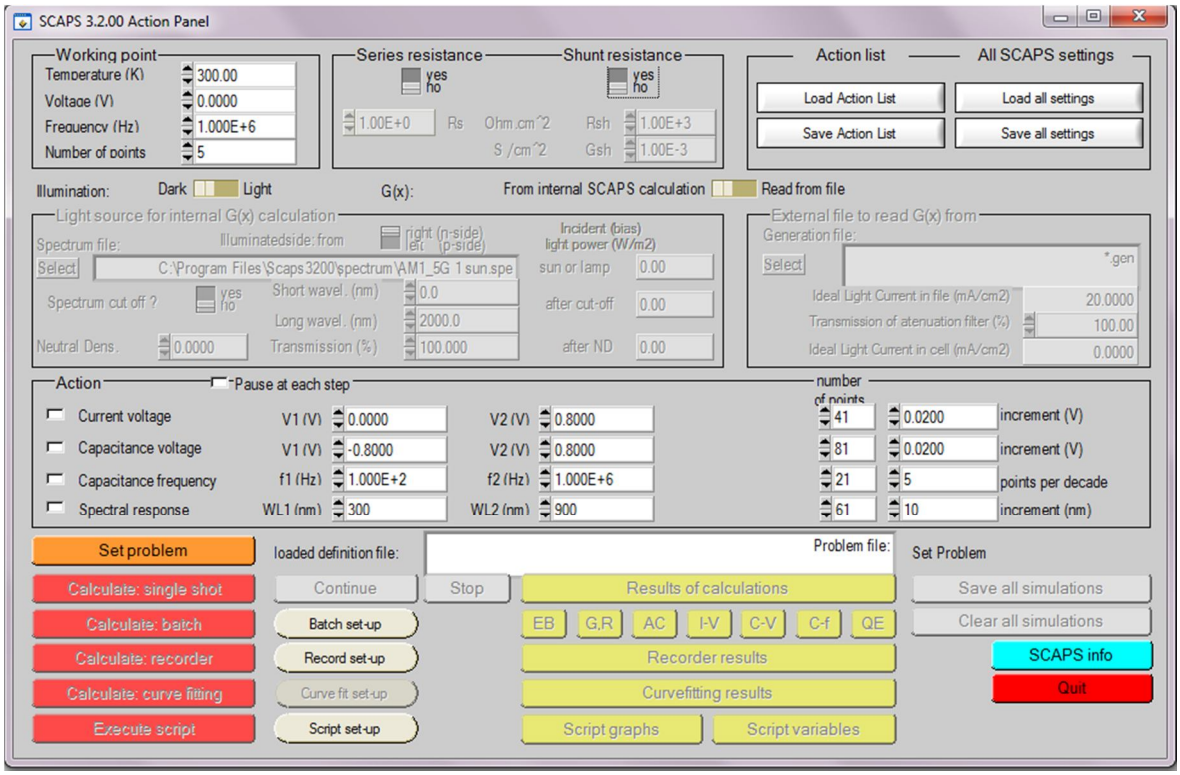


**Figure IV.2: Action Panel of SCAPS 3.2.00.**

### IV.3.3. Solar cell definition:

To define the problem, thus the geometry, the materials and all properties of the solar cell, we click on "set problem" button. The Solar Cell Definition Panel opens up as shown in Figure IV.3. In this panel, we can define structures consisting of up to 9 layers. The first layer is the back contact; the last one is the front contact. The user can specify the properties of the intermediate semiconductor layers. Except for front and back contact, each layer contains the following semiconductor properties:

- Thickness (µm).
- Band gap (eV).
- Electron affinity (eV).
- Dielectric permittivity (relative).
- Conduction band effective density of states ($1/cm^3$).
- Valence band effective density of states ($1/cm^3$)
- Electron thermal velocity (cm/s) .
- Hole thermal velocity (cm/s).
- Donor shallow density ($N_D$).
- Acceptor shallow density ($N_A$).

The optical absorption of the semiconductor layers can be taken from a user file. Examples of such user files are distributed with the program: *Si.abs*, *CdS.abs*, and *GaAs.abs*…etc. we can add other absorption files for other relevant materials.

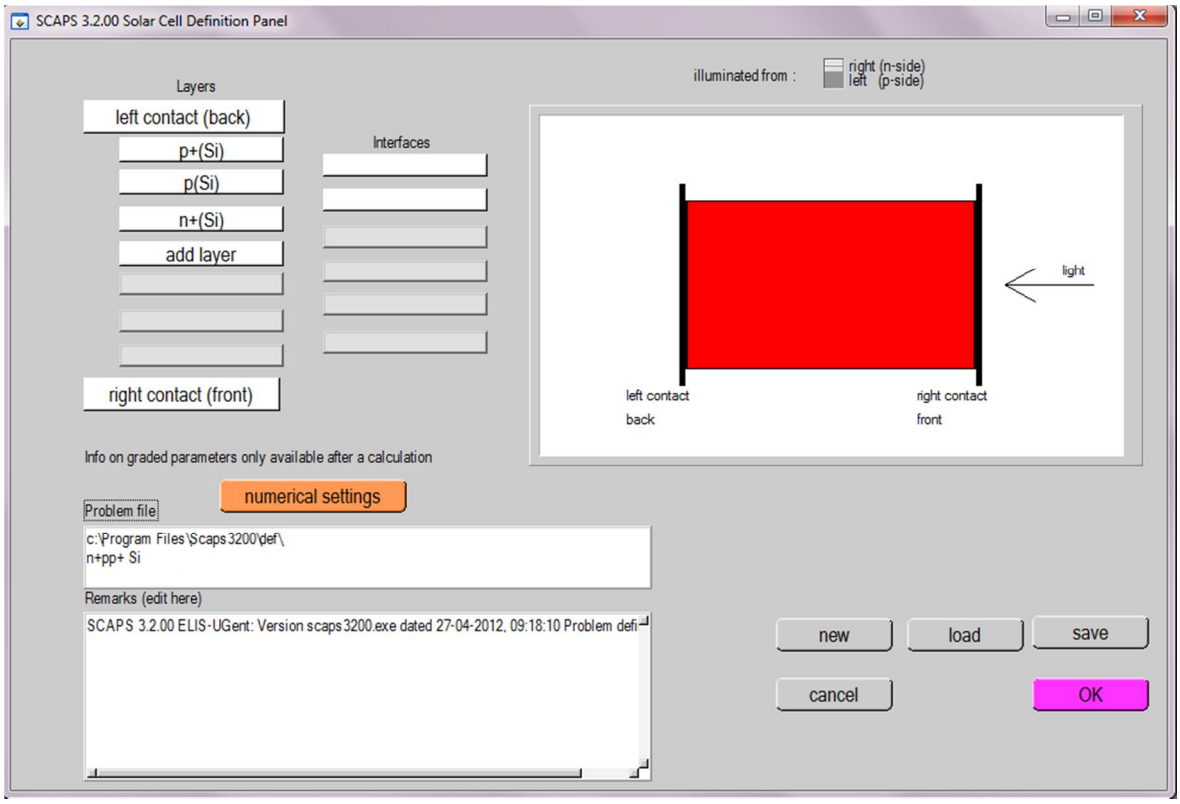


**Figure IV.3: Solar cell definition panel.**

Apart from these basic parameters, we can also modify the absorption model, recombination model and add defects to a layer. A screenshot of the Layer Properties Panel is shown below in Figure IV.4.

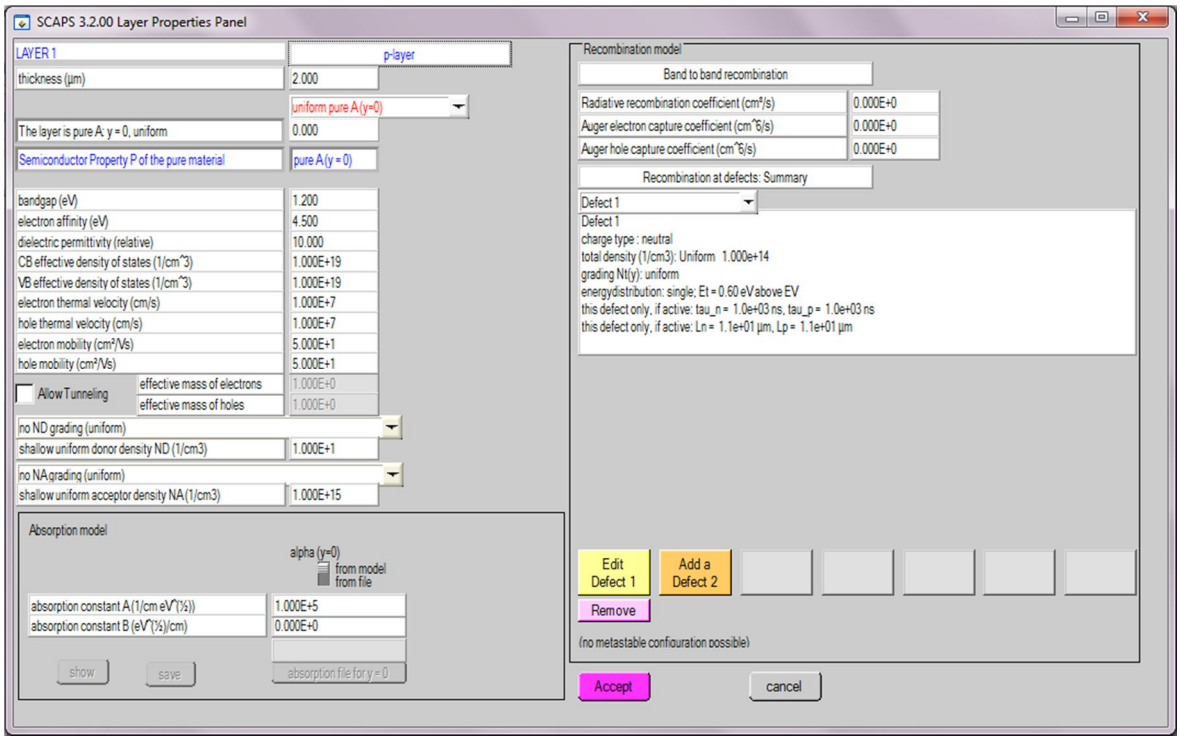


**Figure IV.4: Layer properties panel.**

The contact properties can be set by either clicking the front or back contact button on the cell definition panel, which opens the "contact properties panel", Figure IV.4.

The identification of each contact is made as follows:

- Electron and hole surface recombination velocities.
- Information about the metal work function.

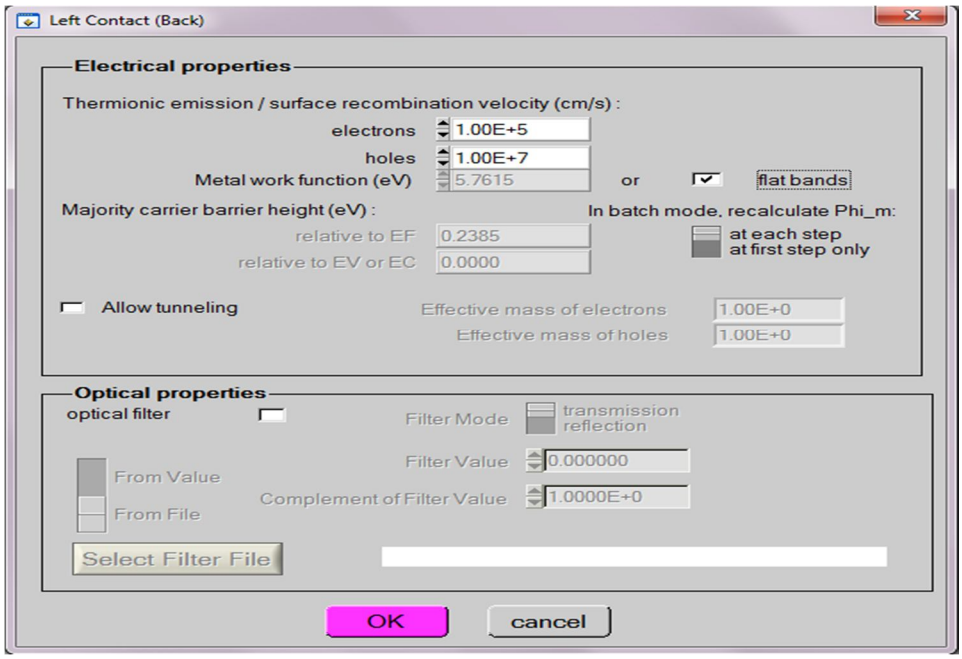


**Figure IV.5: Window to edit electrical and optical properties for a contact.**

### IV.3.4. Define the working point:

Once the solar cell design has been loaded on SCAPS using the Set Problem button, we need to set the working point. The working point specifies the parameters which are not varied in a measurement simulation, and which are relevant to that measurement:

- The temperature T: relevant for all measurements. Note: in SCAPS, only $N_C(T)$, $N_V(T)$ and the thermal voltage $k_BT$ are the only variables which have an explicit temperature dependence.
- The voltage V: is discarded in I-V and C-V simulation. It is the dc-bias voltage in C-f simulation and in QE ($\lambda$) simulation. SCAPS always starts at 0 V, and proceeds at the working point voltage in a number of steps that we also should specify.
- The frequency f: is discarded in I-V, QE ($\lambda$) and C-f simulation. It is the frequency at which the C-V measurement is simulated.
- The illumination: When performing simulations under illumination, we can further specify the illumination conditions. The basis settings are: dark or light, choice of the illuminated side (left/right), choice of the spectrum. A one sun (= 1000 $W/m^2$) illumination with the "air mass1.5, global" spectrum is the default, but we have a large choice of monochromatic light and spectra for specialised simulations. For our simulation we use the spectrum AM0, which is the spectrum out of atmosphere, and is mainly used to predict the behaviour of solar cells for space applications.

### IV.3.5. Defects and recombination:

In a diode, current is converted from hole current at the p-contact to electron current at the n contact. This means that somewhere in the diode recombination must take place, even in the most ideal device. So the user must specify recombination somewhere, at least at one place (in a layer or at an interface). Defects are the most important parameters for our study. In SCAPS, defects are identified by the following parameters:

1. Position of Energy level in the gap.
2. Defect type (i.e. acceptor, donor or neutral).
3. Electron thermal capture cross section.
4. Hole thermal capture cross section.
5. Energetic distribution (single, uniform, ...)
6. Reference for defect energy level (above $E_V$ or bellow $E_C$).
7. Electron optical capture cross section.

8. Hole optical capture cross section.
9. Defect concentration.

### IV.3.6. Select the measurements to simulate:

In the action-part of the Action Panel, we can select one or more of the following measurements to simulate (Figure IV.2): I-V, C-V, C-f and QE (λ). We can adjust if necessary the start and end values of the argument, and the number of steps. Initially, we can do one simulation at a time, and use rather coarse steps: the computer and/or the SCAPS programme might be less fast than we hope, or our problem could be really tough.

### IV.3.6. Calculate and display the simulated curves:

After introducing all the necessary data (layer properties, configuration of the solar cell), we click the button "calculate" in the action panel. The energy bands panel opens and the calculations start. After calculation, energy bands panel window open up with the band diagram, carrier density, current density and occupation probability of deep defects for electrons graph plots as shown in Figure IV.6.

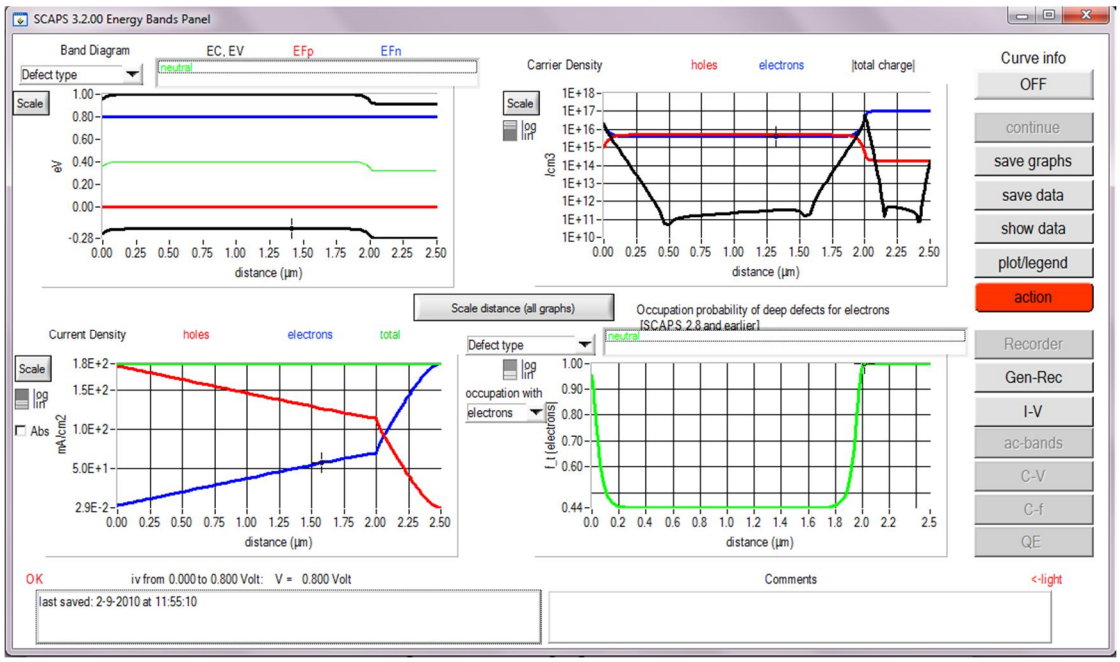


**Figure IV.6: Screenshot of energy bands panel window.**

We can either click on options (Gen-Rec, I-V) from the right side of the energy bands panel window. From the I-V curve we can extract the output of the solar cell such as the short circuit current (Jsc). The results can be saved as ASCII files for further editing and use in other programs (excel for example).

# Chapter V
# Results and discussions

## V.1. Introduction:

For terrestrial applications photovoltaic energy is still battling to find a leading place due its relative high cost compared to other sources. However for space applications it is the most important source of energy. Materials that can be used to make solar cells for this purpose have to withstand harsh conditions that include high temperatures and energetic particles. Only a few materials such as Si and some III-V semiconductors and their all alloys (GaAs, InP and GaInP) can meet these conditions **[6-7]**. Good quality crystals with well controlled doping can be easily achieved due to the mature technology of these semiconductors. Compound semiconductors are preferred because of their higher conversion efficiencies and radiation-resistance, but Silicon still has a better cost effectiveness and reliability.

The solar cells used in space are subjected to charged particles such as protons and electrons of a wide energy range. The highly energetic particles interacting with solar cells induce defects in the semiconductor lattice and, consequently, deteriorate the solar cell performance **[100]**. One of the phenomena observed in Silicon space solar cells exposed to high-energy and high-fluence proton or electron irradiation is the anomalous degradation of the short circuit current **[101]**. It initially decreases followed by a recovery before falling again with increasing proton or electron fluence. This behaviour is usually attributed to type inversion of the solar cell active region (from p-type to n-type).

In this work we have used numerical simulation using the SCAPS (Solar Cell Capacitance Simulator) software developed by Marc Burgelman and collaborators at the University of Gent **[99]** to elucidate this phenomenon. The work is divided in two main parts. In the first part we have studied in details the effect of all defects produced by radiation in Silicon to reproduce the effect of the anomalous degradation of short circuit current in aim to find which of these defects responsible for this anomalous behaviour. In the second part we study the effect of changing the structure of the solar cell in aim to find the best efficiency and hardness to irradiation.

To achieve the aim of the first part we have studied the effect of defects considering their parameter as given by the literature. It will be shown that this does not give the expected

results. Thus we have changed some of the defect parameters to reproduce the experimentally observed anomalous phenomenon.

## V.2. Previous works and aim of the study:

Silicon is one of the most important semiconductors studied concerning solar cells, especially for space applications. The performance degradation of solar cells subjected to energetic electrons and protons in laboratories is well characterized **[102-105]**. It was observed that the space solar figures of merit (the short circuit current $I_{SC}$, the open circuit voltage $V_{OC}$, the maximum output power $P_{MAX}$ , and the conversion efficiency $\eta$) decrease linearly with the logarithm of the fluence. In addition to experimental characterization, analytical modelling is also carried out **[9, 11, 84, 106-108]**. The main goal of this modelling is to predict the effect of the long term exposure of the solar cells to high energetic electrons and protons **[109-110]**. For example, $P_{MAX}$is related to the irradiation fluence by a simple formula of the form **[111]**:

$$P_{MAX}(\varphi) = P_0\left(1 - C\ln\frac{\varphi}{\varphi_0}\right) \qquad \text{V.1}$$

Where $\varphi$ is the irradiation fluence, $\varphi_0$ is the fluence threshold for the power reduction, $P_0$ is the pre-irradiated maximum output power and $C$ is a fitting constant. The other figures of merit follow a similar pattern, in most cases, which means that they decrease monotonically with increasing fluence (in logarithmic scale).

However, in some Silicon solar cells, the short circuit does not strictly follow this behaviour. Instead, it initially decreases and at a certain fluence it slightly increases before decreasing again and sharply **[9, 11, 12, 112]**. An example of experimental results is presented in Figure V.1 **[113]**.

The slight recovery of the short circuit current is usually attributed to a type inversion of the base Silicon (from p to n-type for example) **[11]**. Among the defects created by irradiation are compensating centres which reduce the initial doping density. They are responsible of a phenomenon known as carrier removal which is modeled by an analytical expression **[9]**, thus:

$$p_\varphi = p_0 exp\left(-\frac{R_C\varphi}{p_0}\right) \qquad \text{V.2}$$

$p_0$ is the initial hole density (post-irradiated p-type Si) and $R_C$ is the removal rate. The analytical modelling of the anomalous degradation of the short circuit current divides the $I_{SC}(\varphi)$ curve into four regions **[6, 9, 112]**. The first region is just for $\varphi < \varphi_0$, i.e. when $I_{SC}$

is still not affected by $\varphi$. In this region the created defects have negligible densities compared to shallow doping. The second region is when the short circuit decreases with increasing fluence. This is explained by a decrease in the minority carrier lifetime and hence in their diffusion length. The dependence of $I_{SC}$ on the diffusion length $L$ is roughly given by **[6]**:

$$I_{SC} = q\phi\{1 - \exp(-\alpha W)/(1 + \alpha L)\} \qquad \text{V.3}$$

$\alpha$ is the absorption coefficient and $W$ is the space charge region width and $\phi$ the photon flux. The third region is when the short circuit increases with increasing fluence. This is related to the onset of the type conversion where the space charge width increases instead of decreasing. Therefore the short circuit current increases according to equation (V.3). The fourth region is when the short circuit falls sharply with increasing fluence. This is explained by the increase in the base resistivity associated with the decrease in carrier concentration due to compensation by deep defects.

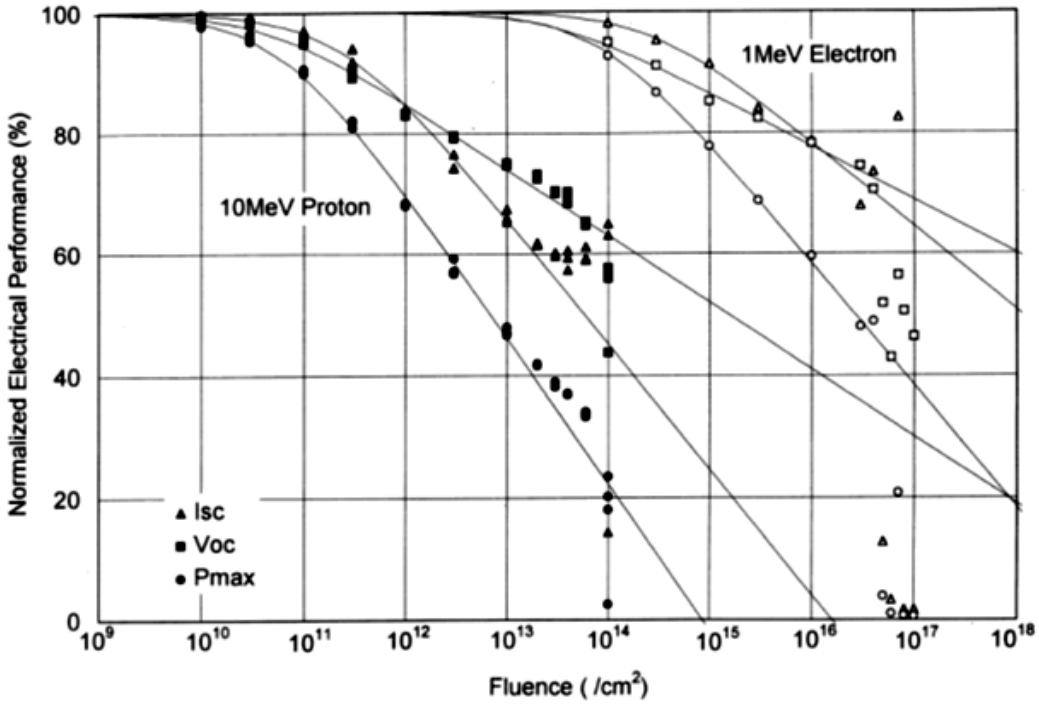


**Figure V.1: Normalized electrical performance versus fluence for Si BSFR solar cells. Black symbols: 10 MeV proton, white symbols: 1 MeV electron [113].**

Another work by Karazhanov **[11]** assumed a simplified model in which the free carriers (holes) are compensated by a single donor deep level. The inversion of the p-type semiconductor to n-type is reached when the deep level concentration surpasses that of holes. This leads to an increase in the short circuit current, also according to equation (V.3).

In the above analysis several simplifications were made. In particular the defects created by irradiation are assumed to act as one effective deep level. In reality and as it is well known, irradiation creates several defects of different types: generation-recombination (GRCs) centres, deep donors (DDs) and deep acceptors (DAs) **[114-119]**.

Experimentally it is not always easy to distinguish between GRs from DDs and DAs. This means that analytical modelling cannot clearly link the observed degradation of the solar cell figures of merit to a particular defect. On the other hand numerical simulation has the ability of unequivocally relate the degradation of each figure of merit to a particular defect **[120-124]**.

In the present work, it can reveal which defect is responsible for the observed phenomenon (the anomalous behaviour of the short circuit current) in Si solar cells. It can also evaluate the behaviour of internal parameters such as the free carrier concentration so that they can be used to explain the observed effect. Numerical simulation is carried out using the software SCAPS (Solar Cell Capacitance Simulator) developed by M. Burgelman and co-workers at the Department of Electronics and Information Systems (ELIS) of the University of Gent, Belgium **[99]**.

## V.3. Silicon solar cell structure and physical parameters used in this work:

The Si solar cell used in this work is similar to that of **[125]**. It is a typical 50 µm thick $n^+$-p-$p^+$ structure used for space applications. The emitter $n^+$ (0,15 µm) doped at $10^{19}$ $cm^{-3}$, the $p^+$ (0,15 µm) serving as back surface field (BSF). The doping of p and $p^+$ layers is fixed at $10^{15}$ $cm^{-3}$ and $5\times10^{18}$ $cm^{-3}$ respectively. Our simulation had been made for room temperature T=300K. The different parameters of this solar cell are presented in Table V.1.

| | Thickness (µm) | Doping density ($cm^{-3}$) | Type |
|---|---|---|---|
| Emitter | 0.15 | $1 \times 10^{19}$ | $n^+$ |
| Base | 49.70 | $1 \times 10^{15}$ | p |
| Back surface field region | 0.15 | $5 \times 10^{18}$ | $p^+$ |

**Table V.1: The parameters of the Si $n^+$-p-$p^+$ solar cell simulated in this work.**

A two-dimensional schematic view of the solar cell is shown in Figure V.2. The emitter side of the solar cell ($n^+$) is illuminated by AM0 spectrum.

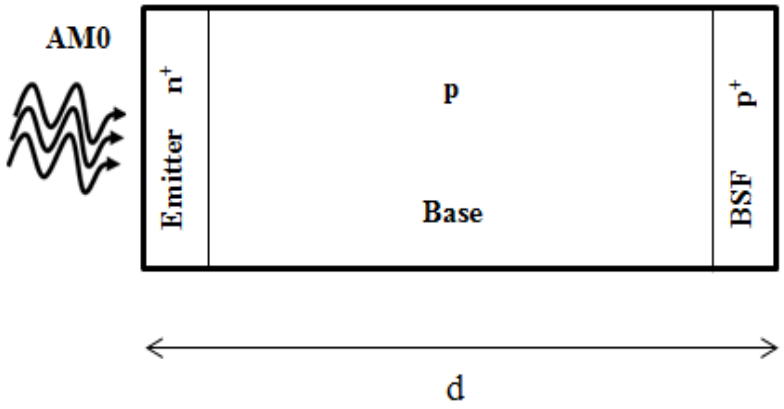


**Figure V.2: A two-dimensional schematic view of the Si $n^+$-p-$p^+$ solar cell.**

For our simulation, the main parameters characterizing Silicon are summarized in Table V.2

| **Property** | **Value** |
|---|---|
| Band gap (eV) | 1.12 |
| Electron affinity (eV) | 4.05 |
| Dielectric constant | 11.9 |
| Effective density of states in conduction band ($cm^{-3}$) | $2.8\times10^{19}$ |
| Effective density of states in valence band ($cm^{-3}$) | $2.65\times10^{19}$ |
| Electron thermal velocity (cm/s) | $1\times10^{7}$ |
| Hole thermal velocity (cm/s) | $1\times10^{7}$ |
| Electron mobility ($cm^2$/Vs) | 1450 |
| Hole mobility ($cm^2$/Vs) | 500 |

**Table V.2: The main parameters for Silicon used in this simulation [22].**

## V.4. Defects induced by irradiation:

Irradiation by energetic electrons or protons creates defects in the Si lattice which manifest as recombination centres or traps for free carriers. A lot of work is carried to characterize these defects so that a large number of defects are detected in Si. For simplicity we have used the most common observed defects **[7, 12]**. These are summarized in Table V.3 Where the introduction rate, k is the proportionality factor between the trap density and the fluence ($k = N_T/\varphi$) **[126-127]**.

| Activation energy (eV) | Capture cross section, σ ($cm^2$) | Introduction rate, k ($cm^{-1}$) | Trap type |
|---|---|---|---|
| $E_V + 0.18$ | $3.1 \times 10^{-15}$ | 0.002 | Majority |
| $E_V + 0.36$ | $6.2 \times 10^{-15}$ | 0.016 | Majority |
| $E_C - 0.20$ | $9.9 \times 10^{-15}$ | 0.002 | Minority |
| $E_V + 0.56$ | $6.3 \times 10^{-13}$ | 0.002 | Majority |
| $E_C - 0.71$ | $3.55 \times 10^{-13}$ | 0.004 | Minority |

**Table V.3: The parameters of the commonly detected defects in Si solar cells irradiated by 1 MeV electrons [7, 12].**

## V.5. Simulation results before irradiation:

Firstly, before irradiation a low density for the native defects is supposed (about $10^{12}$ $cm^{-3}$) which is a typical requirement of good quality solar cells used for space applications. The native defects can be grouped in a single recombination centre with capture cross section of ($\sigma_n = \sigma_p = 10^{-15}$ $cm^2$). The J-V characteristic (before irradiation) of the Silicon solar cell used in this study is shown in Figure V.3.

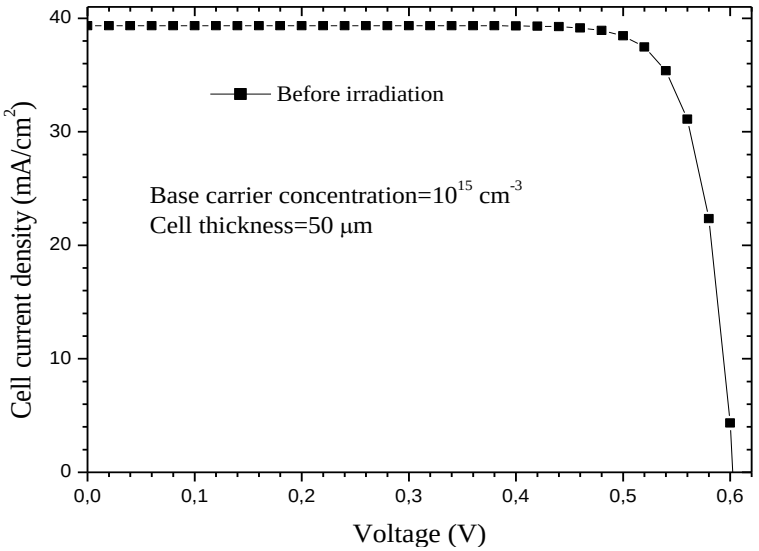


**Figure V.3: The J-V characteristic of the Silicon solar cell before irradiation.**

The output parameters of the solar cell extracted from the J-V curve are presented in Table V.4.

| Parameter | Jsc ($mA/cm^2$) | Voc (V) | FF | η (%) |
|---|---|---|---|---|
| Value | 39.34 | 0.60 | 82.09 | 14.31 |

**Table V.4: Outputs of the cell before irradiation.**

The J-V characteristic is in agreement with that of a well behaved Silicon solar cell. The extracted Jsc, Voc, η before irradiation are fairly in agreement with standard values of Silicon solar cell used in the study of anomalous degradation of Silicon solar cells by electrons and protons **[12, 128]**.

## V.6. Simulation results after 1 MeV electron irradiation:

The J-V characteristics are calculated for different fluences of 1 MeV electrons. Irradiation by these energetic electrons creates defects in the Si lattice. Since the solar cell used in this work has an $n^+$-p-$p^+$ structure, it is expected that the defects will be mainly created within the thickest region which is the p-type base. Hence the majority traps will only contribute to the reduction of the minority carrier lifetime but not to the shallow doping compensation. It is therefore the minority traps which will be responsible for this phenomenon (anomalous behaviour of Jsc). Referring to table V.3, there are only two minority traps: $E_C - 0.20\ eV$ and $E_C - 0.71\ eV$. The second, the deepest, is only observed when the electron irradiation fluence surpasses the critical value where the short circuit current shows the anomalous behaviour. In order to establish which trap is responsible the J-V characteristics are calculated under the effect of each minority (donor-like) trap. Obviously, the majority traps are all taken into account in both cases. It has to be also mentioned that, in numerical simulation, several possibilities may be considered: the two minority traps are considered separately, then together and in each case the trap parameters are adjusted to reproduce the experimental behaviour.

### V.6.1. Effect of the deeper donor trap ($E_C - 0.71\ eV$):

Firstly, we study the effect of the deeper donor trap located at 0.71 eV below the conduction band with the acceptors. We begin with the case of the deeper donor trap with the deep acceptors located in the bottom half of the band gap. The J-V characteristics under different fluences in the presence of the deeper donor trap with deep acceptors ($E_V + 0.18\ eV$) and ($E_V + 0.36\ eV$) are shown in Figure V.4. We observe that the J-V characteristics are degraded.

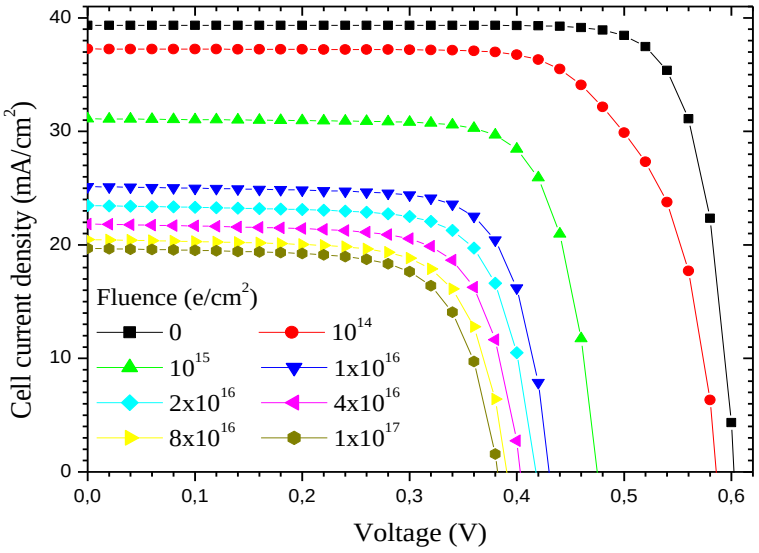


**Figure V.4: The calculated J-V characteristics of the $n^+$-p-$p^+$ Si solar cell under AM0 for different fluences of 1 MeV electron irradiation taking into account acceptors in the bottom half of the band gap with the deeper donor trap, $E_C - 0.71\ eV$**

The normalized parameters extracted from J-V curves are shown in Figure V.5. From these curves, we see that the short circuit current and the open circuit voltage decrease with increasing fluence of electron irradiation. The conversion efficiency follows the same pattern. Although the solar cell figures are degraded, it is also worth to mention that the fill factor is not greatly affected. We can conclude that this case does not produce the experimentally observed effect.

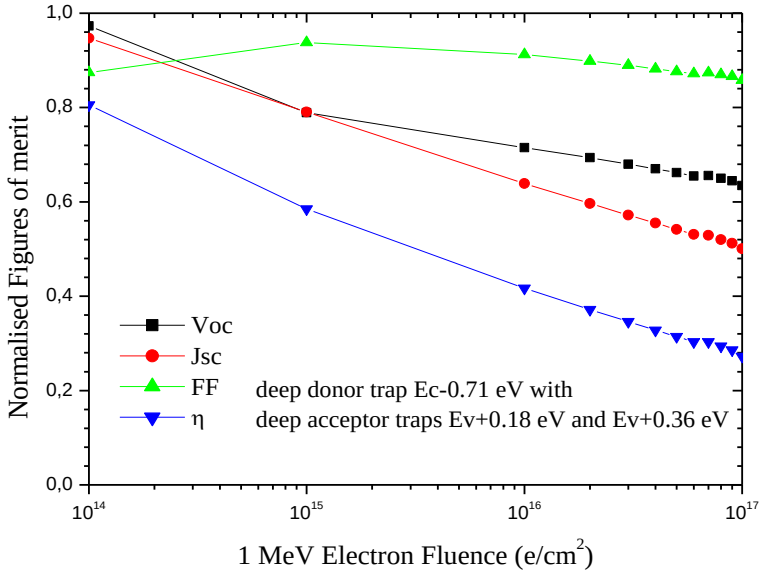


**Figure V.5: The figures of merit extracted from the calculated J-V characteristics (Figure V.4), taking into account acceptors in the bottom half of the band gap and the deeper donor trap ($E_C - 0.71\ eV$).**

Now we consider the case when the mid gap acceptor trap $(E_V + 0.56\,eV)$ is taken into account. The J-V characteristics in this case are shown in Figure V.6. These curves show that the figures of the solar cell are also degraded.

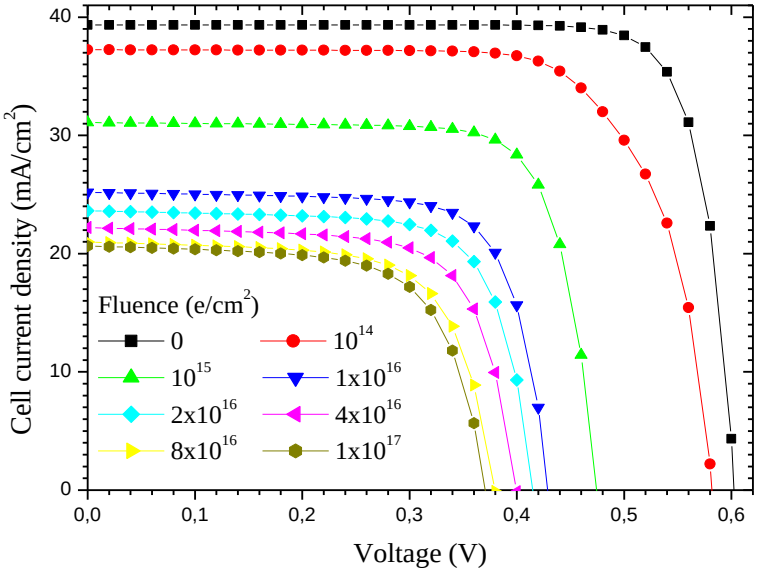


**Figure V.6: The calculated J-V characteristics of the $n^+$-p-$p^+$ Si solar cell under AM0 for different fluences of 1 MeV electron irradiation taking into account the acceptor trap $E_C + 0.56\,eV$ with the deeper donor trap, $E_C - 0.71\,eV$**

The normalized parameters extracted from J-V curves are shown in Figure V.7. The figures of merit are almost similar to the previous case. That is the experimentally observed behaviour is not reproduced.

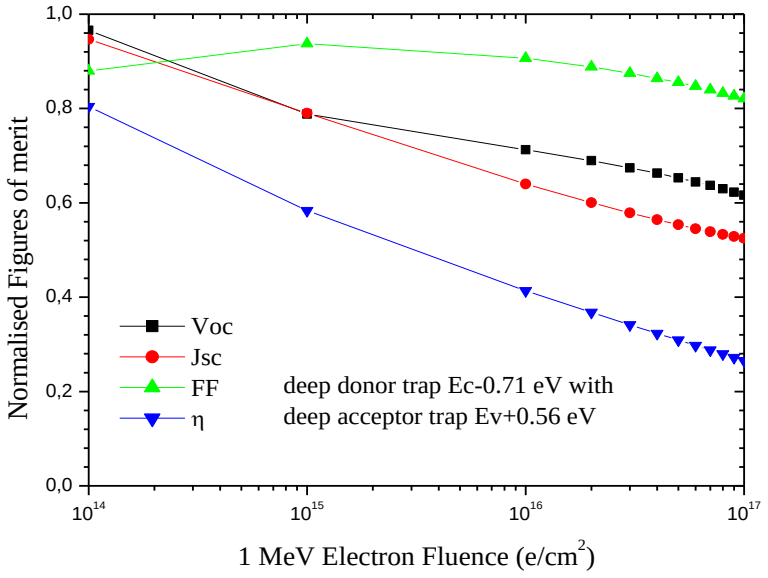


**Figure V.7: The figures of merit extracted from the calculated J-V characteristics (Figure V.6), taking into account the acceptor trap $(E_C + 0.56\,eV)$ and the deeper donor trap $(E_C - 0.71\,eV)$.**

Finally we consider the case of the presence of all acceptors with the deeper donor trap ($E_C - 0.71\ eV$). Figure V.8 shows the J-V characteristics in this case. We can see that the J-V characteristics are degraded but no significant change compared to the previous cases.

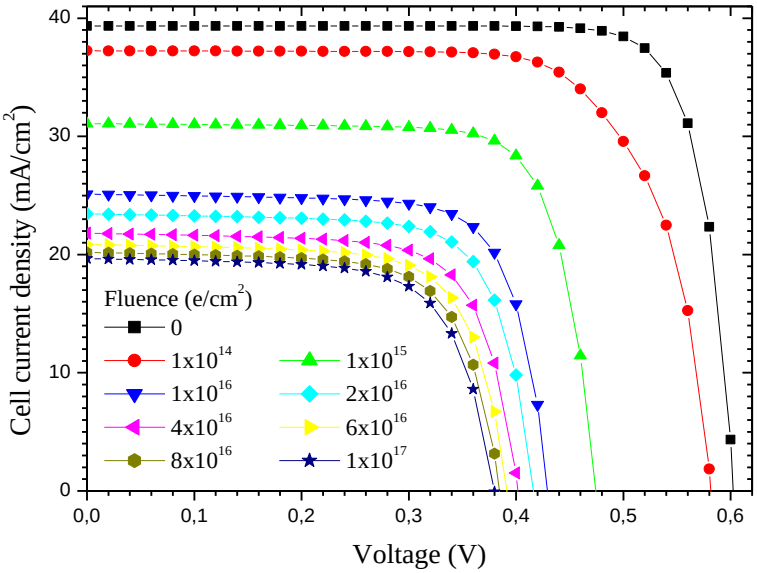


**Figure V.8: The calculated J-V characteristics of the n$^+$-p-p$^+$ Si solar cell under AM0 for different fluences of 1 MeV electron irradiation taking into account all the acceptor traps with the deeper donor trap, $E_C - 0.71\ eV$**

Figure V.9 shows the figures of merit extracted from the J-V curves.

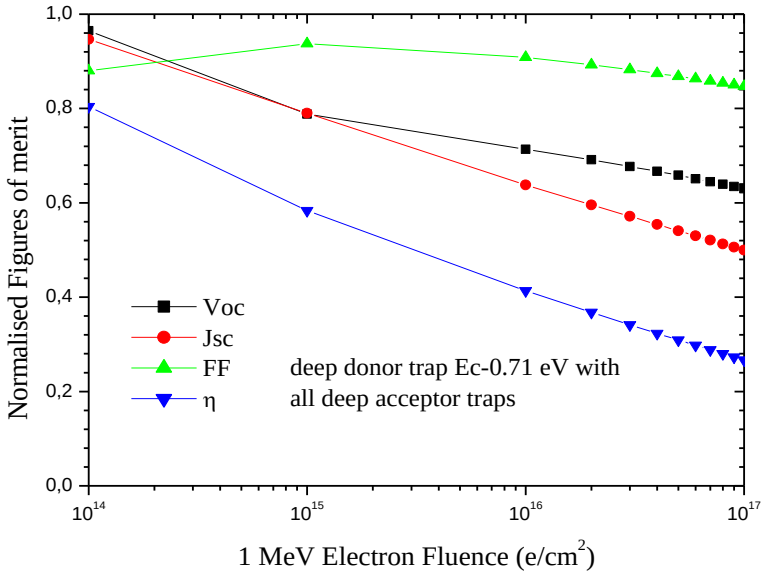


**Figure V.9: The figures of merit extracted from the calculated J-V characteristics (Figure V.8), taking into account all the acceptor traps and the deeper donor trap ($E_C - 0.71\ eV$).**

From these curves we see also that the short circuit current, the open circuit voltage and the conversion efficiency decrease with increasing fluence of electron irradiation. Thus the experimentally behaviour is not reproduced.

### V.6.2. Effect of the shallower donor trap ($E_C - 0.20\ eV$):

Secondly, we study the effect of the shallower donor trap located at 0.20 eV below the conduction band together with the deep acceptors.

The J-V characteristics in the case when we consider the shallower donor trap with the deep acceptors ($E_V + 0.18\ eV$) and ($E_V + 0.36\ eV$) are shown in Figure V.10.

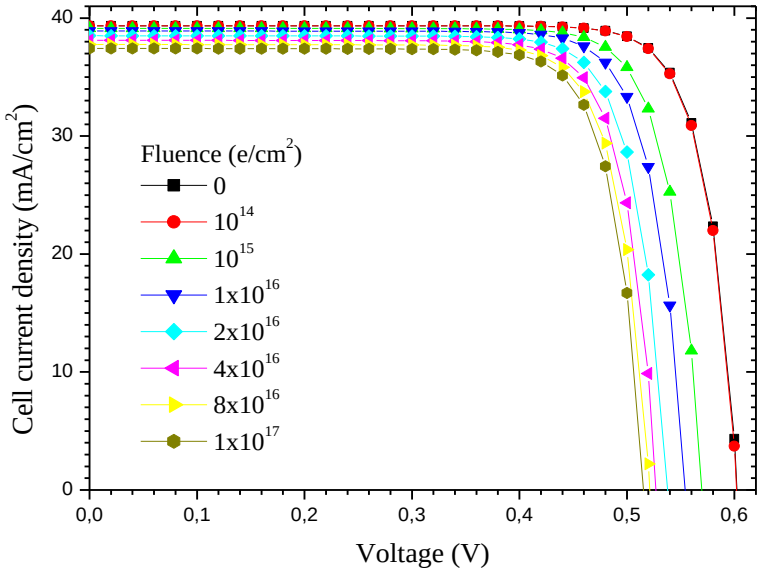


**Figure V.10: The calculated J-V characteristics of the $n^+$-p-$p^+$ Si solar cell under AM0 for different fluences of 1 MeV electron irradiation taking into account acceptors in the bottom half of the band gap with the shallower donor trap, $E_C - 0.20\ eV$**

The normalized parameters of the cell extracted from J-V curves are shown in Figure V.11. Here we can see that the characteristics of the cell are not affected so much with increasing fluence of electron irradiation especially the short circuit current and the fill factor. This also means that the experimentally observed behaviour is not reproduced.

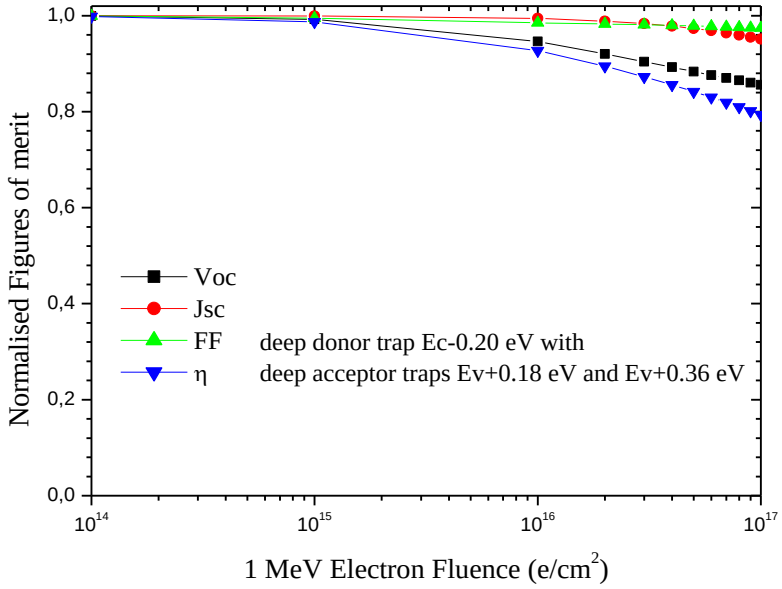


**Figure V.11: The figures of merit extracted from the calculated J-V characteristics (Figure V.10), taking into account acceptors in the bottom half of the band gap and the shallower donor trap ($E_C - 0.20\ eV$).**

When we consider the shallower donor trap with the acceptor trap ($E_V + 0.56\ eV$). The J-V characteristics are shown in Figures V.12. We can see that the J-V characteristics are degraded more than the previous case.

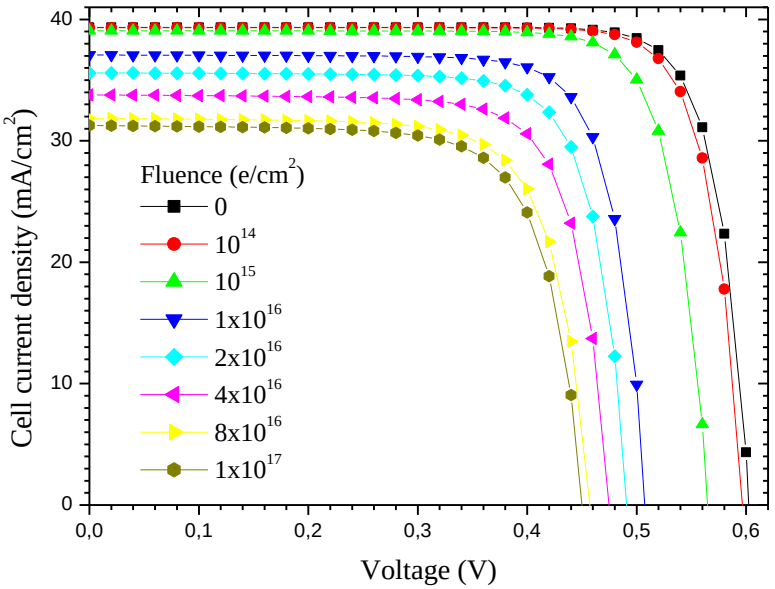


**Figure V.12: The calculated J-V characteristics of the $n^+$-p-$p^+$ Si solar cell under AM0 for different fluences of 1 MeV electron irradiation taking into account the acceptor trap $E_C + 0.56\ eV$ with the shallower donor trap, $E_C - 0.20\ eV$.**

The normalized parameters extracted from J-V curves are shown in Figures V.13. Here we can see that the short circuit current and the open circuit voltage decrease with increasing fluence of electron irradiation. The fill factor is not greatly affected, and the conversion efficiency is more degraded than the other figures of merit. This case also does not produce the experimentally observed behaviour.

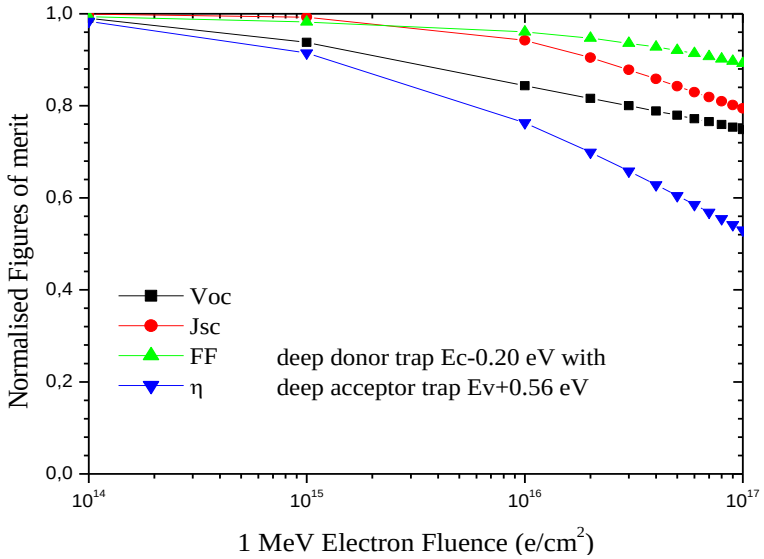


**Figure V.13: The figures of merit extracted from the calculated J-V characteristics (Figure V.12), taking into account the acceptor trap $E_C + 0.56\ eV$ and the shallower donor trap ($E_C - 0.20\ eV$).**

The J-V characteristics of the solar cell when we consider the shallower donor trap with all acceptors are shown in Figure V.14.

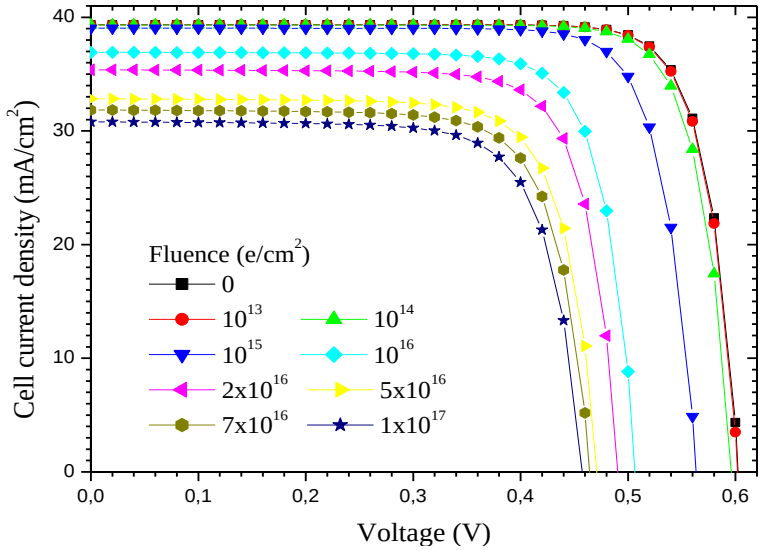


**Figure V.14: The calculated J-V characteristics of the $n^+$-p-$p^+$ Si solar cell under AM0 for different fluences of 1 MeV electron irradiation taking into account all the acceptor traps with the shallower donor trap, $E_C - 0.20\ eV$.**

The extracted parameters are shown in Figure V.15. These characteristics are almost similar to the previous case. Therefore this case is also not responsible for the experimentally behaviour.

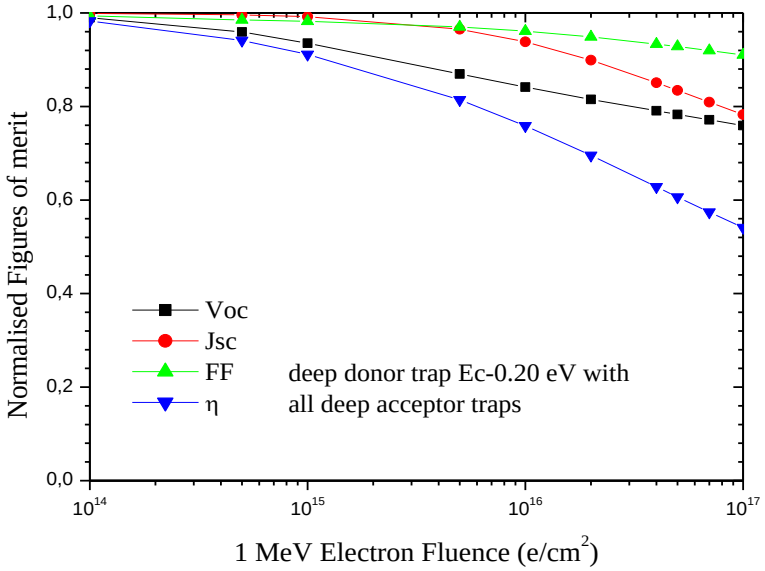


**Figure V.15: The figures of merit extracted from the calculated J-V characteristics (Figure V.14), taking into account all acceptor traps and the deeper donor trap ($E_C - 0.20\ eV$).**

### V.6.3. Effect of the two donor traps:

When the two donor traps are taken together the calculated J-V characteristics under different fluences are shown in Figures V.16. The remaining parameters after irradiation are shown in Figures V.17.

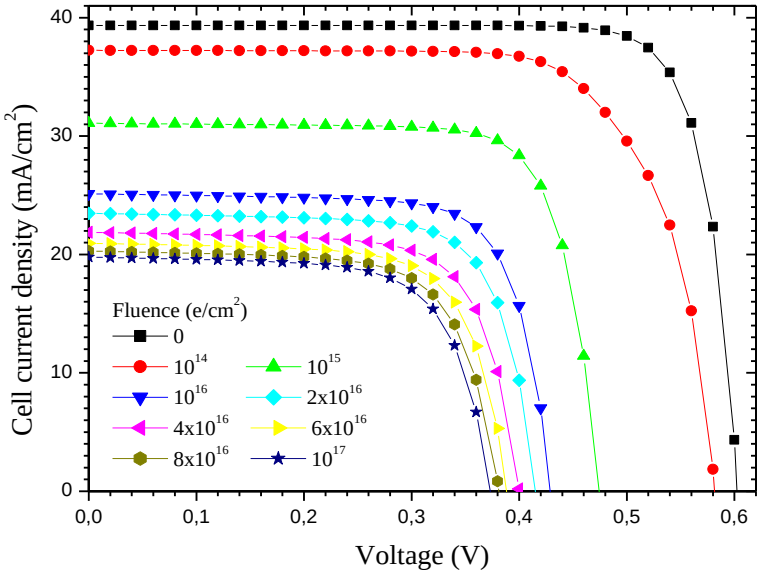


**Figure V.16: The calculated J-V characteristics of the $n^+$-p-$p^+$ Si solar cell under AM0 for different fluences of 1 MeV electron irradiation taking into account all the acceptor traps with the two donor traps, $E_C - 0.20\ eV$ and $E_C - 0.71\ eV$.**

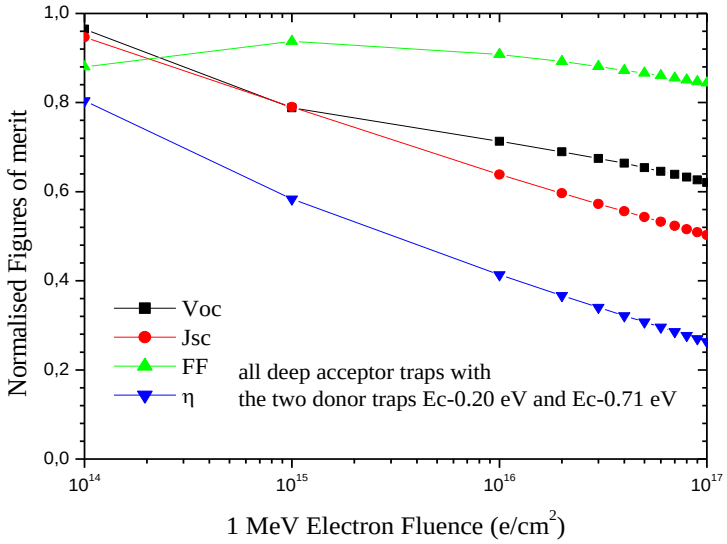


**Figure V.17: The figures of merit extracted from the calculated J-V characteristics (Figure V.16), taking into account all the acceptor traps with the two donor traps, $E_C - 0.20\ eV$ and $E_C - 0.71\ eV$.**

In this case we see also that the short circuit current, the open circuit voltage, and the conversion efficiency decrease with increasing fluence. Thus the experimentally observed behaviour is not reproduced as in the all previous cases.

### V.6.4. Summary:

Since the experimentally observed behaviour is not reproduced in the previous cases, we will have to change some of the parameters of the donor traps since they are responsible for the so-called type inversion. The suggested parameter changes may be justified by the fact that it is not easy to characterize precisely so many traps in one sample even by the most powerful techniques. Amongst all the trap parameters, usually the introduction rate is the most difficult to evaluate precisely by DLTS (Deep Level Transient Spectroscopy),for example, which is the most commonly used in the characterization of traps. It should be noted here that there are several values of the introduction rate of defects for the same author **[7, 12]**. For this reason, we choose to use the introduction rate as a fitting parameter.

## V.7. Changing the parameters of the defects:

### V.7.1. The deeper donor trap ($E_C - 0.71\ eV$):

At first, we change the introduction rate of the deeper donor trap from 0.004 to 0.01 and take all the acceptors without the shallower donor trap. In this case the J-V characteristics are presented in Figures V.18.

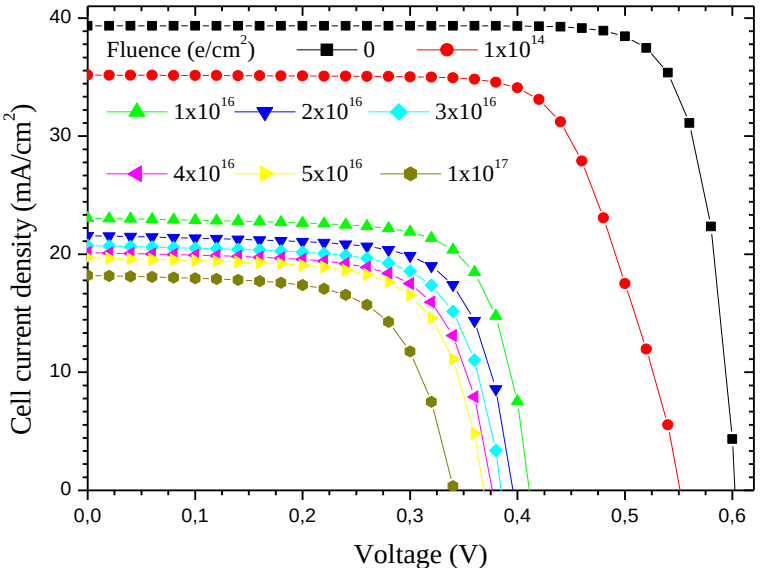


**Figure V.18: The calculated J-V characteristics of the $n^+$-p-$p^+$ Si solar cell under AM0 for different fluences of 1 MeV electron irradiation by taking into account all the acceptor traps together with the deeper donor tarp ($E_C - 0.71\ eV$) only and changing the introduction rate of the later from 0.004 to 0.01.**

The extracted parameters are shown in Figure V.19. From this figures we can see that the figures of merit are degraded but the anomalous behaviour of the short circuit current does not appear.

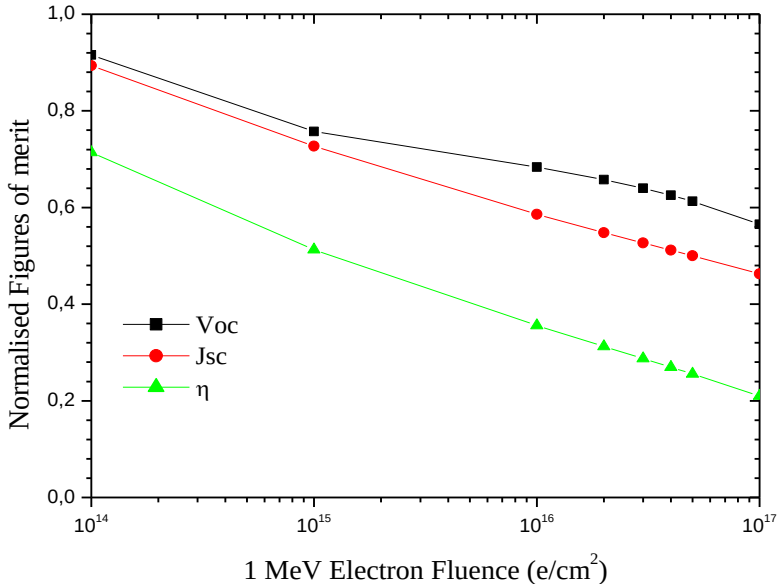


**Figure V.19: The figures of merit extracted from the calculated J-V characteristics (Figure V.18), taking into account all the acceptor traps together with the deeper donor tarp ($E_C - 0.71\ eV$) only and changing the introduction rate of the later from 0.004 to 0.01.**

The J-V characteristics when we change the introduction rate from 0.004 to 0.02 are presented in Figure V.20. The extracted figures of merit are shown in figure V.21. In this case the figures of merit of the solar cell are more degraded but no significant change observed.

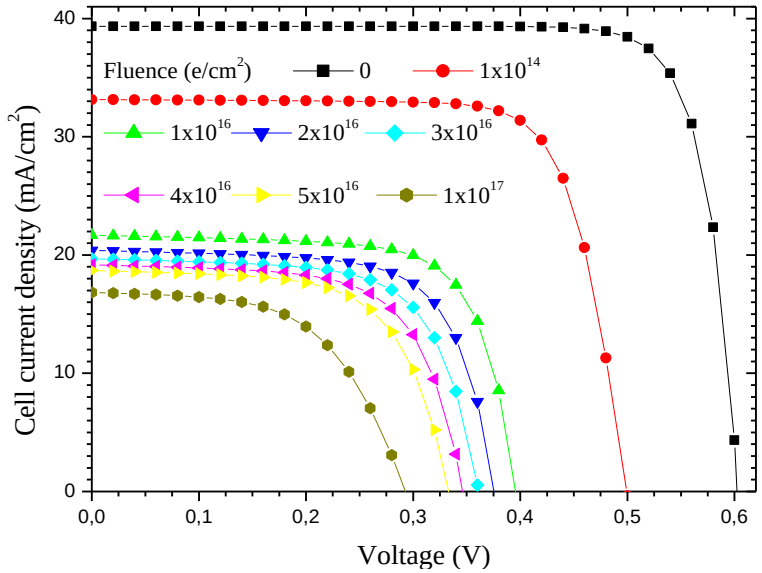


**Figure V.20: The calculated J-V characteristics of the $n^+$-p-$p^+$ Si solar cell under AM0 for different fluences of 1 MeV electron irradiation by taking into account all the acceptor traps together with the deeper donor tarp ($E_C - 0.71\ eV$) only and changing the introduction rate of the later from 0.004 to 0.02.**

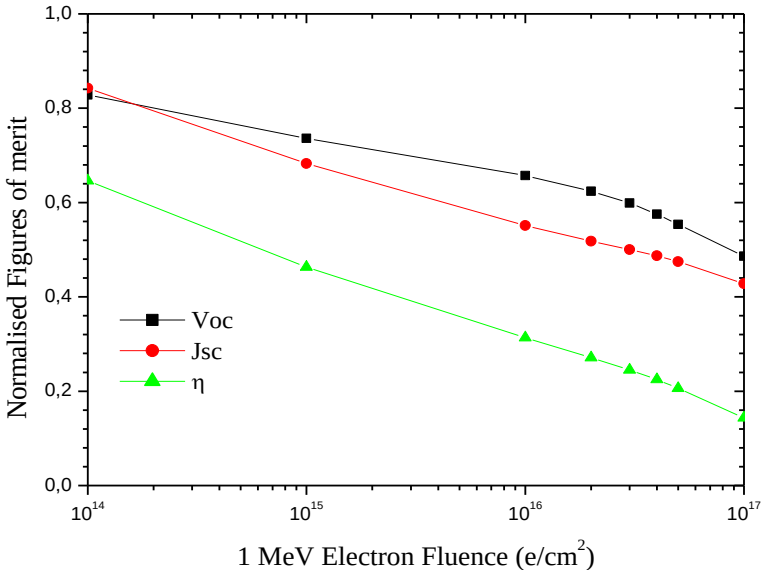


**Figure V.21: The figures of merit extracted from the calculated J-V characteristics (Figure V.20), taking into account all the acceptor traps together with the deeper donor tarp ($E_C - 0.71\ eV$) only and changing the introduction rate of the later from 0.004 to 0.02.**

The J-V characteristics when we change the introduction rate from 0.004 to 0.03 are presented in Figure V.22. The extracted figures of merit are shown in figure V.23. Also, in this case the figures merit of the solar cell are more degraded compared to the previous case, but the anomalous behaviour of the short circuit current again is not observed.

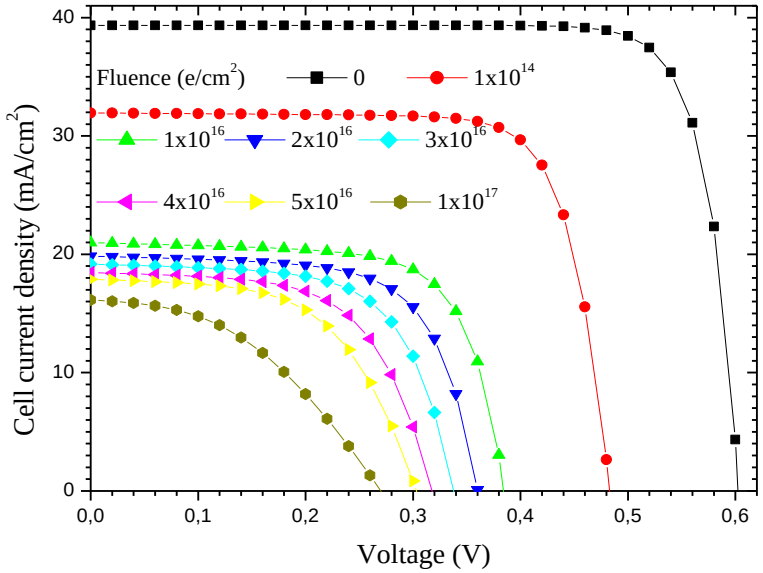


**Figure V.22: The calculated J-V characteristics of the $n^+$-p-$p^+$ Si solar cell under AM0 for different fluences of 1 MeV electron irradiation by taking into account all the acceptor traps together with the deeper donor tarp ($E_C - 0.71\ eV$) only and changing the introduction rate of the later from 0.004 to 0.03.**

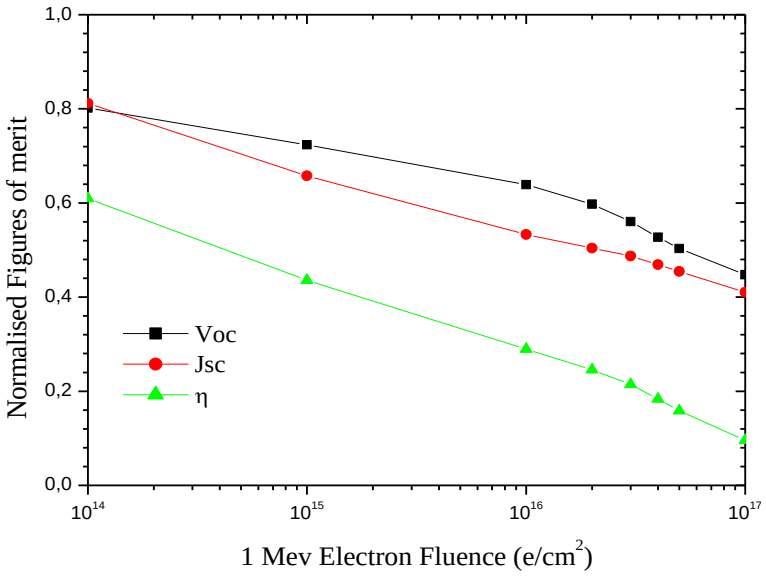


**Figure V.23: The figures of merit extracted from the calculated J-V characteristics (Figure V.22), taking into account all the acceptor traps together with the deeper donor tarp ($E_C - 0.71\ eV$) only and changing the introduction rate of the later from 0.004 to 0.03.**

The J-V characteristics when we change the introduction rate of the deeper donor trap from 0.004 to 0.04 are shown in Figure V.24.

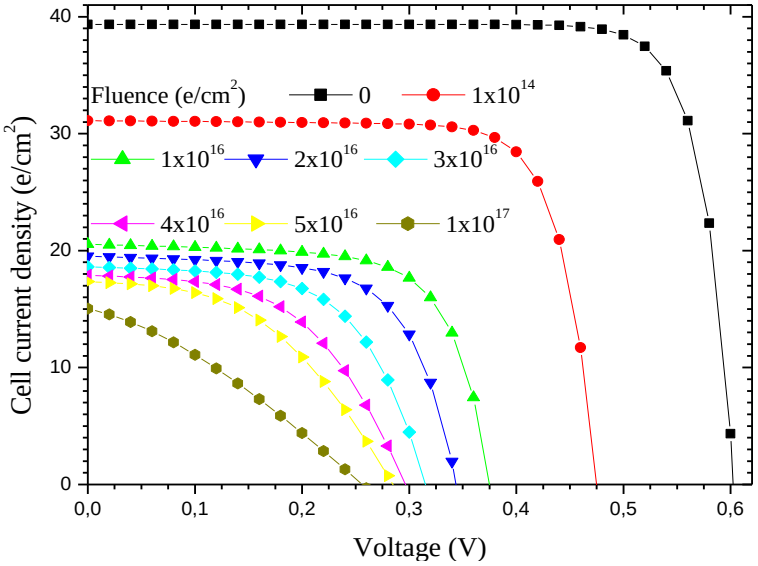


**Figure V.24: The calculated J-V characteristics of the n$^+$-p-p$^+$ Si solar cell under AM0 for different fluences of 1 MeV electron irradiation by taking into account all the acceptor traps together with the deeper donor tarp ($E_C - 0.71\ eV$) only and changing the introduction rate of the later from 0.004 to 0.04.**

The extracted parameters of the solar cell are shown in Figure V.25. We can see that the characteristics of the solar cell are more affected compared to the previous cases. But the experimental behaviour is not reproduced yet.

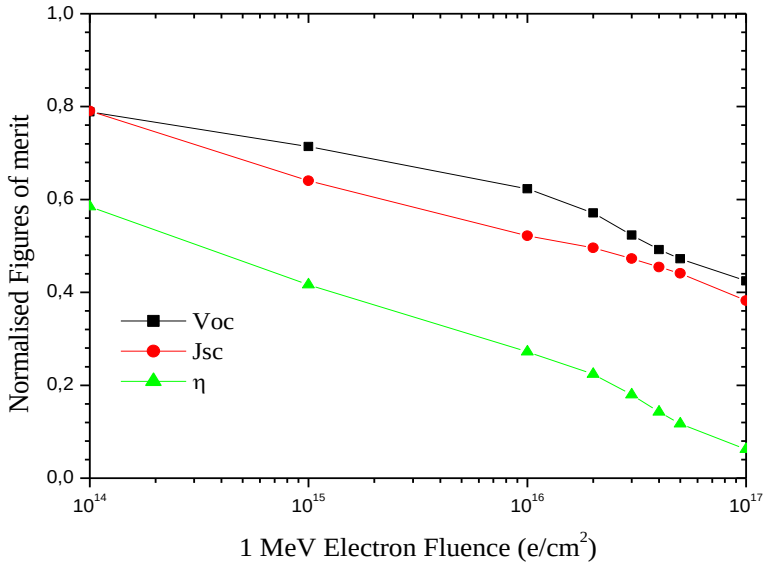


**Figure V.25: The Normalised figures of merit extracted from the calculated J-V characteristics (Figure V.24) by taking into account all the acceptor traps together with the deeper donor tarp ($E_C - 0.71\ eV$) only and changing the introduction rate of the later from 0.004 to 0.04.**

### V.7.2. The shallower donor trap ($E_C - 0.20\ eV$):

We change the introduction rate of the shallower donor trap from 0.002 to 0.01 and take all the acceptors without the deeper donor trap. In this case the J-V characteristics are presented in Figure V.26.

The figures of merit extracted from these curves are presented in Figure V.27. In this case, we observe that the anomalous behaviour of the short circuit current is not reproduced.

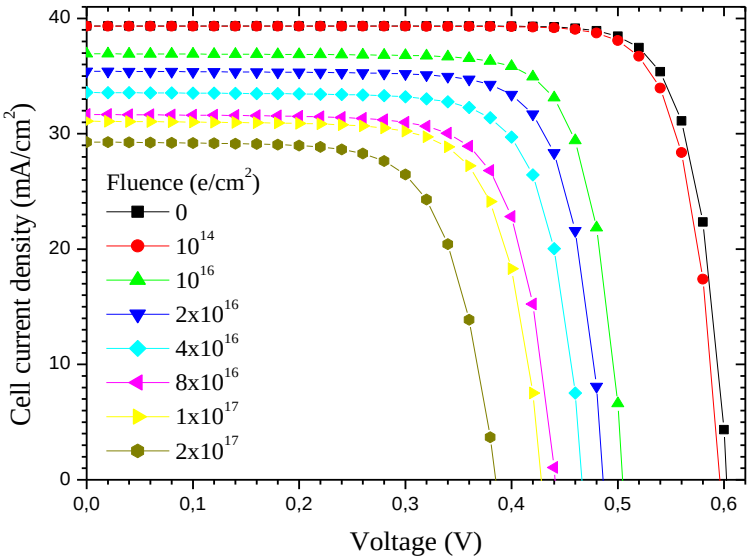


**Figure V.26: The calculated J-V characteristics of the $n^+$-p-$p^+$ Si solar cell under AM0 for different fluences of 1 MeV electron irradiation by taking into account all the acceptor traps together with the shallower donor tarp ($E_C - 0.20\ eV$) only and changing the introduction rate of the later from 0.002 to 0.01.**

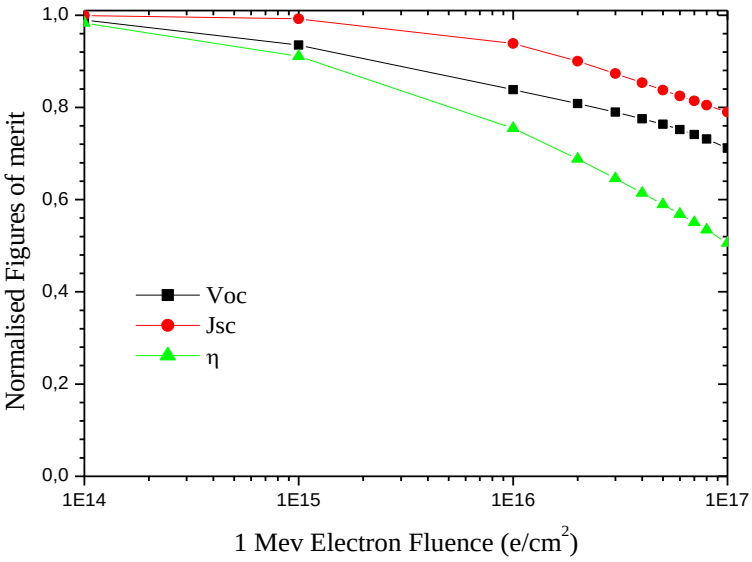


**Figure V.27: The Normalise figures of merit extracted from the calculated J-V characteristics (Figure V.26) by taking into account all the acceptor traps together with the shallower donor tarp ($E_C - 0.20\ eV$) only and changing the introduction rate of the later from 0.002 to 0.01.**

When we take the introduction rate of the shallower donor trap (k=0.02 $cm^{-1}$). The J-V characteristics are shown in Figure V.28. The figures of merit extracted from J-V curves are shown in Figure V.29. From these curves we can see that there is a slight increment in the short circuit current for high fluences near $10^{17}$ $e/cm^2$.

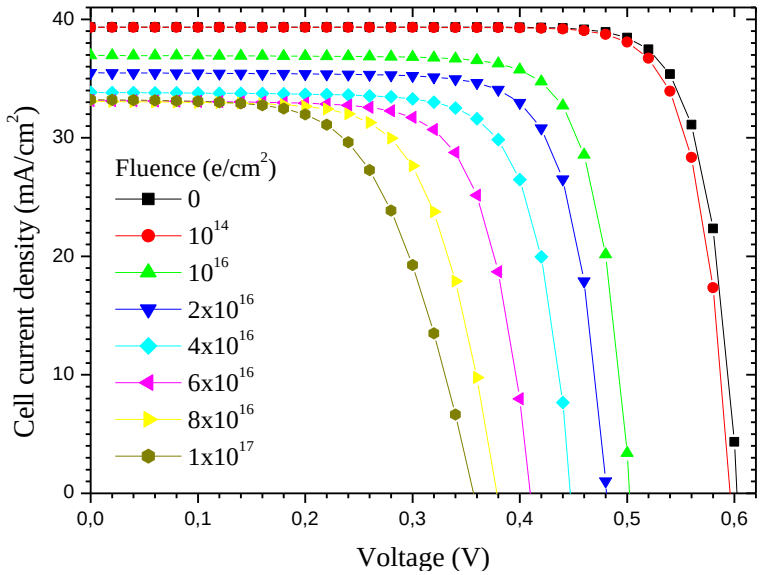


**Figure V.28: The calculated J-V characteristics of the $n^+$-p-$p^+$ Si solar cell under AM0 for different fluences of 1 MeV electron irradiation by taking into account all the acceptor traps together with the shallower donor tarp ($E_C - 0.20$ eV) only and changing the introduction rate of the later from 0.002 to 0.02.**

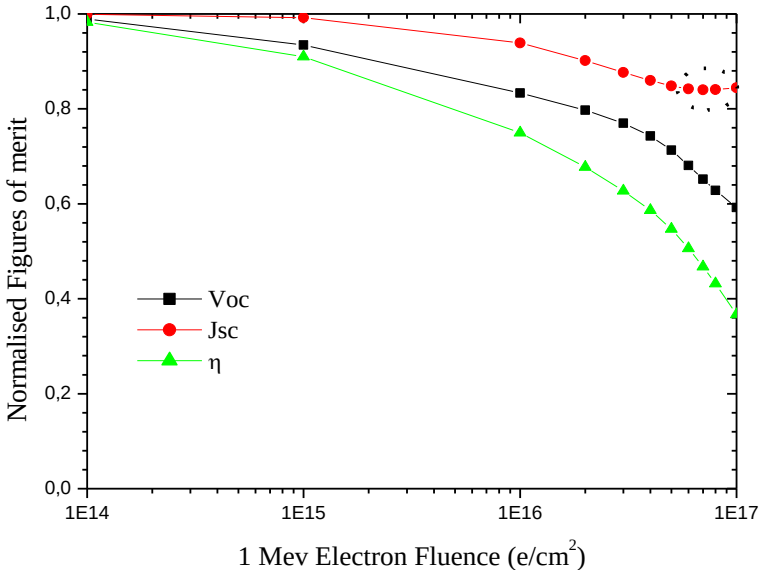


**Figure V.29: The Normalise figures of merit extracted from the calculated J-V characteristics (Figure V.28) by taking into account all the acceptor traps together with the shallower donor tarp ($E_C - 0.20\ eV$) only and changing the introduction rate of the later from 0.002 to 0.02.**

When we take the introduction rate (k=0.03 $cm^{-1}$). The J-V characteristics are shown in Figure V.30. The extracted figures of merit are shown in Figure V.31. Here we can see the anomalous behaviour of the short circuit current but not in the experimentally observed range.

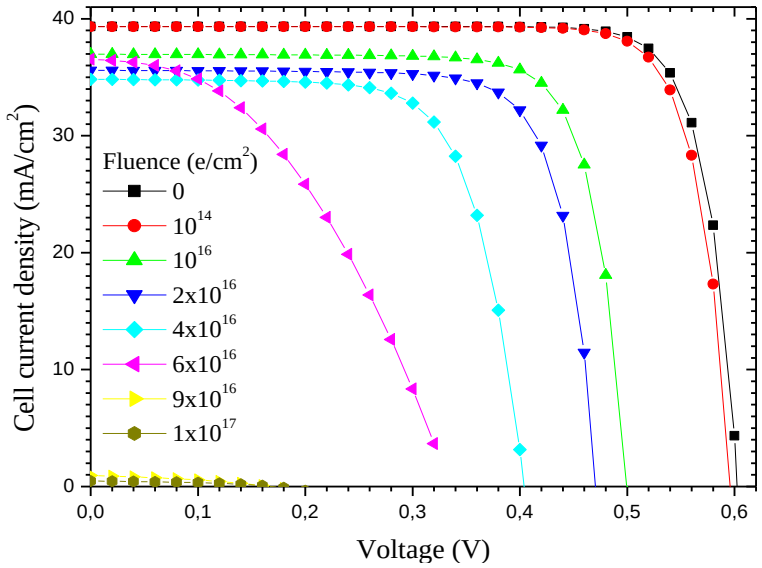


**Figure V.30: The calculated J-V characteristics of the $n^+$-p-$p^+$ Si solar cell under AM0 for different fluences of 1 MeV electron irradiation by taking into account all the acceptor traps together with the shallower donor tarp ($E_C - 0.20\ eV$) only and changing the introduction rate of the later from 0.002 to 0.03**

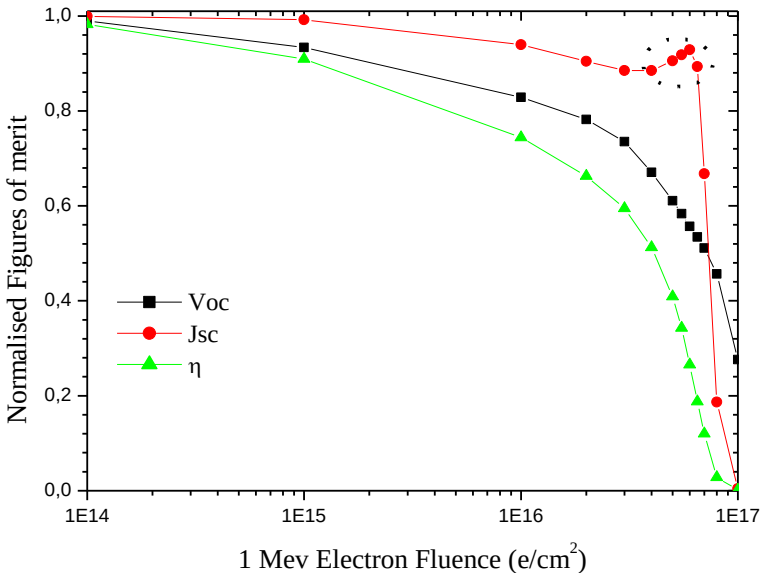


**Figure V.31: The Normalise figures of merit extracted from the calculated J-V characteristics (Figure V.30) by taking into account all the acceptor traps together with the shallower donor tarp ($E_C - 0.20\ eV$) only and changing the introduction rate of the later from 0.002 to 0.03.**

Finally, when we take the introduction rate of the shallower donor trap (k=0.04). The J-V characteristics are shown in Figure V.32. The extracted figures of merit are shown in Figure V.33.

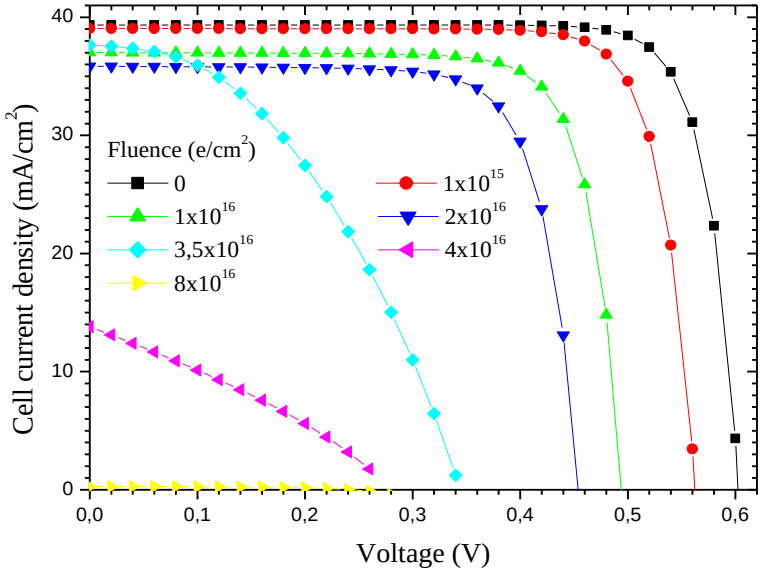


**Figure V.32: The calculated J-V characteristics of the n$^+$-p-p$^+$ Si solar cell under AM0 for different fluences of 1 MeV electron irradiation by taking into account all the acceptor traps together with the shallower donor tarp ($E_C - 0.20\ eV$) only and changing the introduction rate of the later from 0.002 to 0.04.**

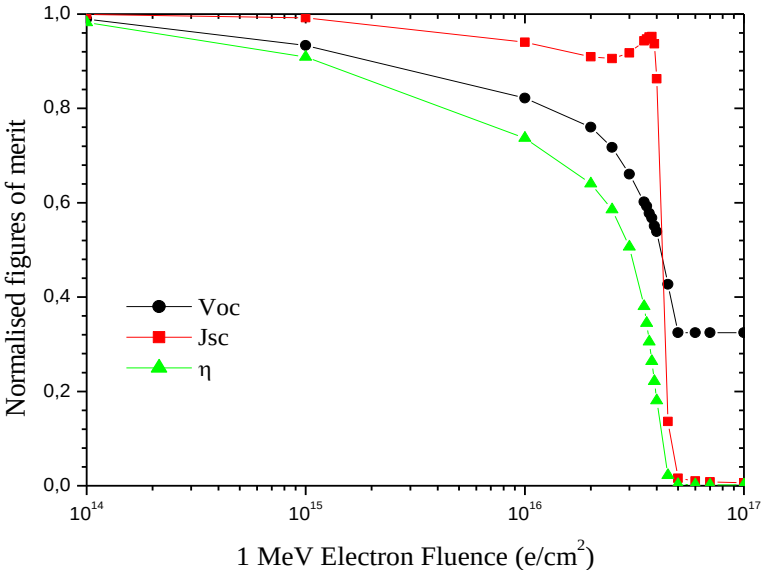


**Figure V.33: The Normalised figures of merit extracted from the calculated J-V characteristics (Figure V.32) by taking into account all the acceptor traps together with the shallower donor tarp ($E_C - 0.20\ eV$) only and changing the introduction rate of the later from 0.002 to 0.04.**

We can see that the open circuit voltage and the conversion efficiency decrease monolithically with increasing electron fluence but the short circuit current shows the anomalous behaviour. It decreases firstly and increases at certain fluence before it decreases abruptly again. The region when the anomalous behaviour of the short circuit current observed is comparable to experimental measurements (between $2x10^{16}$ e/cm$^2$ and $5x10^{16}$ e/cm$^2$) **[113, 125]**.

Although the shape of the experimentally observed phenomenon is reproduced (Figure V.33) but the steepness of its degradation is not. In fact the short circuit degradation is less than 10 % before the appearance of the anomalous phenomenon. The measured degradation is ~30 %. In the following the deeper donor trap ($E_C - 0.71\ eV$) is taken into account and the calculated J-V characteristics in this case are shown in Figure V.34.

It can be seen that the J-V characteristics are more affected. To visualize this larger impact the figures of merit are extracted from the J-V characteristics, normalized and shown in Figure V.35.

In this figure it can be clearly seen that the degradation rate increases and is comparable to values obtained experimentally. It is also worth to mention that the fluence at which this phenomenon appears is very comparable to measurements **[125]**.

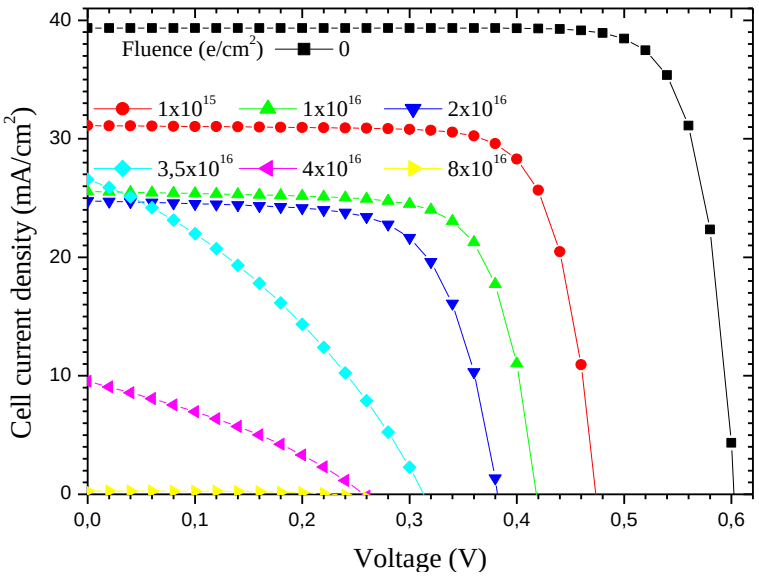


**Figure V.34: The calculated J-V characteristics of the n$^+$-p-p$^+$ Si solar cell under AM0 for different fluences of 1 MeV electron irradiation by taking into account all the acceptor traps together with both the donor traps and changing the introduction rate of the shallower minority tarp ($E_C - 0.20\ eV$) from 0.002 to 0.04.**

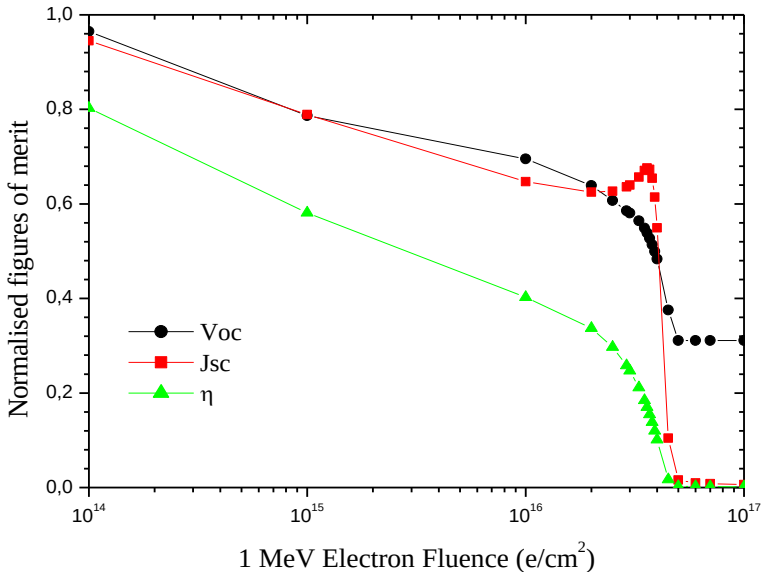


**Figure V.35: The extracted short circuit current, normalized to the unirradiated value, from the calculated J-V characteristics (Figure V.34) of the $n^+$-p-$p^+$ Si solar cell under AM0 for different fluences of 1 MeV electron irradiation by taking into account all the traps and changing the introduction rate of the shallower donor tarp ($E_C - 0.20\ eV$) from 0.002 to 0.04.**

## V.8. Study of the type inversion:

As it was mentioned previously, the anomalous degradation of the short circuit current is usually related to a type inversion of the active region of the solar cell (base) by several authors such as **[11]**. The argument was mainly qualitative and no clear cut evidence was presented. In this work it will be shown that type inversion is not responsible for this phenomenon. For this purpose the electron and hole density distribution in the whole solar cell evolution with the 1 MeV electron fluence is evaluated corresponding to the region where the short circuit current shows the anomalous behaviour (between 2x$10^{16}$ e/cm$^2$ and 5x$10^{16}$ e/cm$^2$ ). This is shown in Figure V.36.

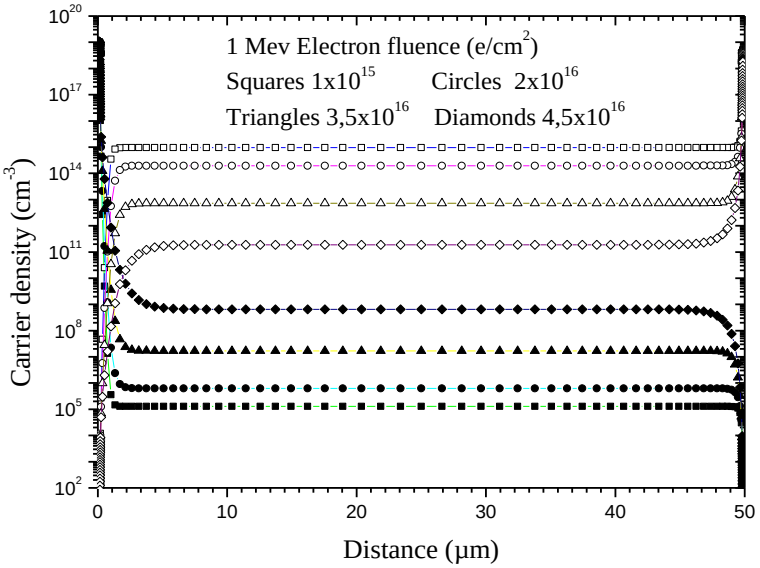


**Figure V.36: The electron (solid symbols) and the hole densities distribution along the $n^+$-p-$p^+$ Si solar cell structure for different fluences of 1 MeV electron irradiation corresponding to the region where the short circuit current shows the anomalous behaviour.**

The hole density decreases and the electron density increases with increasing fluence but the second never surpasses the first although the fluence is larger than the threshold for the short circuit current increase, which is $\approx 3 \times 10^{16}\ e/cm^2$ (see Figure V.35). This means that the base is still p-type and hence the type inversion is not achieved. It is worth pointing out here that numerical simulation has an advantage over experimental characterization and analytical modelling since it can evaluate the internal parameters of the structure such as the electron and hole densities. Such evaluation cannot be realized by experimental characterization and analytical modelling. In order to explain the anomalous behaviour of the short circuit current we will study the evolution of the depletion region ($W$). This parameter can be roughly evaluated from Figure V.36. For this purpose the left side of Figure V.36 is magnified to show the depletion region of the $n^+$-p junction and is shown in Figure V.37.

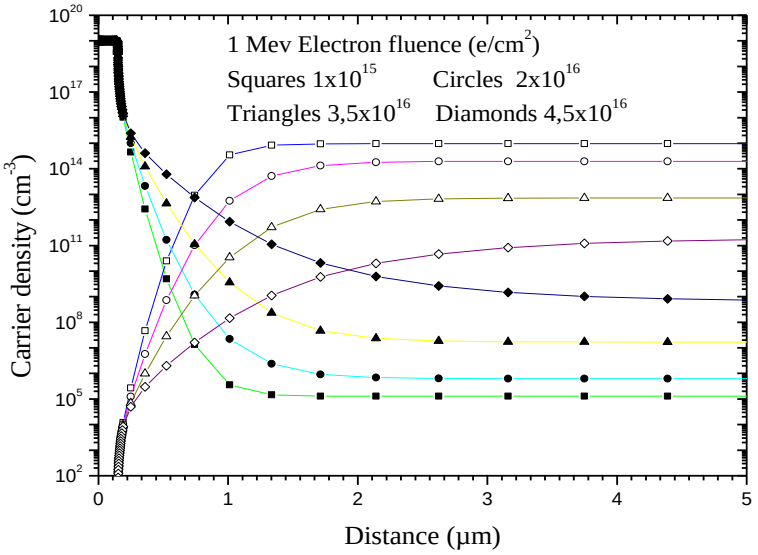


**Figure V.37: Enlargement of the left side of Figure V.36 to show the depletion region at the $n^+$-p junction (left side) of the $n^+$-p-$p^+$ solar cell.**

As the fluence, corresponding to the region where the short circuit shows the anomalous behaviour, increases the depletion region width increases since the hole density decreases. This will lead to an increase in the short circuit current according to equation V.3.

Figure V.38 shows the densities of electrons and holes for the fluences $5x10^{16}$ e/cm$^2$ and $10^{17}$ e/cm$^2$ which are the fluences after the pic of Jsc (anomalous behaviour of the short circuit current). In this figure we can see that the density of electrons is greater than holes, this confirms that the type inversion of the solar cell from p to n type does not appear until after the pic of Jsc.

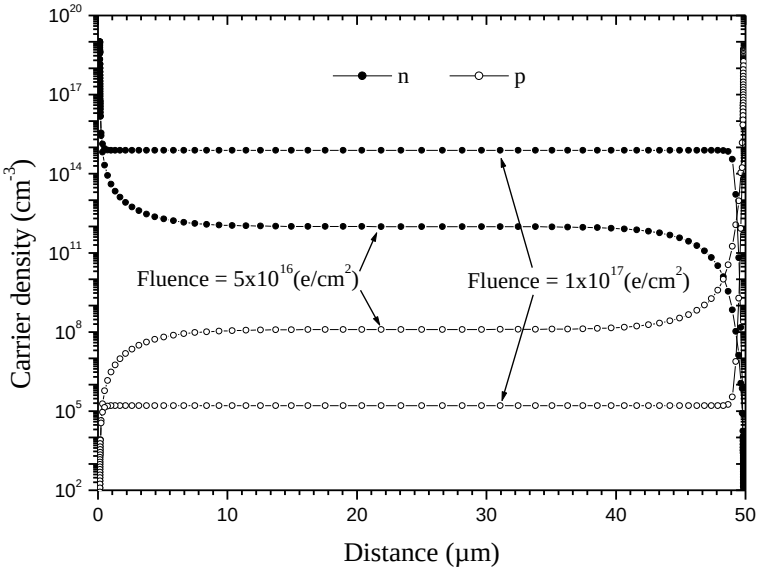


**Figure V.38: The electron (solid symbols) and the hole densities distribution along the $n^+$-p-$p^+$ Si solar cell structure for the fluences ($5x10^{16}$ e/cm$^2$) and ($1x10^{17}$ e/cm$^2$).**

On the other hand, the type inversion of the solar cell can also confirmed by studying the change in the quantum efficiency of the solar cell as a function of 1 MeV electron fluence. The spectral response of the solar cell is illustrated in Figure V.39. Curve (a) is a typical initial result for non-irradiated Silicon solar cell. The other curves (b), (c) and (d) correspond to fluences during the increase of the short-circuit current, during the rapid decrease of the short-circuit current, and after the cell failure, respectively. In the region where the anomalous behaviour of Jsc is observed, the QE at longer wavelengths decreases and no significant change at shorter wavelengths (curve b). In the region where the rapid decrease of the short circuit current, the QE at shorter wavelengths is diminished but that of long wavelengths does not change so much (curve c). After the cell failure (η almost zero), the QE at shorter wavelengths becomes almost zero but a weak response is observed at longer wavelengths (curve d).

The change in spectral response (small remaining response of the cell) for high fluences (fluences greater than $5x10^{16}$ e/cm$^2$) can be explained by the change in the cell structure from p to n-type in the base layer **[128]**. This assumption was experimentally confirmed by the EBIC (Electron Beam Induced Current) of the irradiated solar cells **[103, 128-129]**.

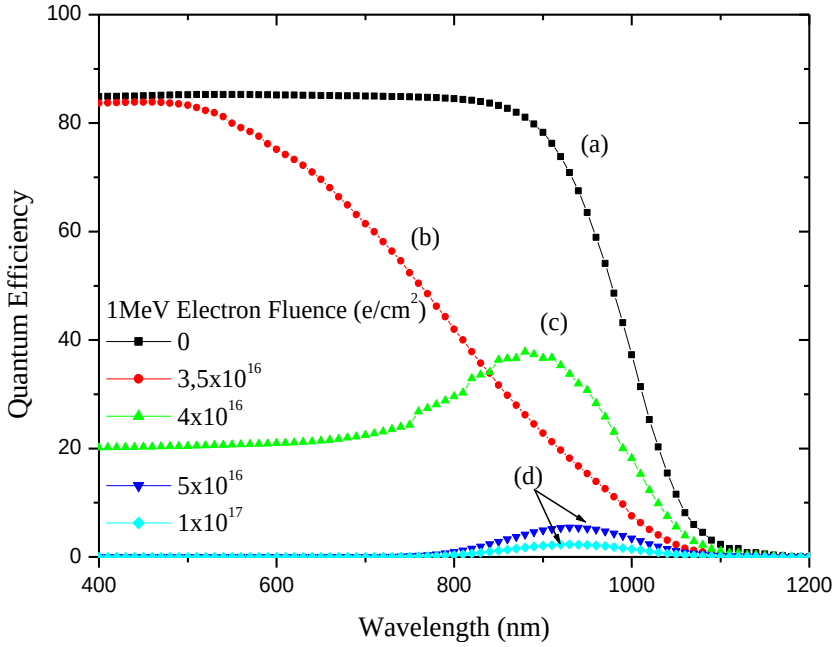


**Figure V.39: Change in spectral response of Silicon solar cell as a function of 1 MeV electron irradiation. (a) Before irradiation, (b) region were current increases, (c) region were the rapid decrease in short circuit current, and (d) after cell failure.**

## V.9. The effect of the cell structure:

### V.9.1. The effect of the base carrier concentration:

Figure V.40 shows the variation of the short circuit current as a function of 1 MeV electron fluence for different base carrier concentrations of the solar cell. Values presented are normalized to those corresponding to the non-irradiated solar cell.

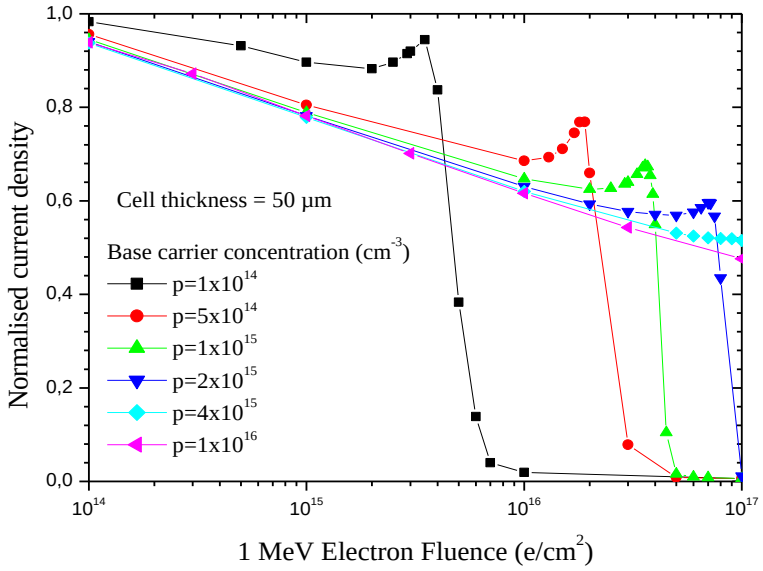


**Figure V.40: Variation of the short circuit current as a function of 1 MeV electron fluence for different base carrier concentrations of the solar cell.**

From this figure we can see that the short circuit current is better for the small base carrier concentration in low fluences. On the other hand, for the small base carrier the anomalous behaviour of short circuit current is shown first; and therefore the cell failure (sharp decrease of Jsc). This can be explained by the carrier removal effect due to compensating centres which compensate first the solar cells that have less value of the base concentration according to equation V.2. By contrast, when the base carrier is increased, the carrier removal effect has almost no influence in the complete range of electron irradiation fluence considered. Therefore the anomalous behaviour of the short circuit current is not observed.

Figure V.41 shows the variation of the open circuit voltage for different base carrier concentrations. From this figure we can see that Voc is not much affected in low fluences, while in high fluences of electrons Voc is better for high base carrier concentrations.

Figure V.42 shows the variation of the efficiency for different base carrier concentrations of the solar cell. From this figure we can see that the efficiency is also not much affected in low fluences and it is better for high base carrier concentration in high fluences of the electrons.

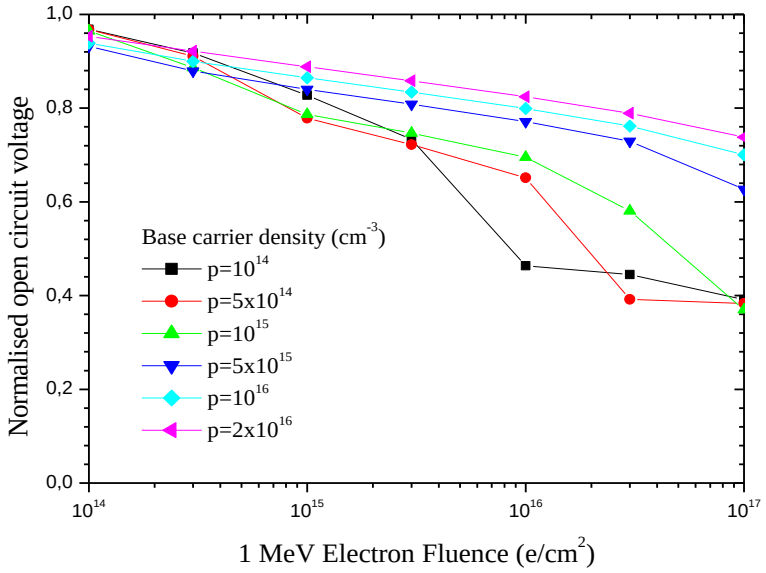


**Figure V.41: Variation of open circuit voltage as a function of 1 MeV electron fluence for different base carrier concentrations of the solar cell.**

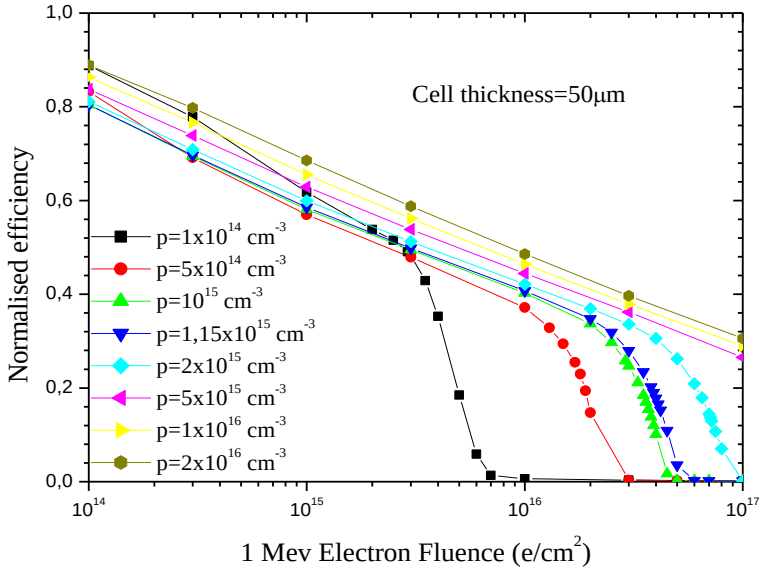


**Figure V.42: Variation of the efficiency as a function of 1 MeV electron fluence for different base carrier concentrations of the solar cell.**

### V.9.2. The effect of the cell thickness:

The variation of the short circuit current as a function of 1 MeV electron fluence for different total thickness of the solar cell is shown in Figure V.43. Here we can see that the short circuit current is better for the small thickness of the solar cells. On the other hand the decrease of the short circuit current after the anomalous behaviour is occurs first for the solar cells which have the highest value of thickness. May be this is due to the penetration of electrons deep in the solar cell. Although the Voc is not affected much by the structure width as shown in Figure V.44.

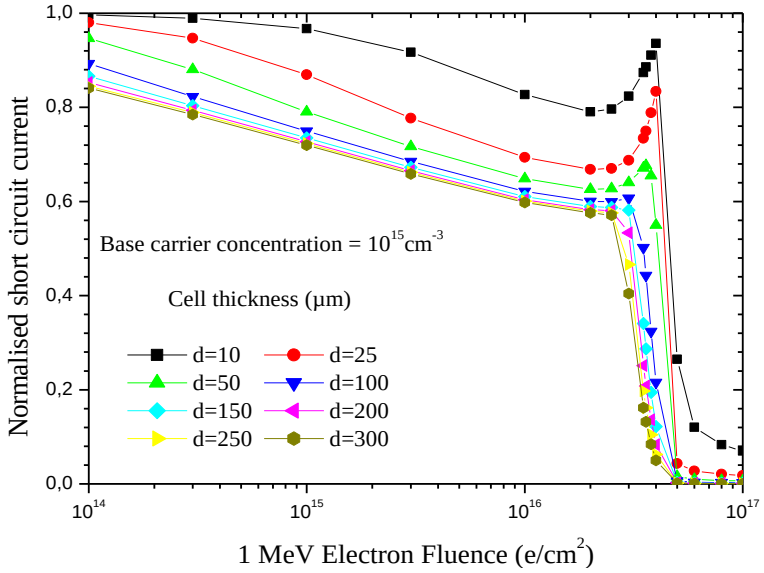


**Figure V.43: Variation of the short circuit current as a function of 1 MeV for different total thickness of the solar cell.**

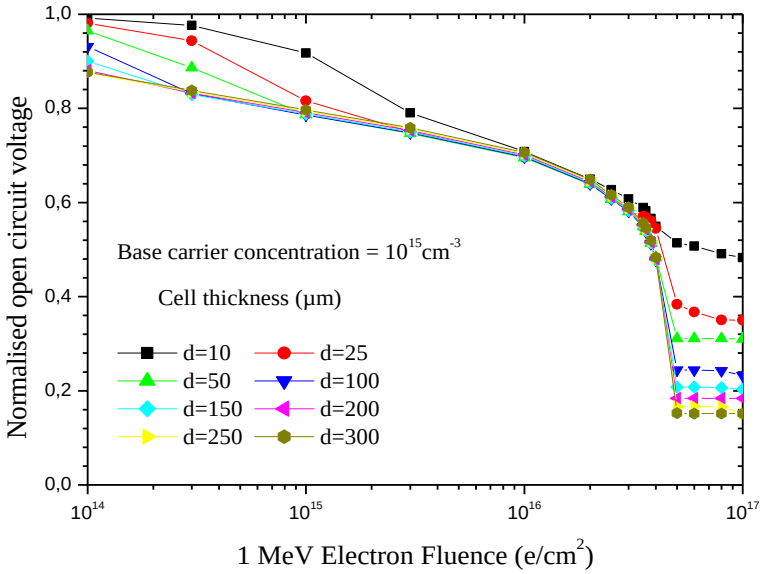


**Figure V.44: Variation of the open circuit voltage as a function of 1 MeV for different total thickness of the solar cell.**

Figure V.45 shows the variation of the efficiency as a function of 1 MeV electron fluence for different thickness of the solar cell. From this figure it can be clearly seen that solar cells with smaller thickness have better radiation tolerance.

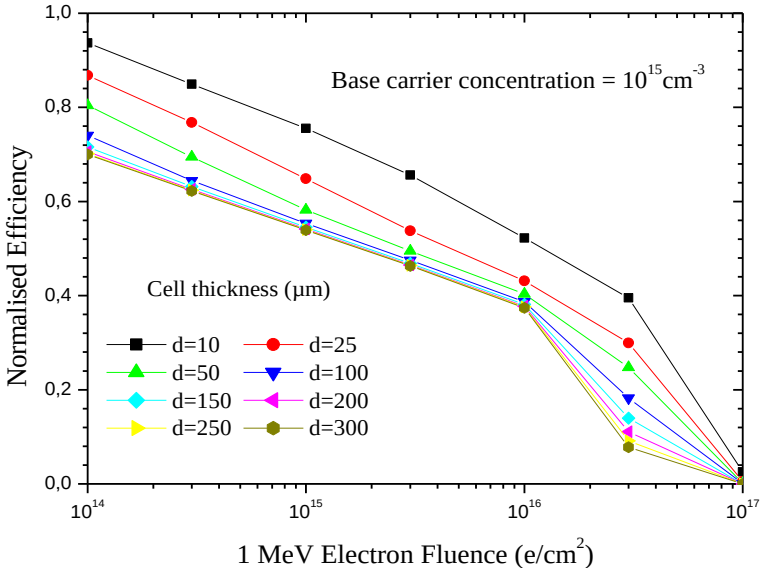


**Figure V.45: Variation of efficiency as a function of 1 MeV electron for different thickness of the solar cell.**

It should be noted here that before irradiation the best efficiency is observed when the highest total thickness of the solar cell is considered as shown in figure V.46. These results are similar to that obtained by other simulation carried out **[124]**.

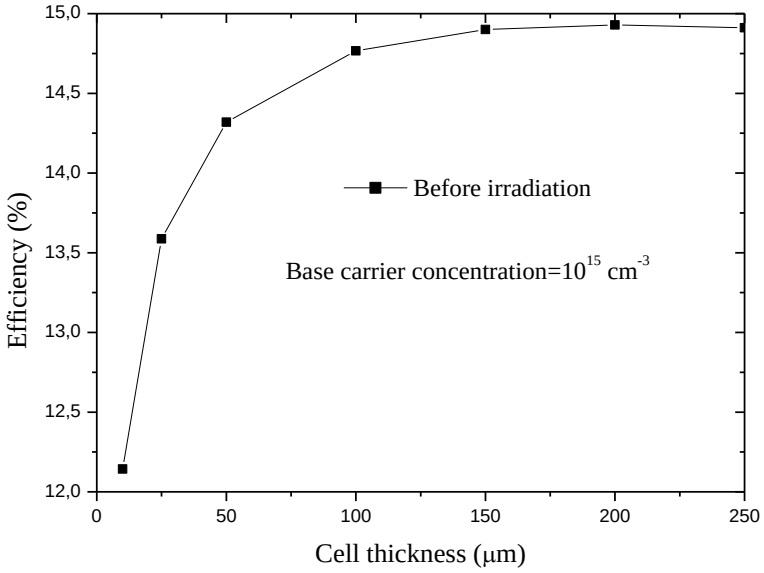


**Figure V.46: Variation of the efficiency before irradiation for different thickness of the solar cell.**

The increase of the efficiency with increasing of the total thickness is due to the fact that the incident photons have more length to travel in the thicker base region and so more region to excite trapped carriers. Then, a larger number of carriers reach the device electrodes to contribute to the generated photocurrent **[124]**.

# Conclusion

Study of the anomalous behaviour of the short circuit current in Silicon solar cells used for space applications is the main aim of this work. In this study we have used the SCAPS simulator to study the electron irradiated solar cell. The current-voltage characteristics of a Si solar cell; having the same structure ($n^+$-p-$p^+$) in which the phenomenon is experimentally observed; are calculated under AM0 spectrum for different fluences of 1 MeV electrons. Knowing that irradiation introduce deep levels in the lattice of the active region of the solar cell; we have studied their effect on the solar cell behaviour. There are several defects created in the active region (p-type base) including deep donors, deep acceptors, and generation/recombination centres. The majority traps only contribute to the reduction of minority carrier lifetime but not to the shallow doping compensation, therefore the minorities which will be responsible for the anomalous behaviour of the short circuit current. In our study therefore; we have concentrated on the two minority traps. For this reason we have studied the effect of these donor traps separately in order to establish which trap is responsible of this phenomenon.

At first, we studied the effect of the deeper donor trap ($E_C - 0.71\,eV$) on the J-V characteristics of the solar cell in many cases:

- When we study the effect of the deeper donor trap with the deep acceptors located in the bottom half of the band gap, we found that the experimentally observed behaviour is not reproduced.
- In the case when we use the deeper donor trap with the deep acceptor located in the mid gap, the anomalous behaviour of the short circuit current is also not reproduced.
- When the deep donor trap with all acceptors is considered it was also found that the experimentally behaviour does not appear.

Secondly, we study the effect of the shallower donor trap ($E_C - 0.20\,eV$) also in many cases:

- When we use the shallower donor trap with the acceptors located in the bottom half of the mid gap we found that the anomalous behaviour of the short circuit current is not reproduced.
- In the case when we use the shallower donor trap with the deep acceptor located in the mid gap, we found that the experimentally behaviour does not appear.

- In the case of the shallower donor trap with all acceptors we found also that the anomalous behaviour of the short circuit current is not reproduced.

Thirdly, when we use the two donor traps together considering their parameters as given in the literature we found also that the experimentally observed behaviour is not reproduced.

Since the experimentally observed behaviour is not reproduced we have changed the introduction rate of the two donor trap separately:

- In all cases when we change the introduction rate of the deeper donor trap, we found that the experimentally observed behaviour does not appear.
- When we change the introduction rate k of the shallower donor trap from 0.002 to 0.01, the anomalous behaviour of the short circuit current does not appear.
- In the case of k=0.03, we observed a slight increment of Jsc for high fluences ($10^{17}$ e/cm$^2$).
- When k=0.04, the region when the anomalous behaviour of Jsc observed is comparable to experimental measurements (between $2x10^{16}$ e/cm$^2$ and $5x10^{16}$ e/cm$^2$) but the steepness of its degradation is not, in this case when we take the deeper donor trap into account we found that the degradation rate of Jsc increases and is comparable to values obtained experimentally and the fluence at which this phenomenon appears is very comparable to measurements.

To study if the anomalous behaviour of the short circuit current is related to the type inversion of the base of the solar cell (from p-type to n-type), we evaluate the electron and hole distribution in the whole solar cell evolution with the 1 MeV electron fluence. This fluence corresponds to the region where the short circuit current shows the anomalous behaviour. We found that the type inversion of the solar cell does not appear until after the pic of the short circuit current.

After that, we studied the effect of the solar cell structure on their figures of merit. We found that when the base carrier concentration is increased the anomalous behaviour of the short circuit current tends to disappear. On the other hand, when we study the effect of the solar cell thickness on the figures of merit of the solar cell, we found that the short circuit current and the efficiency are better for Silicon solar cells which have the smallest thickness. This means that solar cells with the smallest thickness have better radiation tolerance.

In summary, the main results obtained from this study are as follows:

- The shallower donor trap ($E_C - 0.20\,eV$) is the defect responsible for the anomalous behaviour of the short circuit current.

- The deeper donor trap ($E_C - 0.71\ eV$) only enhance the degradation of the solar cell.
- By calculating the free charge profile, the anomalous degradation of the short circuit current is not related to type inversion but to a lateral widening of the space charge region.
- The type inversion of the base of the solar cell is realised after the anomalous behaviour of the short circuit current.
- By studying the solar cell structure effect on the radiation tolerance (the cell thickness, and the concentration of the base), we found that the anomalous behaviour of the short circuit current tends to disappear when the base carrier and the total thickness are increased.
- Silicon solar cells with the smaller thickness have better radiation tolerance.

**Outlook:**

As future work we propose to:

- Study the type inversion in other semiconductor solar cells such as Indium Phosphide (InP).
- Study the type inversion dependence on temperature.
- Obtaining an irradiated solar cell (if possible) for deeper study of the defects parameters.

# References

[1] A. Jungel, "Transport Equations for Semiconductors" Institute fur Mathematik, Johannes Gutenberg Universitat Mainz (Winter 2004) Preliminary Lectures Notes (2005).

[2] M. J. Kerr, "Surface, Emitter and Bulk Recombination in Silicon and Development of Silicon Nitride Passivated Solar Cells", PhD thesis, the Australian national University, (2002).

[3] L.Bruce, "The effect of space environments on solar cells" Available from: https://depts.drew.edu/govschl/NJGSS2010/Journal/TeamPapers/Team7.pdf

[4] M. F. Salerno**, "**Electroluminescence of a-Si/c-Si Heterojunction Solar Cells after High Energy Irradiation", PhD thesis, University of Hagen, (2009).

[5] N. S. Fatemi, H. E. Pollack, H. Q. Hou, P. R. Sharps, "Solar array trades between very high-efficiency multi-junction and Si space solar cells", in Conference Record of the Twenty-Eighth IEEE Photovoltaic Specialists Conference, p. 1083, (2000).

[6] J.C. Bourgoin, N. de Angelis, "Radiation-induced defects in solar cell materials", Solar Energy Materials & Solar Cells 66, 467-477, (2001).

[7] M.Yamaguchi, "Radiation-resistant solar cells for space use", Solar Energy Materials & Solar Cells 68, 31-53, (2001).

[8] A. Klaver, "Irradiation-induced degradation of amorphous silicon solar cells in space", PhD thesis, Delft University of Technology, (2007).

[9] M. Yamaguchi, S. J. Taylor, S. Matsuda, O. Kawasaki, "Mechanism for the anomalous degradation of Si solar cells induced by high fluence 1 MeV electrons irradiation", Appl. Phys. Lett., vol. 68, pp. 3141–3143, (May 1996).

[10] H. Kitahara, S. Tanaka, Y. Kanamori, T. Itoh, in 46th International Astronautical Congress, Oslo, Norway, October 2-6, (1995).

[11] S.Zh. Karazhanov, "Mechanism for the anomalous degradation of proton- or electron irradiated silicon solar cells", Solar Energy Materials & Solar Cells 69, 53-60, (2001).

[12] M.Yamaguchi, A. Khan, Stephen J. Taylor, K. Ando and T. Yamaguchi, S. Matsuda and T. Aburaya, "Deep level analysis of radiation induced defects in Si crystals and solar cells", J. Appl. Phys. 86, 217 (1999).

[13] M. A. Green, "Photovoltaic principles", Physica E 14, 11-17, (2002).

[14] http://www.uccs.edu/~rtirado/PES_1600_SolarEnergy/fotovoltaic_effect.pdf

[15] L. Fraas, L. Partain, "solar cells and their applications", 2nd edition, John Wiley & Sons, (2010).

[16] C. J. Chen, "Physics of Solar Energy", John Wiley & Sons, Inc., Hoboken, New Jersey, (2011).

[17] M. Grätzel, "Perspective for Dye-Sensitized Nanocrystalline Solar Cells", Prog. Photovolt. Res. Appl, 8, 171-185, (2000).

[18] S. Tiwari, N. C. Greenham, "Charge mobility measurement techniques in organic semiconductors" Opt. Quantum Electron, 41, 69-89, (2009).

[19] P. A. Lynn, "Electricity from Sunlight: An Introduction to Photovoltaics", John Wiley &Sons, (2010).

[20] www.uprm.edu/aret/docs/Ch_5_**PV**_systems.**pdf**

[21] H. J. Möller, "Semiconductors for solar cell applications", Progress in Materials Science, 35, 205-418, (1991).

[22] S. M. Sze, Kwok. K. Ng, "Physics of Semiconductor devices", 3rd edition, John Wiley & Sons, New Jersey, (2007).

[23] M. A. Green, "Solar cells, Operating Principles Technology, and Systems Application", Prentice-Hall, (1982).

[24] P .A. Nwofe, "Deposition and Characterisation of SnS Thin Films for Application in Photovoltaic Solar Cell Devices", PhD thesis, University of Northumbria at Newcastle, (2013).

[25] J. V. Holm, "Nanowire Groth for Photovoltaics", PhD thesis, University of Copenhagen, (2013).

[26] G. Altamura, "Development of CZTSSe thin Films based solar cells", PhD thesis, University of Grenoble, (2014).

[27] A. Das, "Development of high-efficiency Boron diffused Silicon solar cells", PhD thesis, Georgia Institute of Technology, (August 2012).

[28] A. Luque, S. Hegedus, "Handbook of Photovoltaic Science and Engineering", John Wiley & Sons Ltd, The Atrium, Southern Gate, Chichester, West Sussex PO19 8SQ, England, (2003).

[29] M. A. Green, "The Path to 25% Silicon Solar Cell Efficiency: History of Silicon Cell Evolution", Prog. Photovolt: Res. Appl, 17, 183-189, (2009).

[30]T. Markvart, L. Castañer, "Chapter IA-1- Principles of Solar Cell Operation", Practical Handbook of Photovoltaics (Second Edition), (2012).

[31] C. Honsberg, S. Bowden, http://pveducation.org/pvcdrom.

[32] M. Zeman, Solar Cells. Chapter 3: "Semiconductor materials for Solar cells", Delft University of Technology.

[33] Md. Atikur Rahman, "A Review on Semiconductors Including Applications and Temperature Effects in Semiconductors", American Scientific Research Journal for Engineering, Technology, and Sciences (ASRJETS**),** 7, No 1, 50-70, (2014).

[34] L. Kazmerski, "Best Research Cell Efficiencies", 2010. Available from: http://en.wikipedia.org/wiki/File:PVeff%28rev100414%29.png.

[35] D. A. Neamen, "Semiconductor Physics and Devices, Basic Principles", third edition, McGrew Hill, New York, (2003).

[36] K. Jäger, O. Isabella, A. H. M. Smets, René A.C.M.M. van Swaaij, M. Zeman, "Solar Energy: Fundamentals, Technology, and Systems", Copyright Delft University of Technology, (2014).

[37] A. Sharma, S. K. Kar, "Energy Sustainability Through Green Energy", Springer New Delhi Heidelberg New York Dordrecht London Springer, India, (2015).

[38] P. Jayakumar, "Solar Energy, Resource Assessment Handbook", Asian and Pacific Centre for Transfer of Technology of the United Nations-Economic and Social Commission for Asia and the Pacific (ESCAP), (2009).

[39] J. A. R. Gonzalez, "Characterization, Modeling and Optipization of industrial Silicon thin film solar cells", PhD thesis, University of Santiago De Compostela, (2013).

[40] Z. Fang, X. C. Wang, H. C. Wu, C. Z. Zhao, "Achievements and Challenges of CdS/CdTe Solar Cells", International Journal of Photoenergy, Volume 2011, Article ID 297350.

[41] V. M. Fthenakis, "Life cycle impact analysis of cadmium in CdTe PV production", Renewable and Sustainable Energy Reviews, 8, 303-334, (2004).

[42] P. Jackson, D. Hariskos, E. Lotter, S. Paetel, R. Wuerz, R. Menner, W. Wischmann, M. Powalla, "New world record efficiency for Cu(In,Ga)Se2 thin film solar cells beyond 20%", Progress in Photovoltaics: Research and Applications 19, 894‑897, (2011)..

[43] O. Mah, "Fundamentals of Photovoltaic Materials", National Solar Power Reasearch Institute, Inc. (1998). Available from: www.nspri.org

[44] M. Bertolli, "Solar Cell Materials", Course: Solid State II, Department of Physics, University of Tennessee, (2008).

[45] A. Md. Bagher, M. M. A. Vahid, M. Mohsen. "Types of Solar Cells and Application". American Journal of Optics and Photonics, 3(5), 94-113, (2015).

[46] M. P. Stéphane, "Nouvelles architectures distribuées de gestion et de conversion de l'énergie pour les applications photovoltaïques" thèse de doctorat, Université de Toulouse, (2009).

[47] W. J. Potscavage, Jr, "Physics and Engineering of Organic Solar Cells", PhD thesis, Georgia Institute of Technology, (May 2011).

[48] S. G. Bailey et al, "Solar Cell and Array Technology for Future Space Science Missions", Internal NASA report to Code S, (2002).

[49] K. Loh, "Solar cells for space applications", Delft University of technology, (2013), available from: www.academia.edu/5253076/Solar_Cells_for_Space_Applications

[50] A. Romeo et al, "Development of Thin-film Cu(In,Ga)$Se_2$ and CdTe Solar Cells", Prog. Photovolt: Res. Appl, 12, 93-111, (2004).

[51] A. Mohsin, "Electrical charactrization of III-V antimonide/GaAs heterostuctures grown by interfacial misfit molecular beam epitaxy technique", PhD thesis, University of Nottingham, (2014).

[52] M. U. Khandaker, "High purity germanium detector in gamma-ray spectrometry", IJFPS, 1, N°.2, 42- 46, (June 2011).

[53] P. Y. Yu, M. Cardona "Fundamentals of Semiconductors**,** Physics and Materials Properties", Fourth Edition, Springer Heidelberg Dordrecht London, New York, (2010).

[54] S. Mukherjee, "Applied Mineralogy: Applications in Industry and Environment", Springer, India, (2012).

[55] A. Rockett,"The Materials Science of Semiconductors", Springer Science+Business Media, LLC, (2008).

[56] C. Nyamhere, "Characterization of process and radiation induced defects in Si and Ge using conventional deep level transient spectroscopy (DLTS) and Laplace-DLTS", PhD thesis, University of Pretoria, (September 2009).

[57] D. S. Aidhy, "Evolution of Intrinsic Point Defects in Fluorite-Based Materials: Insight from Atomic-Level Simulation", PhD thesis, University of Florida, (2009).

[58] W. D. Callister, Jr. "Materials Science and Engineering. An Introduction", seventh edition, John Wiley & Sons, Inc. (2007).

[59] U. K. Bhaskar, "Preparation and Microstructure Characterization of some Metal Nitride", PhD thesis, University of Burdwan, India, (2013).

[60] W.Mtangi, "Electrical characterization of process, annealing and irradiation induced defects in ZnO", PhD thesis, University of Pretoria, (2012).

[61] A. K. DEB, "Lacunes chargées, étude dans des nano-agrégats de silicium", thèse de doctorat, Université de Grenoble, (2012).

[62] J. W. Morris, Jr. "A Survey of Materials Science I. Structure", Department of Materials Science and Engineering, University of California, Berkeley Fall, (2007).

[63] M .D. McCluskey, E.E. Haller, "Dopants and Defects in semiconductors", Taylor&Francis Group LLC, (2012).

[64] M. Schmidt, "Space Charge Spectroscopy applied to Defect Studies in Ion-Implanted Zinc Oxide Thin Films", PhD thesis, University of Leipzig, (2012).

[65] W. Shockley and W. T. Read, "Statistics of the recombinations of holes and electrons", Phys. Rev, 87, 835-842, (1952).

[66] R. N. Hall, "Electron-Hole Recombination in Germanium". Phys. Rev, 87, 387, (1952).

[67] R. J. Walters, G. P. Summers, "Space Radiation Effects in Advanced Solar Cell Materials and Devices", Mat. Res. Soc. Symp. Proc. Vol. 692, (2002).

[68] N. Nagai, M. Sumitomo, M. Imaizumi, R. Fukasawa, "Characterization of electron-or proton-irradiated Si space solar cells by THz spectroscopy", Semicond. Sci. Technol, 21, 201-209, (2006).

[69] A. Vasic, P. Osmokrovic, N. Marjanovic, M. Pejovic, "Radiation Effects in Solar Cells and Optoelectronic Devices", International Journal of Photoenergy Volume 2013, Article ID 171753.

[70] X. Wang, Z. M. Wang, "High-Efficiency Solar Cells Physics, Materials, and Devices", Springer Series in Materials Science, Volume 190, (2014).

[71] S. R. Elkington, "Simulating Electron Radiation Belt Dynamics ", PhD thesis, Dartmouth College, Hanover, NewHampshire, (2000).

[72] S. Duzellier, "Radiation effects on electronic devices in space", Aerospace Science and Technology, 9, 93-99, (2005).

[73] J.W. Howard, D.M. Hardage, "Spacecraft Environments Interactions: Space Radiation and Its Effects on Electronic Systems", Nati**o**nal Aer**o**naut**i**cs and Space Administration, Space Center for AeroSpace Informati**o**n, (july 1999).

[74] J. R. Schwank, "Basic mechanisms of radiation effects in the natural space environment", in Proc. IEEE Nuclear and Space Radiation Effects Conference, Short Course, Section II, Tucson, AZ, USA, 1-109, (1994).

[75] M. R. Reddy, "Space solar cells-tradeoff analysis," Solar Energy Materials & Solar Cells, 77, 175-208, (2003).

[76] T. Mikaelian, "Spacecraft Charging and Hazards to Electronics in Space", York University, (May 2001).

[77] Ö. Amutkan, "Space Radiation Environment and Radiation Hardness Assurance Tests of Electronic Components to be Used in Space Missions", PhD thesis, Middle East Technical University, (2010).

[78] R. L. Pease, A. H. Johnston, J. L. Azarewicz, "Radiation Testing of Semiconductor Devices for Space Electronics", Proceedings of the IEEE, Vol. 76, $N^0$. 11, (November 1988).

[79] J. R. Srour, J. M. McGarrity, "Radiation Effects on Microelectronics in Space", Proceedings of the IEEE, Vol. 76, $N^0$. 11, (November 1988).

[80] E. Segre, "Nuclei and Particles, An Introduction to Nuclear and Subnuclear Physics", W.A. Benjamin Inc., New York, (1965).

[81] W. R. Leo, Techniques for Nuclear and Particle Physics Experiments. Berlin and Heidelberg: Springer, (1994).

[82] H.Y. Tada, J.R. Carter, Jr. "Solar Cell Radiation Handbook", Third Edition, Jet Propulsion Laboratory Pasadena, CA, (1982).

[83] J. R. Srour, J.W. Palko, "Displacement Damage Effects in Irradiated Semiconductor Devices", IEEE Transactions on Nuclear Science, Vol 60, N° 3, (2013).

[84] M. Alurralde, M.J.L. Tamasi, C.J. Bruno, M.G. Martínez Bogado, J. Plá, J. Fernández Vázquez, J. Durán, J. Schuff, A.A. Burlon, P. Stoliar and d, A.J. Kreiner, Experimental and theoretical radiation damage studies on crystalline silicon solar cells, Solar Energy Materials & Solar Cells, 82, 531–542, (2004).

[85] D. V. Lang, "Deep-Level Transient Spectroscopy: A New Method to Characterize Traps in Semiconductors", J. Appl. Phys, 45, 3023-3032, (1974).

[86] M. A. Green, "Silicon Solar Cells: Advanced Principles and Practice", UNSW, Sydney, (1995).

[87] H. Mathieu, "Physique des semi-conducteurs et des composants électroniques", Masson,$4^{ième}$ édition, Paris, (1998).

[88] C.C.Hu, "Modern Semiconductor Devices for Integrated Circuits", New. Jersey: Prentice Hall, (2010).

[89] D. Diouf, "Cellules photovoltaïques silicium à hétérojonctions et à structure interdigitée en face arrière", thèse de Doctorat, Université Paris-Sud11, (2010).

[90] H. J. Möller, "Semiconductors for Solar Cell Applications", Progress in Materials Science 35, 205-418, (1991).

[91] J. Dziewior, W. Schmid, "Auger coefficients for highly doped and highly excited silicon", Applied Physics Letters, 31, 346-348, (1977).

[92] D.A. Clugston, P.A. Basore, "PC1D version 5: 32-bit solar cell modelling on personal computers", Conference Record of the 26th IEEE Photovoltaic Specialists Conference, 207–210, (1997).

[93] H.Zhu, A.K. Kalkan, J. Hou, S.J.Fonash,"Applications of AMPS-1D for Solar Cell Simulation", AIP Conference Proceedings 462, 309, (1999).

[94] B. E. Pieters, J. Krc, M. Zeman, "Advanced numerical simulation tool for solar cells-ASA5," in Proceedings of the Conference Record on 4$^{th}$ WCPEC, 2, 1513-1516, (2006).

[95] R.Stangl, M.Kriegel, M.Schmidt. "AFORS-HET, version 2.2, a numerical computer program for simulation of heterojunction solar cells and measurements", Proceedings of the 4th World Conference on Photovoltaic Energy Conversion, Hawaii, USA: 1350-1353. (2006).

[96] S. Michael, A. Bates, M. Green, "SILVACO ATLAS as a Solar Cell Modeling Tool", Proceedings of the 31st IEEE Photovoltaic Specialists Conference, Orlando, FL, 719-721, (January 2005).

[97] A.Niemegeers, M. Burgelman, S. Degrave, J. Verschraegen, K. Decock, "SCAPS manual", (Version 24 April 2012).

[98] E. K. Chiew, M. Yahaya, A. P. Othman, "Investigation of recombination process of P3HT:PCBM organic solar cell", Solid State Science and Technology, 20, No 1 & 2, 102-108, (2012).

[99] M. Burgelman, P. Nollet, S. Degrave, "Modelling polycrystalline semiconductor solar cells", Thin Solid Films, 527, 361-362, (2000).

[100] J.C. Bourgoin, R. Kiliulis, C. Gonzales, G. Strob, C. Flores, K. Bogus and C. Signorini, "Deep space degradation of Si and GaAs solar cells", 25th PVSC; Washington, D.C, (May 13-17, 1996).

[101] Y. Yamamoto, O. Kawasaki, S. Matsuda, Y. Morita, Proc. European Space Power Conf. ESPCt, Poitiers, France, esa SP-369, 2, 573-578, 4-8 (September 1995).

[102] G.H.Shin, K.S. Ryu, H.M. Kim, K.W. Min, "Radiation Effect Test for Single-Crystalline and Polycrystalline Silicon Solar Cells", Journal of the Korean Physical Society, 52, No. 3, 843-847, (March 2008).

[103] M.Imaizumi, S.J. Taylor, M. Yamaguchi, T. Ito, T. Hisamatsu, S. Matsuda, "Analysis of structure change of Si solar cells irradiated with high fluence electrons", J. Appl. Phys. 85, 1916, (1999).

[104] B. Danilchenko, A. Budnyk, L. Shpinar, D. Poplavskyy, S.E. Zelensky, K.W.J. Barnham, N.J. Ekins-Daukes, "1MeV electron irradiation influence on GaAs solar cell performance", Solar Energy Materials & Solar Cells, 92, 1336-1340, (2008).

[105] M. Yamaguchi, S. J. Taylor, M .J. Yang, S. Matsuda, O. Kawasaki, T.Hisamatsu, "High-energy and high-fluence proton irradiation effects in silicon solar cells", J. Appl. Phys. 80, 4916, (1996).

[106] M. Yamaguchi, A. Khan, S. J. Taylor, M. Imaizumi, T. Hisamatsu, S. Matsuda, "A Detailed Model to Improve the Radiation-Resistance of Si Space Solar Cells", IEEE TRANSACTIONS ON ELECTRON DEVICES, 46, NO. 10, 2133, (OCTOBER 1999).

[107] J. H. Warner, S. R. Messenger, R. J. Walters, G. P. Summers, J. R. Lorentzen, D. M. Wilt, Mark A. Smith, "Correlation of electron radiation induced-damage in GaAs solar cells", IEEE Transactions on Nuclear, 53, NO. 4, (AUGUST 2006).

[108] S. Makham, G.C.Sun, J.C.Bourgoin, "Modelling of solar cell degradation in space", Solar Energy Materials & Solar Cells, 94, 971-978, (2010).

[109] S. Makham, M. Zazoui, G.C. Sun, J.C. Bourgoin, "Prediction of proton-induced degradation of GaAs space solar cells", Solar Energy Materials & Solar Cells, 90, 1513-1518, (2006).

[110] M Mbarki, G. C. Sun, J. C. Bourgoin, "Prediction of solar cell degradation in space from the electron–proton equivalence", Semicond. Sci. Technol, 19, 1081–1085, (2004).

[111] R. J. Walters, M.A. Xapsos, G. P. Summers, "Radiation response of single and dual junction p+-n InGaP/GaAs space solar cells", Proceedings of the 26$^{th}$ IEEE Photovoltaic Specialist Conference, 29 September-03 October 1997, 843–846, Anaheim, CA, (1997).

[112] N. de Angelis, J.C. Bourgoin, T. Takamoto, A. Khan, M. Yamaguchi, "Solar cell degradation by electron irradiation. Comparison between Si, GaAs and GaInP cells", Solar Energy Materials & Solar Cells, 66, 495-500, (2001).

[113] T. Hisamatsu , O. Kawasakia, S. Matsudaa, K. Tsukamotob, "Photoluminescence study of silicon solar cells irradiated with large fuence electrons or protons", Radiation Physics and Chemistry, 53, 25-30, (1998).

[114] X. Xianbi, D. Wenhui, C. Xiulan, L. Xianbo, "Electron irradiation and thermal annealing effect on GaAs solar cells", Solar Energy Materials & Solar Cells, 55, 313-322, (1998).

[115] A. Khan, M. Yamaguchi, T. Aburaya, S. Matsuda, "Comparison of the effects of electron and proton irradiation on type-converted silicon space solar cells upon annealing", Semicond. Sci. Technol, 15, 403-407, (2000).

[116] C. A. Londos, P. C. Banbury, "Defect studies in electron-irradiated boron-doped silicon", J. Phys. C: Solid State Phys. 20, 645-650, (1987).

[117] N. Chandrasekaran, T. Soga, Y. Inuzuka, M. Imaizumi, H. Taguchi, T. Jimbo, "1MeV electron irradiation effects of GaAs/Si solar cells", Mater. Res. Soc. Symp. Proc, Vol. 836, L6.7.1-6. (2005).

[118] A. Khan, M. Yamaguchi, T. Takamoto, N. de Angelis, J.C. Bourgoin, "Recombination centers in electron irradiated GaInP: application to the degradation of space solar cells", Journal of Crystal Growth, 210, 264-267, (2000).

[119] T. Hisamatsu, S. Matsuda, T. Nakao, Y. Matsumoto, S. J. Taylor, M. Yamaguchi, "Thermal recovery of degraded space silicon solar cells due to large fluence irradiation", 26th PVSC; Anaheim, CA, 991-4, (Sept. 30-0ct. 3,1997).

[120] AF. Meftah, N. Sengouga, A. Belghachi, AM. Meftah, "Numerical simulation of the effect of recombination centres and traps created by electron irradiation on the performance degradation of GaAs solar cells", J. Phys.: Condens. Matter, 21, 215802, (2009).

[121] AF. Meftah, N. Sengouga, AM. Meftah , S. Khelifi, "Numerical simulation of the effect of the Al molar fraction and thickness of an $Al_xGa_{1-x}As$ window on the sensitivity of a $p^+$–n–$n^+$ GaAs solar cell to 1 MeV electron irradiation", Renewable Energy, 34, 2426-2431, (2009).

[122] AF. Meftah, N. Sengouga, AM. Meftah, A. Belghachi, "Detailed numerical simulation of the effect of defects created by electron irradiation on the performance degradation of a $p^+$–n–$n^+$ GaAs solar cell", Renewable Energy, 34, 2422–2425, (2009).

[123] AF. Meftah, AM. Meftah, N. Sengouga, S. Khelifi, "The $Al_xGa_{1-x}As$ window composition effect on the hardness improvement of a $p^+$–n–$n^+$ GaAs solar cell exposed to the electron irradiation", Energy Conversion and Management, 51, 1676-1678, (2010).

[124] M. A. Cappelletti, G. A. Casas, A. P. Cédola, E. L. Peltzer y Blancá, "Theoretical study of the maximum power point of n-type and p-type crystalline silicon space solar cells", Semicond. Sci. Technol, 28, 045010, (2013).

[125] T. Hisamatsu, O. Kawasaki, S. Matsuda, T. Nakao, Y. Wakow, "Radiation degradation of large fluence irradiated space silicon solar cells", Solar Energy Materials and Solar Cells, 50, 331-338, (1998).

[126] Y. Tokuda, N. Shimizu, A. Uzami, "Studies of Neutron-Produced Defects in Silicon by Deep-Level Transient Spectroscopy", Japanese Journal of Applied Physics, 18 N°2, 309-315, (February 1979).

[127] A.G.M. Das, C. Nyamhere , F.D. Auret , M. Hayes, "A comparative study of electronic properties of the defects introduced in p-Si: (i) During electron beam deposition of Ti/Mo, (ii) by proton irradiation, and (iii) by electron irradiation", Surface & Coatings Technology, 203, 2628-2631, (2009).

[128] M. Imaizumi, S. J. Taylor, M. Yamaguchi, T. Hisamatsu, S. Matsuda, O. Kawasaki, "Analysis of the spectral response of Silicon solar cells irradiated with high fluence electrons/protons", 26th PVSC, Anaheim, CA 983-986, (Sept. 30-0ct. 3,1997).

[129] S. J. Taylor, M. Yamaguchi, M. J. Yang, M. Imaizumi, S. Matsuda, O. Kawasaki, T. Hisamatsu, "Type conversion in irradiated silicon diodes", Appl. Phys. Lett. 70, 2165, (1997).